University of Exeter
Department of Mathematics

Mathematical modelling and Data Analysis for Parkinson's Disease Gait

Midhun Parakkal Unni

Submitted by Midhun Parakkal Unni, to the University of Exeter as a thesis for the degree of Doctor of Philosophy in Mathematics, October, 2021.

I certify that all material in this thesis which is not my own work has been identified and that any material that has previously been submitted and approved for the award of a degree by this or any other University has been acknowledged.

Signed: .....

Abstract

Freezing is an involuntary stopping of gait observed in late-stage Parkinson's disease (PD) patients. It is a highly debilitating symptom lacking a clear understanding of its causes and is challenging to predict. This thesis addresses (1) machine-learning-based prediction of freezing for better management of the disease and (2) neuromechanical modelling to explain the underpinnings of the symptom.

A data-driven approach is proposed in chapter 4 for predicting freezing events using a machine learning approach, specifically Random Forrest (RF), Neural Network (NN), and Naive Bayes (NB). Data sampled using a force platform were used for this purpose. This data was collected from PD subjects as they stepped in place until they had at least one freezing episode. The F1 scores of the machine learning algorithms were computed for different windowing parameters. These parameters represent the input data length (IL) and how early the freezing event is predicted (GL). The IL that maximised the F1 score is approximately equal to 1.13 s, indicating the physiological changes leading to a freeze take effect at least one step before the freezing incident. The prediction deteriorated as one tried to predict it early, evidenced by a negative correlation between GL and F1 scores. Our algorithm has the potential to support the development of devices to detect and then potentially prevent freezing events in people with Parkinson's, which might occur if left uncorrected.

As the second contribution, mathematical models of PD-Gait are developed with varying complexity and generality to explain the observed gait characteristics of PD. The first mathematical model described in chapter 5 consists of the stance leg modelled as a simple inverted pendulum acted upon by the ankle-push off forces from the trailing leg and pathological forces by the plantar-flexors of the stance leg. Freezing and irregular walking are demonstrated in a biped model as well as

the inverted pendulum model. The inverted pendulum model is further studied semi-analytically to show the presence of horseshoe and chaos to explain the cause of variability in PD-Gait. The model reveals that these opposing forces generated by the plantar flexors can induce freezing and variability. The model also explains gait abnormalities such as reduction in step length close to a freeze and irregular walking patterns. However, the model proposed in chapter 5 does not explicitly address the effect of central pattern generators (CPG), feedback from the limbs, and the transition to walking from FoG observed in PD-Gait. Therefore, a generalisation of the model is developed in chapter 6 by coupling the hybrid mechanical model with a model of CPG and event dependent feedback. The model demonstrates gait characteristics relevant to PD, such as freezing, high variability and stable gait. The model's ability to capture the PD-related characteristics across a wide parameter range showed its robustness. Moreover, the effect of augmented feedback on the model is studied to understand different FoG management methods, such as sensory and auditory cues. While this model explains variability, freezing, the effect of feedback, and transitions from freezing to walking, there is further scope to generalise this model, considering that phase coordination is affected in PD-Gait. This generalisation requirement is addressed in chapter 7. Here, a set of maps are derived, combining both the neural and mechanical aspects of the PD-Gait. Phase reset curves (PRC) that correspond to the oscillators are used to abstract the neuronal dynamics, and a simple inverted pendulum model is used to describe the motion. Gait variability, freezing, the effect of PPN stimulation in PD-Gait are explained using this model. The model is also extensible to be used with different PRCs. To summarise, the thesis has potential implications in FoG management using sensory cues, and it takes a step forward in explaining the underpinnings of PD-Gait characteristics such as freezing and variability.

Acknowledgements

Firstly, I would like to express my sincere gratitude to the University of Exeter for funding my PhD through the International excellence scholarship. I want to thank my primary supervisor, Dr Prathyush Menon, for his excellent guidance and kind support through each stage of the process, from mathematical modelling to the publication of the results, and for helping me develop an interest in hybrid system's theory. I also would like to thank my supervisors, Prof Mark R Wilson and Dr Lorenzo Livi, for their valuable input to the thesis and publications. I express my gratitude to Prof Krasimira Tsaneva-Atanasova, for guiding me in the early stages of the thesis and publication of the results. Moreover, I thank Dr William R. Young and Prof Helen M. Bronte-Stewart for sharing the data and valuable input in work. I want to acknowledge my mentor Prof Peter Ashwin for inspiring my interest in dynamical systems theory and paving my way to the subject.

I sincerely thank my examiners, Dr Jan Sieber and Dr Genevieve Williams, for their critical inputs throughout my PhD period. I also thank Dr Ana Rodrigues, Prof Gino Krkac, Ms Sarmishtha Ghosh and the post-graduate research support team for their help throughout my challenging times. Moreover, suggestions from Dr Ana Rodrigues has been of great help in making me understand the richness of discrete maps in modelling dynamic behaviours. I am incredibly grateful to my family and friends for supporting me throughout my PhD journey.

Contents

Abstract i

Acknowledgements iii

Contents vii

List of Figures ix

List of Tables x

Nomenclature xiii

1 Introduction 1

1.1 Approach 5

1.2 Contribution 7

1.3 Thesis Organization 8

2 Background - Physiology of Gait and Pathophysiology of FoG 10

2.1 Physiology of Walking and Pathology of FoG 11

3 Background - Data Analysis and Modelling for FoG 16

3.1 Data driven prediction of freezing 16

3.1.1 Sensory cues for managing PD 20

3.2 Mathematical Modelling of FoG 21

3.2.1 Central Pattern generators and its relevance to PD-Gait . . . 21

3.2.2 Robotics related models of gait 24

3.2.3 Addressing motor redundancy 25

3.2.4 Walking is a hybrid system . . . 26
3.2.5 Introduction to Hybrid systems . . . 27
3.2.6 Phase and phase response curves . . . 29
3.2.7 Neural oscillators and phase . . . 31

4 Data-Driven Prediction of Freezing of Gait Events From Stepping Data 36

4.1 Methodology . . . 37
4.1.1 Experimental Data Used . . . 39
4.1.2 Preprocessing . . . 40
4.2 Labelling . . . 41
4.3 Cross Validation . . . 42
4.3.1 Integrating the Classifier Outcomes . . . 43
4.3.2 Parameter Analysis Procedure . . . 43
4.3.3 Classifiers and Related Parameters . . . 44
4.3.4 Classifier Comparison . . . 46
4.3.5 Procedure for Real-Time Prediction . . . 47
4.4 Results . . . 48
4.4.1 Classification Performance . . . 48
4.4.2 Real-Time Prediction Demonstration . . . 52
4.5 Discussion . . . 53

5 Ankle Push-Off Based Mathematical Model for Freezing of Gait in Parkinson's Disease 56

5.1 Materials and Methods - Modeling . . . 58
5.1.1 Physiology . . . 58
5.1.2 Dynamics of Walking . . . 59
5.1.3 Derivation of the Forcing Terms . . . 63
5.1.4 Rationale for Using a Low dimensional Model for Analysis . . . 67
5.2 Analysis of the Reduced System . . . 68
5.2.1 Gait Cycle . . . 68

5.2.2 Heel Strike Condition 70
5.2.3 Analytical and Numerical Solution of the Equations of Motion 72
5.2.4 Derivation of a Map to Describe Successive Stance Phases . . 74
5.2.5 Graphical Analysis of the Map Between Stance Phases 76
5.3 Results 77
5.3.1 Freezing in a Biped Model 78
5.3.2 Freezing in an Inverted Pendulum Model 80
5.3.3 Parameter Exploration of Inverted Pendulum: Study of the Map $\tilde{f}_\omega$ 83
5.3.4 Bifurcations of the One Dimensional System for the Inverted Pendulum Model 88
5.4 Discussion 92

6 Central Pattern Generator Based Extension of the Freezing of Gait Model 96

6.1 Background 97
6.1.1 Physiology 98
6.2 Mathematical Modelling 99
6.2.1 Equations of Motion 99
6.2.2 Neuronal Dynamics as Locomotion Control 103
6.2.3 Mechanical model and Definition of Freezing 104
6.3 Numerical Simulation of Freezing and Normal Gait 105
6.4 Stability 109
6.5 Effect of External Input in the Absence of Proprioceptive Feedback . 114
6.5.1 Effect of external input on neuronal activity 114
6.5.2 Effect of External-Input on the *Freezing Fraction* 116
6.6 Effect of feedback on the overall system 117
6.6.1 Parameters $\alpha,\ \tau,\ K,\ S_t$ 119
6.7 Discussion 119

7 Phase Reset Curve Based Generalization of the Freezing of Gait

Model **123**

7.1 Modelling . . . 124

7.1.1 Neural oscillators and phase . . . 124

7.1.2 Mechanics . . . 125

7.1.3 The General PRC Based Model for Constant Step Size . . . 127

7.2 Relevant functions . . . 130

7.2.1 Forcing Function . . . 130

7.2.2 PRC Function . . . 131

7.2.3 Form of the PRC Functions Used in the Model . . . 132

7.2.4 Freezing fraction . . . 134

7.3 Results . . . 135

7.3.1 Simulation of Normal Gait and Freezing . . . 135

7.3.2 Effect of Changes in T, m_f, and η . . . 137

7.3.3 Varying the shape of the PRC . . . 139

7.4 Discussion . . . 141

8 Summary and Conclusion **144**

8.1 Future Work . . . 147

A Appendix: Background Physiology **150**

A.1 Motor Control Physiology - General structure and function . . . 150

A.2 Pathophysiology of Parkinson's Disease . . . 151

A.3 PD interventions . . . 153

B Appendix: PRC Model **155**

B.1 Another way to arrive at the equation of motion . . . 155

List of Figures

2.1 Hierarchy of motor control 10

2.2 Pathophysiology of walking 12

3.1 Explanation of FoG/pre-FoG 17

3.2 Figure adapted from (Palmerini et al., 2017) 17

3.3 Illustration of the trajectory in the hybrid system. The dashed line correspond to the discrete mode dynamics, whereas the solid line corresponds to the continuous part of the hybrid system. 28

3.4 Explanation of PRC 30

4.1 The windowing and data conditioning methodology. 38

4.2 The effect of GL and IL on the median F1-scores. 49

4.3 The effect of IL, GL on the F1-scores of the classifiers. 50

4.4 The comparison of the freezing prediction using NN, RF and NB . . 51

5.1 Anatomical representation of the stance phase from ankle push-off to heel strike. 56

5.2 The toe-off, mid stance and heel strike instances of the biped 60

5.3 Free body diagram of the forces. 64

5.4 The toe-off, mid stance and heel strike instances of the inverted pendulum 69

5.5 Proof of horseshoe in the map 76

5.6 Numerical simulation of biped during freezing 78

5.7 Numerical simulation parametric for biped 79

5.8 Numerical simulation of inverted pendulum during freezing 81

5.9 Numerical simulation parametric for inverted pendulum 82
5.10 Period doubling as ϕ is varied 84
5.11 Maps obtained by varying the parameter τ_l. 85
5.12 Maps obtained by varying the parameter ϕ 86
5.13 Maps obtained by varying the parameters τ_r and θ_{reset} 87
5.14 Period-1 orbits and stable regions 91
5.15 Period-3 and period 1 orbits and stable regions 92

6.1 The physiology and the associated modelling assumptions 98
6.2 CPG model block diagram 100
6.3 Normal gait and freezing in CPG based model 107
6.4 Numerical simulation of the hybrid-CPG-based system 108
6.5 The effect of external input on the low f_b 109
6.6 The value of Ξ as it changes between S and $\tilde{S}$ 110
6.7 3D plot of stable periodic points 113
6.8 Synchronization in CPG 115
6.9 Synchronization effect of external input 117
6.10 Parameter exploration 118

7.1 Inverted pendulum model - PRC 125
7.2 A sketch of a trajectory of one of the oscillator's phase and angular velocity close to a *limit cycle* 128
7.3 $PRC_m(\cdot)$ parametrized by a 133
7.4 $PRC_e(\cdot)$ parametrized by a 133
7.5 Numerical simulation of the discerete model 136
7.6 Bifurcation diagram for parameter T 137
7.7 Bifurcation diagram of m_f 138
7.8 Bifurcation diagram of η 138
7.9 Freezing and walking regimes corresponding to PRC_m and PRC_e . . 140

A.1 A detailed description of the basal ganglia functional dynamics 152

List of Tables

3.1 Gait literature relevant to PD 22

5.1 Summary of qualitative behaviour of the map 90

6.1 The values of different parameters of the model and initial conditions 106

7.1 Discrete Simulation parameters 135

Nomenclature

AMD Amygdala

CD Coeffient of dispersion

CLR Cerebellar locomotor region

CoM Centre of mass

CP Caudate Putamen

CPG Central pattern generators

CV Coeffient of variation

DBS Deep brain stimulation

ECG Electrocardiogram

EEG Electroencephalogram

FoG Freezing of gait

GL Gap Length

GPe Globus pallidus externus

GPi Globus pallidus internus

Hipp Hippocampus

IL Input length

LC Locus coeruleus

MC Motor cortex

MFN Mean false negatives

MFP Mean false positives

MLR Mesencephalic locomotor region

MN Motor neurons

MRF Midbrain reticular formation

NB Naive Bayes

NN Neural Network

NRGc Nucleus reticularis gigantocellularis

NRMc Nucleus reticularis magnocellularis

OL Offset Length

PC Parietal cortex

PCA Principal component analysis

PD Parkinson's disease

PPN Pedunculopontine nucleus

PRC Phase reset curve

PRF Pontine reticular formation

RF Random forest

RN Raphe nuclei

SD Standard Deviation

SF Sensory feedback

SLR Subthalamic locomotor region

SNc Substantia nigral pars compacta

SNr Substantia nigra pars reticulata

STN Subthalamic nucleus

TL Target Length

TS Time series

VC Visual cortex

VP Ventral pallidus

VTA Ventral tegmental area

WL Window length

cs Centisecond

m Meter

$N\ m$ Newton meter

rad Radians

s Second

1. Introduction

Parkinson's disease (PD) is a neurodegenerative disorder affecting more than 16 million people worldwide (Mazilu et al., 2015) which includes approximately 1% of the population over the age of 60 years (Lewis and Barker, 2009). The aetiology of the disorder involves the death of dopaminergic neurons in the substantia nigra pars compacta of the basal ganglia (Kandel et al., 2000). Both cognitive (e.g., depression and sleep difficulties) and motor (e.g., tremor, rigidity, bradykinesia, changes in speech and Freezing of gait (FoG)) symptoms are associated with PD (Schapira, Chaudhuri and Jenner, 2017). FoG is a motor disability in PD patients where subjects experience an "episodic absence or marked reduction of forward progression of the feet despite the intention to walk" (page 734, (Nutt et al., 2011)). The onset of FoG typically occurs in advanced stages of the disease progression (Giladi et al., 2001) and is one of the most debilitating features of PD, affecting the well-being and quality of life between 20-80% of patients. Additionally, falls and FoG are interconnected in PD patients (Bloem et al., 2016; Bloem et al., 2004) further complicating the problem. Furthermore, PD could also result in defective utilization of afferent feedback inputs, (Dietz and Colombo, 1998) necessitating augmented feedback (Hwang et al., 2012).

One could divide the domains of research associated with PD-Gait into two. Firstly, the one related to the cure and management of PD, where one aims to develop solutions to manage or cure the disease. The second one is associated with understanding the disorder, where one seeks to discover the underlying mechanisms linked to FoG. There is no permanent cure for PD. Current therapies include medications (e.g., Levo-Dopa) and Deep Brain Stimulation (DBS) (Gilat et al., 2018b; Marsden and Parkes, 1977; Breit, Schulz and Benabid, 2004; Anidi et al., 2018; Syrkin-Nikolau et al., 2017). However, freezing pathology is often resistant

to pharmacological and surgical interventions, thus emphasizing a need to develop alternative strategies to help people avoid freezing in daily life (Nonnekes et al., 2015). Cueing strategies (augmented feedback Hwang et al., 2012) form one of the most non-invasive and effective management options available to the patients affected with for stabilising (Nonnekes et al., 2015; Rubinstein, Giladi and Hausdorff, 2002; Dean et al., 2020) and, potentially delaying onset (Gilat et al., 2018b). However, it is not practical for users to continuously listen to sensory cues and focus their attention on walking as sensory systems such as vision are required for other functions such as route planning and avoiding hazards. This poses a potential requirement for predicting the possible onset of such that the total time of application of the sensory feedback is minimum. The pathophysiology of is not yet conclusively established, and further neurophysiological and biomechanical explanations related to are to be sought. While a set of correlations between the neural inputs (e.g. dysfunction of visuomotor and occipito-parietal pathways) and bio-mechanical variables (e.g. gait pattern generation) of have been studied (Heremans, Nieuwboer and Vercruysse, 2013a), its causality is not well established. Apart from freezing, abnormal gait patterns in PD consist of high stride time variability with less reduction in stride length (Heremans, Nieuwboer and Vercruysse, 2013a). The relationship between the abnormal gait patterns and freezing is also not well understood.

Detection and prediction of freezing have been attempted using kinematic and electrophysiological data extracted using wearable sensors such as electrocardiograph, skin conductance device, and accelerometer (Mazilu et al., 2015; Pham et al., 2017; Pardoel et al., 2019). These methodologies do not use kinetic data, which could have subtleties related to the loading and unloading dynamics, necessitating further exploration. Additionally, methods that use pre-/ based classification (Mazilu et al., 2013) may not be accurate, as the stream of data could contain a combination of and pre- states. The techniques involving multiple sensors such as EEG and accelerometer are often inconvenient from the perspective of personalized daily use. This, therefore, necessitates the exploration of other sensor modalities.

Mathematical modelling of normal gait has been around for quite some

time (McGeer et al., 1990), yet, to the best of our knowledge, modelling in PD has only been attempted recently in literature (Muralidharan et al., 2018). The study of bipedal gait historically has been along two lines: firstly, to build machines that mimic human or animal locomotion and secondly, to understand the biological underpinnings of locomotion. While there are several commonalities between these two approaches, such as understanding the stability of gait and bifurcations, there are stark contrasts. For example, physiologically relevant gait models aim to reproduce pathological gait and relate to the experimental motor-control and human-gait literature. However, models built for robotics can deviate from the experimental motor control literature focusing more on developing a stable and robust walking system, rather than understanding and reproducing the pathophysiology of human gait.

Mathematical models of passive gait have been studied extensively by several researchers to understand their stability and different bifurcations present in their governing equations (Goswami, Thuilot and Espiau, 1996a; Manchester et al., 2011; Dai and Tedrake, 2013; Sadeghian and Barkhordari, 2020; Iqbal et al., 2014; Fathizadeh, Taghvaei and Mohammadi, 2018; Mahmoodi, Ransing and Friswell, 2013; Znegui, Gritli and Belghith, 2020; Fathizadeh, Mohammadi and Taghvaei, 2019). In McGeer et al., 1990 the effect of environmental condition ramp on stability was addressed. Impulsive dissipation at heel strike is studied for a multidimensional biped model in Ros et al., 2015. There are other motor control models where minimization of a cost functional is used for the control of motor action, or for parameter extraction, from the motor control data (Dorschky et al., 2019; Pekarek, Ames and Marsden, 2007; Flash and Hogan, 1985; Parakkal Unni et al., 2017; Delp et al., 2007). These models are not sufficient to understand human locomotion in PD patients, as these papers have focused on generating stable periodic behaviour and its control. They do not address explicitly how the external stimuli result in high variability, and freezing observed in PD-Gait (Heremans, Nieuwboer and Vercruysse, 2013a).

On the other hand, general biophysical models of gait such as the ones proposed in (Taga, 1995; Aoi et al., 2010) considers the interaction with the Central

Pattern Generators (CPG). The aim of these models are primarily to demonstrate walking as a stable limit cycle that emerges from the dynamic interaction between neural oscillation originating in CPG and the pendulum oscillation of body linkages, rather than involuntary stoppage of gait and variability. CPG-based model, proposed in Aoi et al., 2010 and Taga, 1995 depends on multiple parameters such as the strength of neural connections, the magnitude of the coefficients in the rhythmic force controller, and strength of sensory inputs, to yield a desired locomotor pattern. The dependency on an excessive number of intricate and sensitive parameters become a stumbling block in the adaptability of the model for wider generic use. To identify and tune such parameters for attaining involuntary freezing and variability of gait behaviour for a wider population of patients is rather an arduous trial-and-error or learning and optimization based task. Involuntary stoppage of gait and variability are the two key aspects that a model needs to exhibit to be considered as a PD-Gait model. The model by Muralidharan et al., 2018 make use of the neural dynamics of basal ganglia (BG) but does not focus on the mechanics of movement. A model combining the Lorentz system with the passive dynamic walker by Montazeri Moghadam et al., 2018 do not model . Their model combines the bipedal walking mechanics with a chaotic system to generate variability. This makes it less relevant biophysically. In Sarbaz et al., 2012, a 'sine circle map' based discrete model is proposed, and this model exhibits the variability in PD-Gait. However, the biophysical meaning of this map-based model is difficult to ascertain. The motivation here is to develop a model which exhibits and variability in PD-Gait while addressing the mechanical and neurophysiological aspects of the gait pathophysiology. Though there exist vast literature using mathematical models to understand the effect of sensory feedback on normal gait (Taga, 1995; Aoi and Tsuchiya, 2006; Tamura et al., 2020) there is a need for further mathematical modelling research looking into how FoG relates to feedback.

Aim: The overall aim of the thesis is to develop mathematical explanations of the underpinnings of PD-Gait and design machine-learning-based tools striving to improve the sensory cue-based management of FoG. The biophysical modelling

aims to explain the attributes of PD-Gait such as variability, freezing, 'reduction in step size before a freeze' and the effect of proprioceptive feedback. Modelling also attempts to address the role of phase, its synchronisation against feedback, and the desynchronisation on FoG. Ultimately, the object is to develop a modular system to study phase perturbations due to feedback and higher-level neuronal control.

In the data analysis front, the aim is to develop a machine learning-based solution for the real-time prediction of FoG in PD-Gait using stepping time series data. The analysis seeks to develop a real-time application to be used in the future with sensory and auditory cueing.

1.1 Approach

In this thesis, force-plate based measurements and machine learning ideas have been used to predict FoG. This prediction is aimed to be one with the potential to be used with sensory cues to prevent freezing of gait. Secondly, simple lower-order mathematical models have been proposed which effectively show FoG and variability common in people affected with PD. The mathematical model also explains the effect of feedback and external inputs on gait. The word model is used in this thesis in the most general sense. In the context of machine learning, the word *model* is used to represent the ML algorithm after fitting to data. In the biophysical approach, *models* represent the equations that are used to describe the biophysics.

Data analysis approach: Freezing of gait (FoG) is often resistant to pharmacological interventions. The prediction of freezing events might optimize novel treatment options that make use of auditory or sensory cues. These predictions can help trigger external sensory cues when walking behaviour is changed to indicate an impending freeze. Therefore, these predictions could help deliver cues when the user needs them the most rather than continuously providing cue information, improving walking performance less obtrusively. A data-driven approach is proposed for predicting freezing events using three different machine learning algorithms - Random Forrest (RF), Neural Network (NN), and Naive Bayes (NB) classifiers. Data from a force platform were collected from a set of patients affected with PD as they stepped

in place for the analysis. The performance scores of RF/NN/NB based algorithms were computed for different size of inputs to the machine learning algorithm and how early the freezing event is predicted. Moreover, the system's real-time-performance capability is demonstrated, and the ability to control sensitivity and specificity in FoG prediction by way of combining the ensemble of ML models is also tested. The algorithm's real-time performance capability is achieved by ensuring the algorithm uses only a window of data *before* the target data for prediction. Furthermore, the time that the algorithm takes for prediction is negligible (compared to the gait cycle and how early the algorithm could make predictions).

Modelling approach: Physiologically relevant mathematical modelling is used for explaining the underpinnings of the PD-Gait and the abnormal characteristics associated with it. Specifically, modelling aims to understand the underlying mechanism of freezing, high variability and the effect of feedback on the PD-Gait. The modelling is accomplished in three stages. Firstly, a simple inverted pendulum based, hybrid mathematical model under ankle push-off forcing is built and is tested for its ability to explain FoG and variability in PD-Gait as a function of model parameters, specifically the phase difference between the opposing forces. Secondly, the model is extended to include CPG oscillators, where the phase difference between the opposing forces naturally emerge. This model is tested for its capacity to explain the effect of feedback and external inputs on gait and the transition of PD-Gait from walking to freezing and vice-versa. Thirdly, a discrete phase reset curve (PRC) based model is built simultaneously, generalizing and simplifying the previous modelling approaches. This is accomplished through abstracting away the perturbations on the CPG oscillators using PRC functions. The capability of the model to test multiple PRC functions representing different characteristics of the neuronal system against perturbation is also evaluated.

1.2 Contribution

Specifically, this work makes the following contributions:

Data analysis contributions: A machine learning-based approach is proposed to predict freezing events from force data collected from the people affected with PD while they stepped in place. This 'Kinetic' data is used in such a way that can be used for real-time prediction. A systematic analysis is carried out to determine how the performance changes for different windowing parameters characterising the training data.

Research outcomes:

- *M. Parakkal Unni, P. P. Menon, L. Livi, M. R. Wilson, W. R. Young, H. M. Bronte-Stewart and K. Tsaneva-Atanasova (2020a). 'Data-Driven Prediction of Freezing of Gait Events From Stepping Data'. In:Frontiers in Medical Technology, p. 13.*

Modelling contributions: In this thesis, a novel hybrid dynamical model has been proposed to explain FoG and high variability in PD-Gait. Subsequently, this model is extended using the ideas of the CPG oscillators to explain the effect of feedback, external inputs representing augmented feedback and transitions from freezing to walking and vice versa. Finally, the mathematical description of the PD-Gait is further generalized to a discrete system by abstracting away the role of the CPG, higher-level neural control and sensory feedback using the concept of phase reset curves. The discrete model, apart from explaining the characteristics of PD-Gait, is highly extensible to test different neuromechanical hypotheses associated with PD-Gait.

Research outcomes:

- *M. Parakkal Unni, P. P. Menon, M. R. Wilson and K. Tsaneva-Atanasova (2020c). 'Ankle Push-Off Based Mathematical Model for Freezing of Gait in Parkinson's Disease'. In:Frontiers in Bioengineering and Biotechnology, p. 1197.*

- *M. Parakkal Unni, P. P. Menon. 'Modeling and Analysis of Parkinsonian Gait' In:Nonlinear Dynamics (In Review).*

1.3 Thesis Organization

Chapter 2 starts by providing the general background of the motor control physiology, pathology of PD, focusing specifically on FoG. As part of FoG pathology, a summary of connections governing gait is described, along with a description of the current understanding of PD-Gait and its treatment options. Successively, the prior literature on the data analysis for FoG prediction and the mathematical models governing FoG is provided, focusing on CPG based walking models, gait models in robotics and how motor redundancy is addressed in different fields. The chapter ends with a description of dynamical system models and the role of phase and phase response curves in neuro-mechanical models.

Chapter 3 addresses one of the problems posed in the introduction, namely the prediction of freezing of gait using stepping data to aid the treatment methodologies that use augmented feedback. The chapter describes the methodology used for developing a machine learning algorithm for predicting freezing from the stepping data, a cross-validation procedure, a real-time demonstration of the algorithm and the performance scores.

Chapter 4 develops a mathematical model of FoG based on the ankle push-off forces acting on the stance legs, where the stance leg is modelled as an inverted pendulum. This model forms the preliminary framework to understand PD-Gait mainly from the limb mechanics perspective. Here, a mathematical model and a map governing the PD-Gait is prescribed and analysed to show characteristics of PD-Gait, such as variability, 'reduction in step length' before a freeze and freezing.

Chapter 5 provides a generalised version of the ankle push-off model extending the simple model developed in chapter 4, using oscillators, phenomenologically representing the CPG controllers. The effect of augmented feedback on gait is demonstrated and analysed to understand its frequency-dependent behaviour. The chapter also analyses the parameters governing the neural control to understand its

effect on the freezing fraction and variability.

Chapter 6 further generalises the FoG modelling using a discrete map-based model. The oscillator dynamics governing the PD-Gait are accommodated in this model in a PRC function. The PRC function also implicitly models the effect of augmented feedback. The model is analysed to show the high variability, chaos and freezing in PD-Gait. This model has the advantage of being modular, where one could replace the PRC function with another experimentally obtained PRC function to understand its effect on gait. Moreover, the relatively simpler nature of the model permits the use of this model in systems with lower computational capabilities.

2. Background - Physiology of Gait and Pathophysiology of FoG

Movement is the crucial aspect of physiology that differentiates animals from plants, making motor physiology one of the most critical aspects of animal biology. Human motor control is hierarchical (Grillner, 2003) with the control flowing from brain through spinal-cord to the limbs and the sensory information flowing the other way around as shown in Fig 2.1. Gait is shown in the Fig. 2.1 as an example of motor control. The brain (basal ganglia, cortical and subcortical areas) control the spinal cord central pattern generators (CPG) which in turn control motor control physiology (e.g. gait).

CPG are neuronal circuits that can generate rhythmic motor patterns in the absence of sensory inputs (Grillner, 2021) - a structure which is still not fully understood (Grillner, 2021). While CPG produces the underlying motor pattern the higher brain areas and sensory inputs control the timings, and the magnitude of the activations (Büschges, 2005)

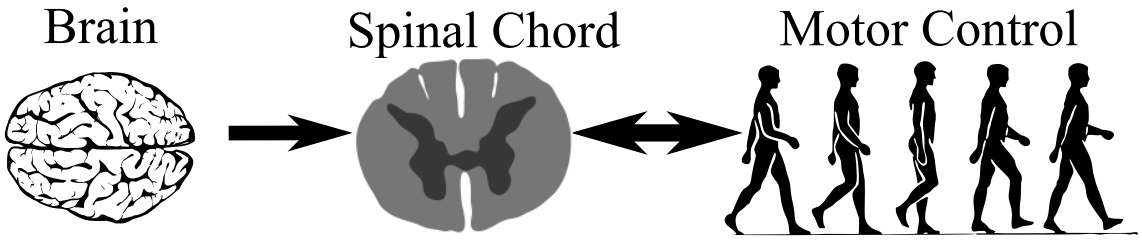

Figure 2.1: Hierarchy of the motor control in general is depicted.

The pathophysiology relevant to PD-Gait and physiology of gait is described in the coming sections in this chapter. The control of bipedal gait is highly complex at the level of the brain, which gets simpler at the level of the spinal cord and limb

dynamics. The system's complexity increases as one moves from the lower level structures (e.g. limbs and CPG) to higher-level structures (e.g. cortex, subcortical structures and brain stem). This hierarchy is described in the following sections starting from 2.1 essentially delineating how several structures converge to CPG and motor neurons (MN). A bottom-up approach is chosen for the modelling of gait by several authors (Taga, 1995; Aoi et al., 2019), and a similar strategy for modelling PD-Gait in this work. In this bottom-up approach, first, the lower limb kinetics relevant to PD-Gait is modelled. Successively, the model is extended into a CPG based control of lower limb kinetics. This approach has the potential to investigate different mechanisms that lead to PD-Gait. Moreover, the models developed this way could be modified further as more findings on the higher structures emerge.

2.1 Physiology of Walking and Pathology of FoG

Understanding the physiology of gait is paramount to understanding the pathophysiology of FoG. This section aims to shed light on the physiology and pathophysiology of gait and related anatomical structures relevant to FoG. FoG is also seen in diseases such as progressive supranuclear palsy, multiple system atrophy, and vascular parkinsonism (Factor, 2008; Gurevich and Giladi, 2003). In the case of PD, while the basal ganglia (BG) and the related dynamics explain the PD pathology, the lower structures determine how it reflects in PD-Gait. Fig. 2.2 shows the elaborate connections between different regions of the brain ending in motor neurons (MN). The nodes with high degree-centrality have been used to scale the size of the nodes.

At the lowest level, the gait is believed to be controlled by CPG, however, this is debatable (Minassian et al., 2017). In the current section, the focus is on the connectivity and physiology of subcortical and brain stem structures and their relation to the CPG in the spinal cord.

Anatomically positioned below the BG, various areas in the brain stem play their own critical roles in the physiology of walking as well as FoG via their inputs to the CPGs, either directly or indirectly via intermediate areas. As shown in Fig. 2.2, the areas include the Nucleus reticularis gigantocellularis (NRGc), Nucleus reticularis

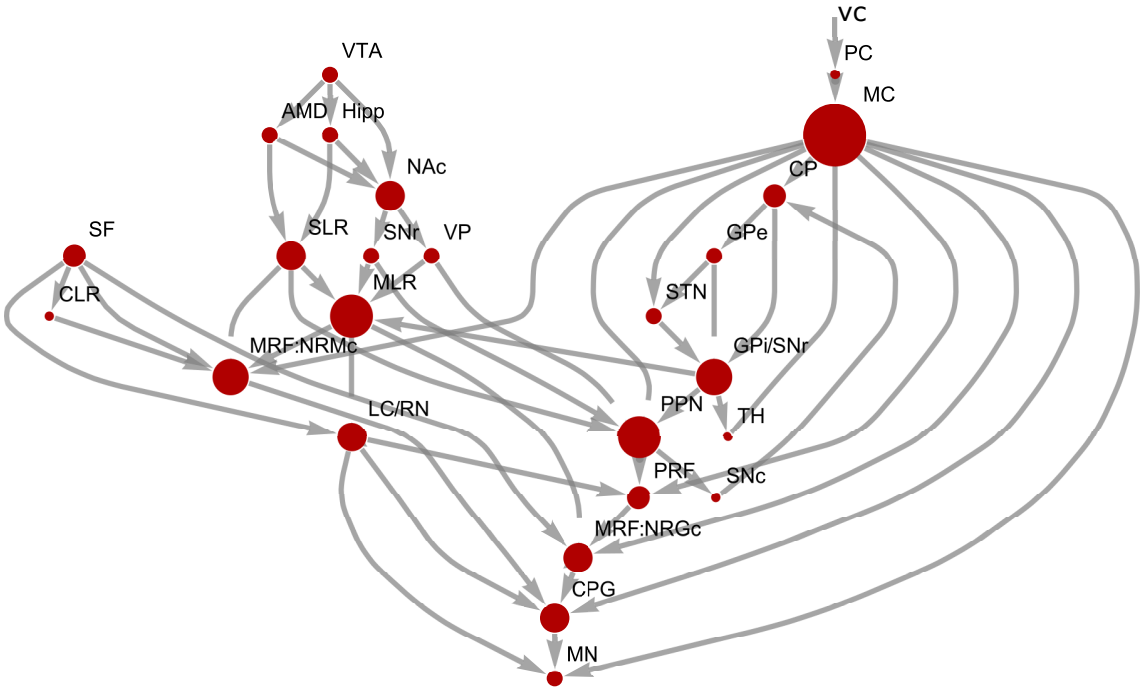

CPG	Central pattern generators	NAc	Nucleus accumbens
MN	Motor neurons	Hipp	Hippocampus
MRF	Midbrain reticular formation	VTA	Ventral tegmental area
NRMc	Nucleus reticularis magnocellularis	VP	Ventral pallidus
NRGc	Nucleus reticularis gigantocellularis	CLR	Cerebellar locomotor region
LC	Locus coeruleus	SF	Sensory feedback
RN	Raphe nuclei	GPi	Globus pallidus internus
PRF	Pontine reticular formation	GPe	Globus pallidus externus
PPN	Pedunculopontine nucleus	STN	Subthalamic nucleus
SNr	Substantia nigra pars reticulata	CP	Caudate Putamen
MLR	Mesencephalic locomotor region	SNc	Substantia nigral pars compacta
SLR	Subthalamic locomotor region	MC	Motor cortex
AMD	Amygdala	VC	Visual cortex
PC	Parietal cortex		

Figure 2.2: Physiology of walking. The size of the nodes represent the degree centralities associated with the nodes.

magnocellulari (NRMc), Locus coeruleus (LC)/Raphe nuclei (RN) and Corticospinal tract (from motorcortex). CPG, which control the limbs, are affected by the inputs from NRGc, NRMc, LC/RN and Corticospinal tract (from motor cortex). Inhibitory NRGc input is modulated by the Pontine reticular formation (PRF) regulated by Pedunculopontine nucleus PPN. PPN, an area that controls posture and regulates muscle tone, receives projections from Globus pallidus internus and Substantia nigra pars reticulata (GPi and SNr), the input to which is defective in PD. Moreover, one could hypothesise that the MRF inputs (midbrain reticular formation, which consists of NRGc and NRMc) and LC/RN regulate CPG neurons (Lemieux and Bretzner, 2019) changing their behaviour against perturbations.

Neuro-mechanical control of bipedal walking can be classified into two. The first one corresponding to mechanical walking without any adjustments to external inputs or perturbations such as auditory or visual proprioceptive inputs and the second one correlates with walking whilst adjusting to external demands/inputs which require refined movements, learning and sensory integration. Even though this categorisation helps to understand the physiology better, the roles of the regions corresponding to mechanical walking and the one corresponding to refined movements are not fully demarcated. Experiments on decerebrate animals have shown that stimulation of mesencephalic locomotor region (MLR) is sufficient to elicit locomotion despite its 'machine-like' nature Snijders et al., 2016. Subthalamic locomotor region (SLR) connections to MLR are believed to be playing the role of postural and equilibrium control. Even though debatable, PPN and the adjacent areas such as the cuneiform nucleus (CN) and the subcuneiform nucleus form the MLR (Alam, Schwabe and Krauss, 2011). Neurons of the PPN region with its connection towards several areas in the brain, such as BG, limbic areas, thalamus, brain stem, spinal cord, and cerebellum, make the different regions' functional understanding quite difficult. PPN neurons suppress the muscle tone and also has a role in modulating locomotion. Loops from motor cortical areas to BG and cerebellum, believed to play a role in the adaptive control of locomotion (Takakusaki, 2013). BG controls locomotion through GABAergic SNr outputs, and these outputs are affected in

PD. SNr has connections to MLR. Lateral SNr blocks PPN induced suppression of muscle tone, and medial SNr suppresses locomotion induced by MLR. The excessive inhibition of the MLR through SNr in PD might cause the gait symptoms in PD (Snijders et al., 2016). Supplementary motor area (SMA) and premotor area (PM) are believed to involve movement initiation where finer control is necessary. Furthermore, Sergei et al.'s study on cat lesions has revealed the role of pyramidal tract neurons (PTNs) in the motor cortex in anticipatory postural adjustments (Yakovenko and Drew, 2009). The role of proprioception in human gait is well established (Frost et al., 2015). Ian Waterman's case study illustrates this point accurately, where he lost the sensory perception from the neck down due to a rare autoimmune disorder. Even though he could contract his muscles, he lost control of his movements, including his gait. This difficulty in coordinating gait could be attributed almost entirely to feedback or proprioception (Tuthill and Azim, 2018). Ankle proprioceptive feedback is affected in the case of people affected with PD (Khudados, Cody and O'Boyle, 1999; Klockgether et al., 1995; Rickards and Cody, 1997). Dysfunction of the affected ankle proprioceptive feedback seems to contribute to the gait abnormalities (Teasdale, Preston and Waddington, 2017; Khudados, Cody and O'Boyle, 1999). As the actual sensory signal is believed to be unaffected in PD, the effect of the proprioceptive signal on the motor circuit is assumed to be affected (Khudados, Cody and O'Boyle, 1999). BG neurons are shown to respond to the passive and active movements of the limbs (Konczak et al., 2009). However, studies in monkeys treated with MPTP (1-methyl-4-phenyl-1,2,3,6-tetrahydropyridine) to induce parkinsonian show a reduction of BG specificity against sensory inputs, this lack of specificity to sensory inputs affects proprioception (Konczak et al., 2009). The motor neurons from the spinal cord innervate muscles of the lower limbs causing muscle contraction and successively resulting in bipedal gait. Abnormalities such as premature activation of plantar flexors have been shown to accompany a freezing episode in EMG studies by Nieuwboer et al., 2004. The muscles that can help in plantar flexion are gastrocnemius, peroneus longus and soleus (Duysens et al., 1990; Sammarco, 1995). Moreover, during horizontal walking, most of the energy is spent

on lifting the body against gravity, and the ankle muscles accomplish this during plantar flexion. Therefore plantar flexors form a crucial set of muscles for PD-Gait modelling.

The general aspects of motor physiology are described in Appendix A.1, the physiology of basal ganglia in Appendix A.2 and the pharmacological and surgical interventions used in PD in Appendix A.3.

In summary, the cortical inputs to BG and brain stem regions play a significant role in locomotor control. The role of feedback from limbs to CPG, and the effect of stimulation of PPN are key aspects relevant to the future sections of the thesis.

3. Background - Data Analysis and Modelling for FoG

This chapter provides the relevant background to the data analysis for FoG prediction and biophysical mathematical modelling of FoG. The section on the biophysical modelling also briefly covers the general mathematical models of gait relevant to human motor physiology.

3.1 Data driven prediction of freezing

In recent years, there has been much interest in developing novel and practical algorithms for the detection and prediction of FoG by making use of the physiological data. Two main areas of focus are (1) detection of FoG episodes from the time series data collected over a finite duration of time after it has happened (2) prediction (forecasting) of imminent FoG episode using physiological time series data gathered over a finite duration of time.

While there are several studies (Pardoel et al., 2019) on the detection front, the prediction studies are rather limited (Pardoel et al., 2019; Mazilu et al., 2015; Pham et al., 2017). Typically, kinematic measurements using sensors such as accelerometer, gyroscope are used by authors (Pardoel et al., 2019) for detection and prediction of FoG. There is also a prevalence of the use of measurements of EEG (electroencephalogram), EMG (electromyogram), GSR (galvanic skin response) for FoG detection, for example by (Handojoseno et al., 2012), (Cole, Roy and Nawab, 2011) and (Mazilu et al., 2015) respectively.

There are very few research studies reported as of today that present results

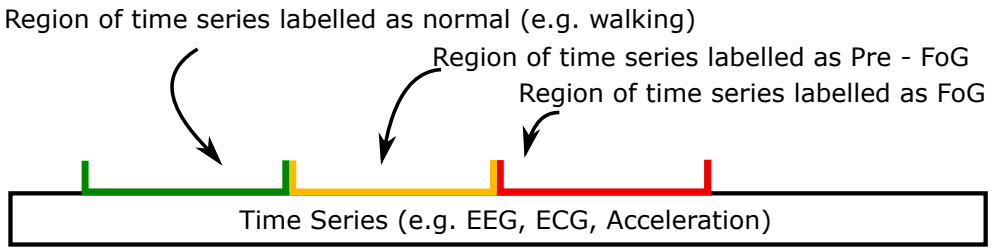

Figure 3.1: Illustration of FoG and pre-FoG. The black square represents an arbitrary time series. The red, yellow and green regions represent part of the time series labelled as FoG, pre-FoG and normal region. The yellow region always precedes an FoG labelled red region.

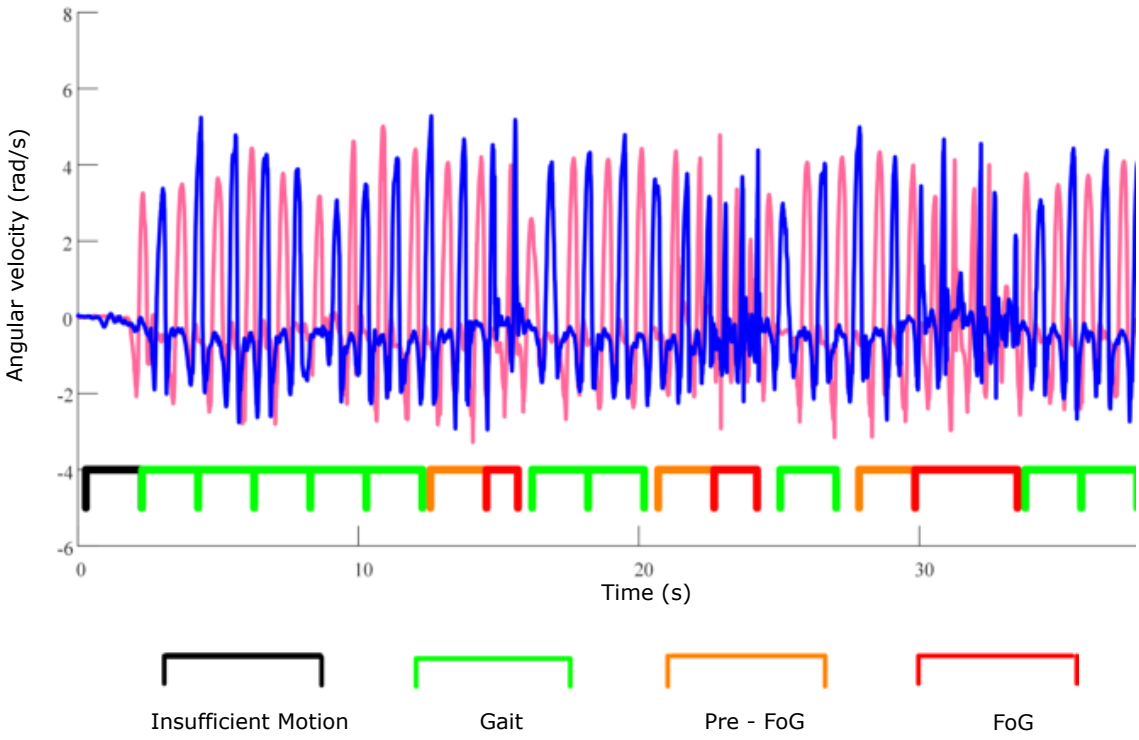

Figure 3.2: The figure shows the angular velocities of the sensors on the left (red) and right (blue) ankles. The segmentation of the data into Insufficient motion, Gait, pre-FoG and FoG are indicated. This is an example to illustrate the literature on pre-FoG/FoG classification. *This figure is adapted from (Palmerini et al., 2017) with permission.* Only a subset of approximately 70 s time-series data from (Palmerini et al., 2017) is depicted here, as this is only for the illustration of data segmentation methods used in previous literature.

on predicting or forecasting FoG using physiological time series. A typical strategy used in the FoG prediction is by converting the problem into a classification problem by segmenting the data into pre-FoG/FoG (Borzì et al., 2021; Arami et al., 2019). The data-segmenting involves partitioning the data into (a) pre-FoG, (b) FoG, and (c) normal where FoG is the time series duration where freezing happens, pre-FoG is the data before the freezing episode for a pre-defined period (e.g. 1 s to 11 s in Mazilu et al., 2013) and normal is the data which is neither FoG nor pre-FoG. In this framework, the two-class classification problem of classifying FoG from every other kind is considered FoG *detection* and the three-class classification problem of classifying data into pre-FoG, FoG and normal is considered as *prediction*. An illustration of the segmentation of the data into pre-FoG and FoG in a general time series is illustrated in Fig. 3.1, and an example of the same adapted from Palmerini et al., 2017 is given in Fig. 3.2. In the particular case of Palmerini et al., 2017 the data segmentation is done on the angular velocity measured in rad. s^{-1}. Mazilu et al., 2013 has developed a decision tree classifier for pre-FoG, FoG, and normal-locomotion classification with an F1-score of 0.56 for FoG prediction.

In Mazilu et al., 2015 their previous work has been extended using skin conductance and ECG measurements with a prediction using multivariate Gaussian model resulted in an accuracy of 71.3%. The accuracy is calculated in this work by computing the fraction of freezing episodes predicted out of the total number of 184 freezing events. Handojoseno et al., 2014 work of EEG based FoG prediction used a multilayer perceptron (MLP) with Fourier and Wavelet-based features and other nonlinear univariate and bivariate features. They also showed that theta oscillations in the human cortex increase during transition to freezing and during freezing, consistent with the earlier studies which suggest a relationship between FoG and motor planning impairments (Knobl, Kielstra and Almeida, 2012). This was later extended using Bayesian neural nets in Gilat et al., 2018a. The study by Palmerini et al., 2017 that tried to identify a common evident pattern coming prior to the occurrence of FoG is done using linear discriminant analysis to differentiate pre-FoG from normal gait. In addition to predicting FoG, a reduction in the symmetry between the limbs before

a freeze is demonstrated in Palmerini et al., 2017, making the work physiologically very interesting. They also show high-frequency movement before a freeze, thereby posing questions for mechanistic explanations. Moreover, several authors recently have tried using neural nets for the prediction of FoG (Torvi, Bhattacharya and Chakraborty, 2018; Zia et al., 2016). More recently, pre-FoG detection work using machine learning by Borzì et al., 2021 show that dopaminergic therapy affects the pre-FoG gait patterns. More recently, a random forest-based classifier with an orthogonal experimental design has been used for the pre-FoG/FoG/normal classification using a random forest algorithm and a set of signals (accelerometer, gyroscope and magnetometer) generated from an inertial measurement unit (IMU; BMI160, Bosch, Germany) at 100 HzChen et al., 2021. Furthermore, there has been other explorations on pre-FoG/FoG/Normal classification using other machine learning approaches such as support vector machines, gradient boosting and naive Bayes classifiers using accelerometer data set Orphanidou et al., 2018.

The FoG prediction literature (Mazilu et al., 2013; Mazilu et al., 2015; Handojoseno et al., 2014; Borzì et al., 2021) focuses on segmenting the data into pre-FoG, FoG and normal states. One drawback with this classification is that in a real-time prediction scenario, the window of data used for prediction at a given time can contain a combination of these states. For example, the data may contain a walking region and transition to a freeze (pre-FoG) region. Here, an algorithm trained using the three-state classifications may not be suitable as it has not been trained in combinations of the states. This three-class classification scheme also will be affected by the offset between the windows used for sampling the data before being fed to the prediction algorithm. Furthermore, even though the sensing modalities such as EEG, accelerometers, skin conductances, ECG are explored in literature, there is a need to explore sensing modalities that make kinetic measurements such as force-plates.

3.1.1 Sensory cues for managing PD

As defined by Konczak et al., 2009 proprioception is 'unconscious processing of proprioceptive signals used for reflexive and postural motor control'. The definition encompasses both the sense of limb position and limb movement. This definition is adopted for proprioception throughout this thesis. In other words, proprioception forms the 'feedback' that one uses for executing motor functions. However, one could note that there are alternative definitions where one separates the position sense from the sense of movement (Konczak et al., 2009). Proprioceptive feedback is affected in PD, and the management options of PD focus on providing sensory and auditory cues and augmented feedback (Hwang et al., 2012; Nonnekes et al., 2015; Nieuwboer, 2015) to manage FoG. There are two main types of cueing strategies that one could adopt: (1) open-loop cueing (2) closed-loop cueing. In open-loop cueing, the strategy is to supply sensory cues in a preset manner independent of the user performance (Muthukrishnan et al., 2019). On the other hand, closed-loop cueing depends on the users' gait performance (Muthukrishnan et al., 2019).

One hypothesis of action of the cues on PD-Gait is by increasing cortical activation, thereby reducing the pathological basal ganglia activity (Muthukrishnan et al., 2019). Moreover, it is hypothesised that an alternative pathway involving the cerebellum, sensorimotor cortex, and lateral premotor cortex is activated in the process of compensating for BG deterioration (El-Tamawy, Darwish and Khallaf, 2012). Furthermore, the augmented proprioceptive feedback also could be compensating for the reduced proprioception in PD. However, the exact mechanism of action of these cues is still subject of research (Ginis et al., 2018).

Several cueing strategies (e.g., auditory and visual) exist that often induce clear benefits in terms of stabilizing gait (Nonnekes et al., 2015; Rubinstein, Giladi and Hausdorff, 2002; Dean et al., 2020) and, potentially delaying the FoG onset (Gilat et al., 2018b). However, it is not practical for users to continuously listen to sensory cues and focus their attention on walking as sensory systems such as vision are required for other functions such as route planning and avoiding hazards. Therefore, a more efficient strategy would be to initiate the sensory cues only at times when the

user needs them most (i.e., at a time when they are about to freeze). Understanding the behavioural factors that are predictive of upcoming freeze events could help to progress our understanding of underlying neurophysiological mechanisms that cause and exacerbate freezing. While there are several recent contributions applying machine learning to Parkinsonian tremors (Livi, Sadeghian and Sadeghian, 2016) and gait analysis (Frohlich et al., 2017) as well as the freezing of gait detection (Pham et al., 2017; Amini, Banitsas and Young, 2019), to our knowledge, no work has used measurements of stepping actions, i.e. using kinetic data alone, to predict an upcoming freezing event.

3.2 Mathematical Modelling of FoG

Gait has been studied fundamentally from two different perspectives. One approach is robotics and control, and the second is biophysical. In the area of PD-Gait, only a few studies are available in the literature. The model of PD-Gait by Muralidharan et al., 2014 successfully captures the neural dynamics of basal ganglia (BG) but does not focus on the mechanics. A recent model which combines the chaotic region of the Lorentz system with the passive dynamic walker is provided by Montazeri Moghadam et al., 2018. In this model, chaos is added externally, making it less relevant biophysically. As chaos is known to be absent in the basal ganglia (BG) in PD state (Mandali et al., 2015) the neuromechanical interactions need to be studied to find out the underpinnings of the variability in PD-Gait.

Forthcoming sections explain the modelling of gait in human motor control and robotics from different perspectives.

3.2.1 Central Pattern generators and its relevance to PD-Gait

Central pattern generators (CPG), typically argued to be fundamental to most rhythmic behaviours, are a group of neurons with interconnections that generates a fictive motor pattern when appropriately activated. CPG is used to drive the

Source	Methodology	Results	Limitations
(Muralidharan et al., 2018)	ODE and RL based model of BG & CPG.	Explanation of PD-Gait characteristics such as step length reduction and variability.	No FoG and hybrid nature of walking. Inadequate kinetic aspects of the PD-Gait.
(Montazeri Moghadam et al., 2018)	Rigid body dynamics of the limbs. Externally added chaos through logistic map and Lorenz system.	Explains the PD-Gait variability	The biophysical meaning is difficult to ascertain . Absence of FoG. No neuronal controller.
(Sarbaz et al., 2012)	Discrete map based model	Simple model and easier to be used with the data.	The biophysical meaning is difficult to ascertain. FoG is absent
(Goswami, Thuilot and Espiau, 1996a; Manchester et al., 2011; Dai and Tedrake, 2013; Sadeghian and Barkhordari, 2020; Iqbal et al., 2014; Fathizadeh, Taghvaei and Mohammadi, 2018; Mahmoodi, Ransing and Friswell, 2013; Znegui, Gritli and Belghith, 2020; Fathizadeh, Mohammadi and Taghvaei, 2019)	Rigid body mechanics. Passive gait is modelled.	Explains passive gait and stability, highly relevant to robotics. Plausibly passive gait is disturbed in PD.	Not directly relevant to PD. Do not explain the mechanism of human gait, CPG, variability in PD-Gait or FoG
(Aoi and Tsuchiya, 2006; Aoi et al., 2010; Aoi et al., 2019)	ODE based model of CPG and Rigid body mechanics. Muscle synergy hypothesis is implicitly employed.	Explains the normal gait controlled by the CPG.	Not directly relevant to PD-Gait. Do not explain the pathophysiology in PD-Gait or FoG.

Table 3.1: A summary of gait literature relevant to PD.

mechanical systems in several models of human locomotion. CPG based gait models assume that the CPG receive feedback (perturbations) from the sensory system (or indirectly get modulated by the brain) such that the overall system consisting of the CPG and rigid-bodies representing the limbs are synchronised (Yamasaki, Nomura and Sato, 2003). Yamasaki et al. in (Yamasaki, Nomura and Sato, 2003) take a control systems-based approach to the problem using a simple model for the CPG. Their model also uses an IDM (inverse dynamics model) module, the physiological correlates of which is assumed or speculated to be in the cerebellum. In Aoi et al., 2010 the authors have made the model more physiologically relevant using the experimental findings from Ivanenko, Poppele and Lacquaniti, 2004. There are two difficulties associated with using these models for understanding freezing, (1) a large number of parameters, resulting in a scenario where identifying the cause of freezing becomes difficult (2) the use of dimensionality reduction based approximations, resulting in a model, which explains the normal behaviour well but can not be directly extended to pathological scenarios such as freezing. While Aoi et al.'s model is an excellent candidate for understanding normal walking, it is challenging to use such a model for understanding FoG. This difficulty is because of many tuned parameters and the difficulty of judging which component's failure caused FoG. Also, the muscle synergy and factor analysis based approximations may not be valid in a pathological scenario as these approaches focus on normal walking scenarios. Sensory feedback to the brain and CPG are crucial aspects of gait addressed in the modelling literature over the years (Taga, 1995; Aoi and Tsuchiya, 2006; Tamura et al., 2020); however, to the best of our knowledge, current literature seem to lack details on how FoG is related to feedback from the limbs. Moreover, how PD-Gait changes from walking to freezing and back also needs a physiologically relevant explanation.

Muscle coordination can be quantified using the *phase* associated with the muscle activation. The activation of muscle is assumed to be controlled by the CPG in the spinal cord. CPG is typically modelled as *limit cycle* oscillators (Ijspeert, 2008). These *limit cycle* oscillators can be 'perturbed' by the sensory inputs from the

legs, or inputs from the brain which could lead to entrainment (Taga, 1994). *Phase reset curves* (PRC) can quantify the effect of such perturbations on the state of the CPG (Izhikevich, 2003) close to its *limit cycle*. The brain stem regions connected to the CPG receive perturbations associated with freezing episodes. As an example, an EEG study by Shine et al., 2014 has revealed abnormal oscillatory activity in the brain associated with a freezing episode. Moreover, a transient inhibitory input from the BG resulting in a decreased activity of brain stem structures is claimed to be causing FoG in Lewis and Shine, 2016. These transient changes affecting brain stem structures (Lewis and Shine, 2016) could induce changes in the PRC characteristics of the CPG neurons. Therefore, a careful study is needed on the different PRC characteristics that induce freezing episodes.

3.2.2 Robotics related models of gait

While studying gait, it is impossible to ignore the robotics literature. The passive gait is the link that connects the robotic literature with the biophysical models as the fundamental difference between the robotic models and the biophysical models lie in the control aspect. McGeer et al.'s early work in passive gait models (McGeer et al., 1990) show the stability and effect of external inputs on passive gait. Several others have also studied the passive gait models and their bifurcations (Goswami, Thuilot and Espiau, 1996a; Manchester et al., 2011; Dai and Tedrake, 2013; Sadeghian and Barkhordari, 2020; Iqbal et al., 2014; Fathizadeh, Taghvaei and Mohammadi, 2018; Mahmoodi, Ransing and Friswell, 2013; Znegui, Gritli and Belghith, 2020; Fathizadeh, Mohammadi and Taghvaei, 2019). The fully actuated bipedal robots are in the other end of the spectrum where typically feedback linearization is used to nullify the 'natural' dynamics of the robot (Gupta and Kumar, 2017). On the other hand, underactuated robots use the 'natural' dynamics of the rigid body system while simultaneously providing some actuation (Gupta and Kumar, 2017). However, these models cannot directly explain PD pathology due to the lack of actuation or actuation's biological nature.

3.2.3 Addressing motor redundancy

Muscles act as the actuators of the neuromuscular system. The aim of neuromechanical modelling is to explain the control scheme used by the brain to achieve normal and pathophysiological motor control. Several muscles act on a joint to achieve motion, thereby increasing the number of actuators relative to the degree of freedom. These redundancies in actuation result in a scenario where there are multiple ways to achieve the same movement. Explaining how the brain chooses the set of muscles for a particular movement is one of the problems in neuromuscular control. Optimal-control formalism addresses this issue to some extent and forms an alternative approach to modelling motor control. This approach assumes a cost-functional (e. g. integral of the jerk), which is minimised during motor action. This is very suitable for robotic applications (Ishihara, Itoh and Morimoto, 2019; Pekarek, Ames and Marsden, 2007). Inverse optimal control can be used to circumvent the assumption of the cost functions, such as minimising jerk or overall torque applied by inferring it from the data. Nevertheless, this necessitates formulating the problem in such a way that there is a cost function that is minimised during a motor action (Rebula et al., 2019; Parakkal Unni et al., 2017; Mombaur, Truong and Laumond, 2010).

The equilibrium point hypothesis (Duan, Allen and Sun, 1997; Feldman, 1986) suggests that the limb movements are the result of active changes in the equilibrium state of the motor system. The equilibrium state is governed by the torque-length characteristics of the motor system. A neural controller can change torque-length characteristics of the muscles to achieve motion. It has been shown that the muscles act synergistically to reduce the variability in the targeted action. For example, the uncontrolled manifold hypothesis by Latash, Scholz and Schöner, 2002 explains the variability in the muscle recruitment as 'good' and 'bad' regions of variability, depending on whether they achieve the targeted action or not. The muscle recruitments that achieve targeted action are considered 'good' regions of variability, whereas the muscle recruitments that do not achieve targeted action are considered 'bad' regions of variability. The Equilibrium point approach (Feldman, 1986) makes the electromyogram (EMG) activity implicit. The empirical determina-

tion of invariant characteristics (Sainburg, 2015) such as torque-length characteristics (Feldman, 1986) is necessary for validating the equilibrium point hypothesis. A way in which it is achieved is by asking the subjects 'not to intervene' (Sainburg, 2015; Feldman, 1986) while doing a task such as unloading, and assuming these result in stabilisation of central commands to muscles (Sainburg, 2015). However, this assumption is not necessarily true, as there could be involuntary responses resulting in muscle contraction. The use of muscle synergies (Latash, 2010) in models is one way to address redundancies. These models assume co-activation of a set of muscles as motor primitives to address the redundancy associated with muscle activation (Aoi et al., 2019; Tamura et al., 2020). The idea of muscle synergy is still debated and is considered difficult to refute or falsify by any empirical evidence (Popper, 2002; Olszewski and Sandroni, 2011) by some authors (Tresch and Jarc, 2009).

3.2.4 Walking is a hybrid system

Hybrid systems are dynamical systems, which exhibit both continuous and discrete dynamics. Walking involves the interaction of continuous differential dynamics governing the limbs and their neural control and discrete dynamics due to the leg's impact on the ground. Naturally, this results in a hybrid dynamical system. The hybrid systems' theory becomes extremely relevant in modelling PD-Gait and studying its orbital stability. While orbital stability of smooth systems have been well studied (Glendinning, 1994) the study of orbital stability of hybrid systems is relatively recent. Hybrid systems can result from combinations of linear or nonlinear differential equations and discrete dynamics. The emerging hybrid dynamical system can show richer dynamics than that offered by the systems individually. Mathematically, there are three aspects to a hybrid system: (1) A set of differential equations defining the smooth flow, (2) a reset surface or surfaces and (3) a map to apply when the trajectory reaches a reset surface or surfaces. Understanding the stability of the hybrid dynamical system is vital to explain its long term behaviour. One approach to studying the stability of the hybrid dynamical system is by using contraction analysis. A non-singular Jacobian is essential to the contraction analysis of the system, which

is based on variational methods of the differential dynamics (Lohmiller and Slotine, 1998; Tang and Manchester, 2014). However, biologically relevant gait models with event-driven feedback can have a singular Jacobian. A general methodology to address the problems arising in hybrid systems is to use Poincare section based techniques such as the one given by Goswami, Thuilot and Espiau, 1996a.

3.2.5 Introduction to Hybrid systems

Hybrid systems are a class of dynamical systems, which exhibit both continuous and discrete dynamics. These systems are often associated with events such as resets or jumps, and switching. A system of ordinary differential equations typically governs the continuous behaviour, and a vector-valued function governs the discrete part. The general hybrid dynamical system is of the form,

$$\dot{z}(t) \;=\; \mathcal{F}(z(t),\lambda),\; z(t)^- \notin \mathcal{S}\;, \tag{3.1}$$

$$z(t)^+ \;=\; \Delta(z(t)^-,\lambda),\; z(t)^- \in \mathcal{S}, \tag{3.2}$$

where $z \in \mathcal{Z}$ represents the state variables and $\mathcal{Z} \subset \mathbb{R}^n$ is the state manifold. In Eq. 3.1, $\mathcal{F}(z(t),\lambda) : \mathcal{Z} \times \Lambda \to \mathbb{R}^n$ is a continuous vector valued function. Further, $\lambda \in \Lambda \subset \mathbb{R}^m$ represents a vector of adjustable constant parameters of the system and Λ characterises a set of admissible parameter values. In this case, $\mathcal{F}(z(t),\lambda) : \mathcal{Z} \times \Lambda \to \mathbb{T}\mathcal{Z}$ is $\mathcal{C}^\infty$ vector field, in which $\mathbb{T}\mathcal{Z}$ is the tangent bundle of state manifold $\mathcal{Z}$. The solution curve of the system is denoted as $\zeta(t, z_0, \lambda)$, such that $z(t) = \zeta(t, z_0, \lambda)$ is the solution at time $t > 0$ of the system with an initial state $z(0) = z_0$ at time $t = 0$.

In hybrid systems, the state can instantaneously reset to a discrete time part according to a $\mathcal{C}^\infty$ reset map $\Delta(z(t)^-,\lambda) : \mathcal{Z} \times \Lambda \to \mathcal{Z}$ in Eq. 3.2.

The *switching surface* is defined as

$$\mathcal{S} := \{\; z(t) \in \mathcal{Z} \;\big|\; g_r(z(t)) = 0 \;\}\;, \tag{3.3}$$

where $g_r(z(t)) : \mathcal{Z} \to \mathbb{R}$ is a $\mathcal{C}^\infty$ real valued switching function, satisfying the

condition $\frac{\partial g_r}{\partial z}(z) \neq 0$. The system with the reset, or so-called impulse effect, brings forth the possibility of the state's jumping (also known as 'resets') when certain boundaries are crossed. In general, these boundaries are subsets of the space, $\mathcal{S} \subset \mathcal{Z}$. The difference between a smooth system and a hybrid one lies in the fact that when the flow $\zeta(t,\ z_0, \lambda)$ reaches the *switching surface* Eq. 3.3, a *reset map* in Eq. 3.2 is applied.

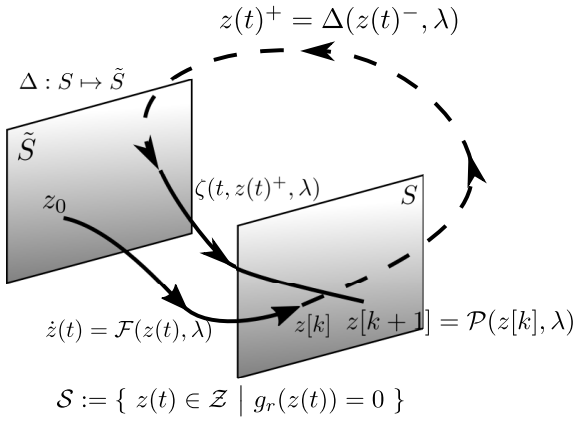

Figure 3.3: Illustration of the trajectory in the hybrid system. The dashed line correspond to the discrete mode dynamics, whereas the solid line corresponds to the continuous part of the hybrid system.

The *time to reset* function is then defined as $T : \mathcal{Z} \times \Lambda \to \mathbb{R}_+$ as the first time at which the continuous part solution $\zeta(t, z_0, \lambda)$ intersects the switching manifold $\mathcal{S}$:

$$T(z_0, \lambda) := \inf\{\ t > 0 \mid \zeta(t, z_0, \lambda) \in \mathcal{S}\ \}\ . \tag{3.4}$$

A *Poincaré map*, which describes the motion of the point of intersection of a differential dynamical system with a lower dimensional subspace traverse to the flow, $P : \mathcal{Z} \times \Lambda \to \mathcal{Z}$, is defined by

$$P(z, \lambda) := \zeta(T(\Delta(z, \lambda), \lambda),\ \Delta(z, \lambda),\ \lambda)\ , \tag{3.5}$$

and describes the evolution of the hybrid model in Eq. 3.1 - Eq. 3.2 on the *switching surface*, $\mathcal{S}$, which is considered as the *Poincaré section* (indicated in Fig. 3.3)

according to a discrete time dynamics

$$z[k+1] = P(z[k], \lambda), \quad k = 0, 1, 2, \cdots \tag{3.6}$$

Typically a periodic orbit is transversal, i.e., not tangent, to the switching manifold $\mathcal{S}$, and the fixed point for the *Poincaré map* in Eq. 3.5 is

$$P(z^*,\ \lambda) = z^*,\ \forall \lambda \in \Lambda. \tag{3.7}$$

In the hybrid walking system described here, a Poincare map may be constructed by choosing the *switching surface* $\mathcal{S}$ as the Poincare section (Wendel and Ames, 2010; Ames, 2014). The discrete dynamics on the *Poincaré section* is defined as follows:

$$\mathcal{P} : z[k+1] = P(z[k],\ \lambda) \tag{3.8}$$

One could note that the variable z when used as an argument to the Poincare map is indicated with square braces to indicate the discrete nature of the map.

3.2.6 Phase and phase response curves

Synchronisation is central to the neuroscience and dynamical-systems theory of oscillators. Typical oscillators observed in biology are limit-cycle oscillators; this partly owes to the homeostatic mechanisms providing the necessary dissipative forcing. *Periodic orbit* is a solution of a dynamical system that repeats itself after a constant time. A "*limit-cycle* is an isolated closed trajectory of a dynamical system" (Sun and Lei, 2013). The neighbouring trajectories spiral into or out of the *limit-cycle*. One could also define an asymptotic phase for the points in the basin of attraction of the limit cycle by mapping points in the basin of attraction to 'points on the limit cycle'. The set of points having the same asymptotic phase is called an isocron. This way of defining an asymptotic phase and isocrons allows a description of the system based on the phase of the system, ignoring the exact amplitude of the oscillation. Applying a brief stimulus (brief so that the point does not leave the basin of attraction) to a

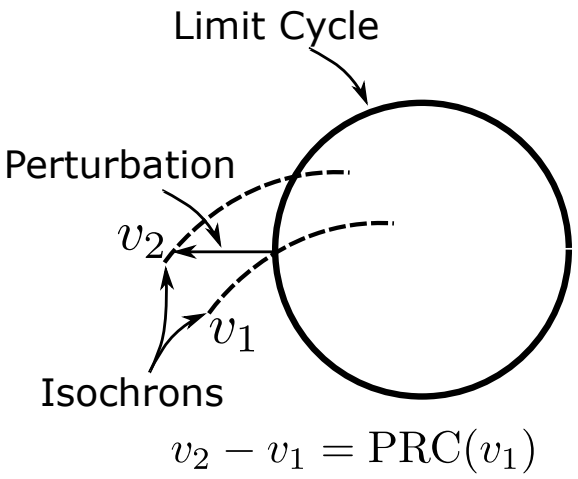

Figure 3.4: Illustration of the relationship between isochrons, PRC and perturbation of a limit cycle.

point on the limit cycle can move it to a different point in the basin of attraction where the asymptotic phase is different. This results in a change in the phase of the system, and the corresponding change in phase is quantified using a phase reset curve (PRC) (Ermentrout and Terman, 2010a). An illustration of how 'a perturbation moves a point from one isochron to another as defined by the PRC' is depicted in Fig. 3.4. The useful aspect of PRC is that it could be measured in real neurons or ensembles of neurons (Ermentrout and Terman, 2010a). Moreover, one could use PRC to convert the differential dynamics of the neurons close to a limit cycle to maps that are easier to study (Izhikevich, 2007).

Neuronal activity is affected by multiple cellular and extracellular perturbations such as channel conductances and synaptic activity. Internal feedback mechanisms and environmental factors such as pH and temperature also influence the cell. However, the earlier notions of one-to-one correspondence between properties of an ion channel and its function need study and further amendments (Goaillard and Marder, 2021). This is because several sets of conductances and associated currents can lead to similar firing patterns in the cells (Alonso and Marder, 2019). Hence, one way to study the effect of the change of conductance (or any other perturbation) on the activity of the neuron and network properties is to look at its effect on PRC. In general, one could perturb a neuron by either a depolarisation (increasing the electromagnetic potential inside the cell) or hyperpolarisation (de-

creasing the electromagnetic potential inside the cell) current. CPGs, when supplied with excitatory (depolarising) feedbacks, need precise tuning to control, which is suggested in literature (Sieling, Canavier and Prinz, 2009) as a plausible explanation why most of the CPG synapses are inhibitory. One could obtain a general shape of PRC corresponding to a CPG against inhibitory perturbation (Oprisan, Thirumalai and Canavier, 2003). In Oprisan, Thirumalai and Canavier, 2003, the point at which the spiking threshold is reached is labelled as the start of the phase (phase '0'). An inhibitory pulse applied during the burst (early part of the phase) makes the next pulse appear faster (or advances the phase). Initiation of a burst is delayed if an inhibitory pulse is applied slightly before the burst. Soofi and Prinz, 2015 show how conductance changes affect the PRC of CPG neurons, especially that an increase in the hyperpolarisation-activated conductance changes the PRC. As conductances are modulated by neuromodulators such as dopamine, these effects become highly relevant in PD.

Furthermore, the use of PRC in human locomotion studies is not new (Yamasaki, Nomura and Sato, 2003; Aoi et al., 2010; Funato et al., 2016; Tamura et al., 2020). The assumption behind the use of this approach is that the CPG receive feedback (perturbations) from the sensory system (from the limbs or indirectly from the brain through visual or auditory feedback) such that the overall system (neural and mechanical system) is synchronised (Yamasaki, Nomura and Sato, 2003). The control systems based approach by Yamasaki et al.'s (Yamasaki, Nomura and Sato, 2003) has a simple model for the CPG but uses an inverse dynamics model, modelling the cerebellum.

3.2.7 Neural oscillators and phase

As described in Sec. 3.2.6 ideas of phase, phase-reduction and PRC can be applied to the *limit-cycle* oscillators describing the CPG. This section defines *phase* mathematically and how PRC can reduce the multidimensional oscillator dynamics into simpler discrete or continous equations.

A conventional phase reduction approach is aimed at explaining the dynamics

of a system near a *limit-cycle*. In this approach, irrespective of the dimension of the system, the underlying dynamics are represented in terms of a single variable, the so-called phase variable. Suppose a generic n-dimensional nonlinear dynamical system,

$$\dot{x} = \mathcal{F}(x),\ x \in \mathbb{R}^n,\ n \geq 2 \tag{3.9}$$

has a stable periodic orbit $\tilde{\varphi}(t)$ with period T.

Definition 3.2.1 *For each point x^* in the basin of attraction of the periodic orbit $\tilde{\varphi}(t)$ of the oscillator, there exists a unique function $\phi(x^*)$ such that*

$$\lim_{t\to\infty} |x(t) - \tilde{\varphi}(t + \phi(x^*))| = 0, \tag{3.10}$$

where $x(t)$ is the flow of the initial point x^* under the vector field $\mathcal{F}(\cdot)$. The value $\phi(x^*)$ is called the asymptotic phase *or* phase *of x^*, and takes values in $[0,\ T)$, or in $[0,\ 2\pi)$ with appropriate scaling (Josic, Shea-Brown and Moehlis, 2006).*

When the oscillator's trajectory is in the basin of attraction of the limit cycle, $\phi(\cdot)$ could be used to determine its *phase* $v := \phi(x^*)$ of the oscillator and *isochrons* are the level sets of the phase function $\phi(\cdot)$. Furthermore, as the flow vector $\mathcal{F}(\cdot)$ maps isochrons to isochrons, on and close to the limit-cycle, the following is true (Izhikevich, 2007),

$$\dot{\phi} := 1 \tag{3.11}$$

$$= \nabla\phi(x).\dot{x} \qquad \text{(by chain rule)} \tag{3.12}$$

$$= \nabla\phi(x).\mathcal{F}(x) \tag{3.13}$$

The system is assumed to be close to the *limit-cycle* $\tilde{\varphi}(t)$ even under small perturbations. Given a system evolving close to a *limit-cycle* and perturbed by a weak input, one could define a function $PRC(\cdot)$ which characterises the response of the system to the weak perturbation.

Infinitesimal PRC: A local approximation to the $PRC(\cdot)$ is known as an *infinitesimal* $PRC(\cdot)$ which maps the current phase of the system v_n to the new phase v_{n+1} *locally*. Here v_n and v_{n+1} denote the current phase and phase after perturbation respectively. This could be obtained by the Taylor series approximation of the derivative of the function $\phi(\cdot)$ (Ermentrout and Terman, 2010b). That is, for arbitrary perturbation δ,

$$\underbrace{v_{n+1}}_{\phi(x_n+\delta)} = \underbrace{v_n}_{\phi(x_n)} + \nabla(\phi(x_n))\delta + O(\|\delta\|^2) \tag{3.14}$$

Hence for small perturbations, one could omit the higher-order terms resulting in the following equation,

$$PRC(v_n, \delta) = \underbrace{v_{n+1}}_{\phi(x_n+\delta)} - \underbrace{v_n}_{\phi(x_n)} = \nabla(\phi(x_n))\delta \tag{3.15}$$

Consequently, for infinitesimal perturbations, the *infinitesimal* $PRC(\cdot)$ given by the following equation fully characterises the system (Ermentrout and Terman, 2010a).

$$PRC(v_n) = \nabla(\phi(x_n)) \tag{3.16}$$

However, one could note that the phase function is challenging to obtain for many practical cases and one has to resort to numerical means to compute the $PRC(\cdot)$. One such practical method to determine the infinitesimal $PRC(\cdot)$ is by solving the adjoint equation on the points of the limit cycle, as discussed in Ermentrout and Terman, 2010b; Izhikevich, 2007.

Continuous Case: When the perturbation is continuous, the n dimensional nonlinear dynamical system becomes,

$$\dot{x} = \mathcal{F}(x) + \epsilon\mathcal{G}(t),\ x \in \mathbb{R}^n \tag{3.17}$$

and ϵ is a small positive constant. The term $\epsilon\mathcal{G}(t)$ represent the stimulus or perturbation. One could make use of the conventional phase reduction concepts to reduce

the forced system to a single dimensional system of the form $\dot{v} = 1 \ + \ \epsilon PRC(v)\mathcal{G}(t)$ where $v := \phi(x)$. This equation could be obtained by several means (Izhikevich, 2007) such as the one given by Winfree or Kuramoto (Winfree, 1967; Izhikevich, 2007). While Winfree arrives at this equation by approximating continuous perturbations as a set of impulses (Izhikevich, 2007) Kuramoto uses the chain rule. The approach by Kuramoto is given below.

Extending Eq. 3.14 to continuous perturbations, one could write the following for the perturbed system, as described in Izhikevich, 2007 as inspired from Kuramoto's approach,

$$\dot{v} = \nabla\phi(x).\dot{x} \tag{3.18}$$

$$= \nabla\phi(x).(\mathcal{F}(x) + \epsilon\mathcal{G}(t)) \tag{3.19}$$

However, the phase function is defined for the non-perturbed system of equations $\dot{x} = \mathcal{F}(x)$. And, using the identities given in Eq. 3.11 - Eq. 3.13, and Eq. 3.16 One obtains,

$$\dot{v} = \nabla\phi(x).\mathcal{F}(x) + \nabla\phi(x).\epsilon\mathcal{G}(t) \tag{3.20}$$

$$= 1 \ + \ \epsilon PRC(v)\mathcal{G}(t) \tag{3.21}$$

The subscript of v can be avoided in the continuous case. In an alternative formulation, if the phase is assumed to vary between $[0, 2\pi)$ and if the limit cycle solution is scaled as $\varphi(\frac{2\pi}{T}t)$ as given in the original paper by Kuramoto (Kuramoto, 1984) one could obtain the following equation for the rate of change of phase.

$$\dot{v} = \frac{2\pi}{T} \ + \ \epsilon PRC(v)\mathcal{G}(t) \tag{3.22}$$

Time is not scaled by $\frac{2\pi}{T}$ in this thesis.

General PRC: In this work, a general approach to $PRC(\cdot)$ has been chosen, and the infinitesimal perturbation or *infinitesimal* $PRC(\cdot)$ is not assumed. Therefore, the $PRC(\cdot)$ becomes a function of both phase and amplitude of the perturbation. For a

given phase, the perturbation to the PRC is a vector. However, once the direction of perturbation is fixed, only the magnitude needs to be specified. In this work, the perturbations which can be specified by a single number are only considered.

Remark 1 *$PRC(\cdot)$ functions for the purposes of this thesis is defined as a parameterized family of functions which maps the current phase to the phase after perturbation.*

4. Data-Driven Prediction of Freezing of Gait Events From Stepping Data

One of the central ideas outlined in the previous chapters is the fact that lack of permanent cure in PD necessitates management methodologies such as providing augmented feedback. This chapter addresses the problems associated with developing tools for the prediction of an FoG episode detailed in Sec. 3.1 which in turn has the potential to be used with a cueing technique. The methodologies adopted in this chapter can be directly extended to other signals and can be used in conjunction with auditory and sensory cueing techniques.

There is a need for the use of kinetic data to address the problem of prediction. While kinematic aspects of PD-Gait is crucial, the kinetic aspects such as the loading and unloading aspects of the PD-Gait also need due consideration. The pre-FoG/FoG based classification methodologies may not be suitable for real-time prediction of FoG as the real-time signals can contain a combination of these states. There is also a need for personalizable algorithms where one can control the sensitivity and specificity associated while in use.

In this chapter, an approach is proposed to predict freezing events from force data obtained while stepping. This prediction is accomplished using machine learning techniques—random forest, neural networks and naive Bayes, and the results are compared. "Kinetic" data, as is used in this work, likely contains subtleties in the loading and unloading phases of the stance that would directly translate to clear kinematic outcome measures. Moreover, as stepping data is produced

throught the same oscillation generators, this data is relevant for walking gait as well. The methodologies developed here could be translated to walking gait with minor modifications. Kinetic data is not translated into kinematic data such as position and velocity in the proposed approach. The work systematically analyses how the performance changes for different windowing parameters that characterize the training data. A sliding window approach is used to avoid the problems associated with Pre-FoG and FoG based classification when used for real-time prediction. An ensemble-based approach is employed in this work such that the sensitivity and specificity of the algorithm have the potential to be personalized after training. The work done in this chapter has been published in the following article.

- M. Parakkal Unni, P. P. Menon, L. Livi, M. R. Wilson, W. R. Young, H. M. Bronte-Stewart and K. Tsaneva-Atanasova (2020a). 'Data-Driven Prediction of Freezing of Gait Events From Stepping Data'. In:*Frontiers in Medical Technology*, p. 13.

The chapter is structured as follows. The methodology Sec. (4.1) starts with the preprocessing and labelling (in Sec. 4.2) of the data. Further, the classification procedure and the procedure for comparing classifiers are discussed in Sec. 4.3. Results are discussed in Sec. 4.4. Conclusions and future research directions in Sec. 4.5.

4.1 Methodology

The methodology consists of preprocessing the data, generating models from this data using machine learning approaches, and testing the obtained models to compute performance scores. The input-output pairs of training and testing data are generated by windowing the data as shown in Fig. 4.1a.

In Fig. 4.1a the sample window is split into three sections IL (input length), GL (gap length), and TL (target length). The force data in the first part of the window (IL) is used as the input to forecast the freezing state in TL part of the window ('1' for freezing and '0' for not freezing). GL is the temporal distance between

(a)

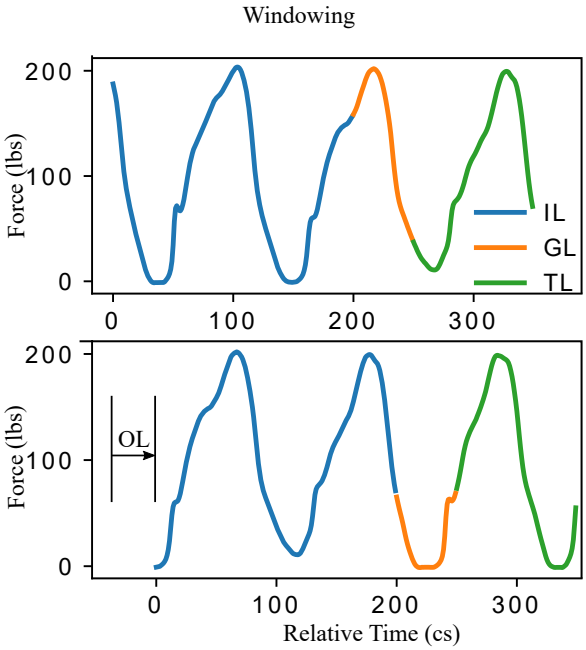

(b)

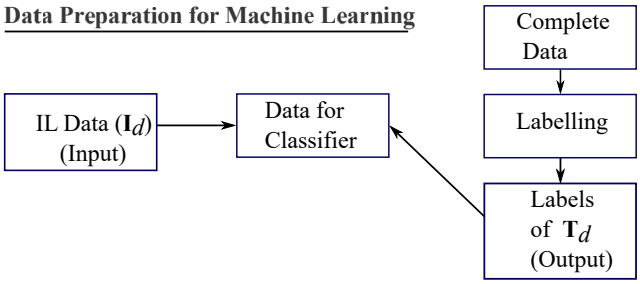

Figure 4.1: The windowing and data conditioning methodology. (a) The data for machine learning are obtained by considering a specific instance of input, gap, target and offset length. By varying these parameters, one obtains different datasets and, accordingly, different classification problems. Specifically, IL (Input Length) and label extracted from TL (Target Length) determine the input and output, defining the classification problem. GL (Gap Length) indicates how early the event can be detected. OL (Offset Length) determines the distance between two windows. A larger value of TL is shown for clarity while it is chosen to be 1 in this work to predict the immediate event. The ordinate is given in pounds (lbs) and abscissa is given in centiseconds (cs) (b) Summary of data preparation for training/testing the classifiers. IL and the labels obtained from TL region of the data formed the input and output data respectively. The labelling procedure is given in Sec. 4.2. This procedure of data conditioning is repeated for all data obtained by moving the window at an offset of OL. Centiseconds is adopted in this work as the unit of time as the sampling frequency is 100Hz. This results in the discrete number of time points available for analysis in any time interval matching exactly the quantity of time elapsed from start to end of that interval.

IL and TL, and it determines how early the predictions can be made, while OL (offset length) determines the offset interval between windows. When the total window length (IL+GL+TL) is greater than OL, there will be an overlap between windows. The details about windowing are given in the preprocessing section.

The data vector contained in the IL is represented as $\mathbf{I}_d$ and the dimension of the data vector depends on the value of IL and the sampling frequency. Similarly, vectors $\mathbf{T}_d$ and $\mathbf{G}_d$ depend on TL and GL respectively. IL, GL, OL and TL are windowing parameters for data preprocessing and not internal parameters of the classifier. The label for $\mathbf{I}_d$ is assigned as 'one that is representative of a future freezing' (labelled '1') or 'not freezing' (labelled '0') episode using a binary value that corresponds to the $\mathbf{T}_d$ using an automated process described in the labelling section. This results in $\mathbf{I}_d$ and $\mathbf{T}_d$ forming the input and output for training the classifiers as illustrated in Fig. 4.1b.

The data used for training/testing depends on windowing parameters. Therefore, the impact of these parameters on classification performance is determined. The following subsections provide the details of preprocessing and training/testing of machine learning algorithms using the data.

4.1.1 Experimental Data Used

The current data constitute data from a previous study (Young et al., 2016), collected using 'two force plateslates customized to fit a SMART Equitest from Neurocom'. Nineteen subjects with Parkinson's disease were recruited from the Stanford Movement Disorder clinic. The exclusion criteria were dementia, significant hearing loss, or any musculoskeletal or neurological issue (other than Parkinson's) that significantly affected their walking. Data from the nine patients who had freezing episodes is used in this work. All the trials with different attentional focus with freezing episodes have been used. This provides the algorithm with an opportunity to train against various plausible stepping characteristics leading to a freeze. Inclusion criteria were that participants scored at least three or greater to the third item of the FoG questionnaire. Participants were ON medication (i.e. they were testing 1-2h after taking medication).

No participants had undergone surgery for deep brain stimulation, although some were candidates undergoing evaluation for surgery. All participants had idiopathic Parkinson's and no other known neurological impairment. Participants were excluded from the study if they were unable to stand unsupported for the 90s. The testing session comprised six trials of 90s and lasted approximately 20-30 minutes depending on the time participants rested between trials. Data without FoG episodes are removed from this study resulting in at least two trials per subject. The detailed experimental protocol is given in Young et al., 2016.

This Force plate data were collected at 100 Hz (uniformly sampled) from the subjects as they stepped in place until they at least had one freezing episode or for a duration of 90 s. The data included force and moments in all three coordinates as time series (TS). The participant characteristics are as follows; age was 62.827 ($\pm$ 8.82), Unified Parkinson Disease Rating Scale (UPDRS) score of 32.6 ($\pm$ 21.33), Hoehn and Yahr Scale (H & Y) of 2.4 ($\pm$ 0.53), years since diagnosis being 10.71 ($\pm$ 6.01) (Young et al., 2016).

4.1.2 Preprocessing

A PCA (principal component analysis) of the data in a 3D-coordinate system measuring force and moments in x (frontal), y (lateral) and z (vertical) directions were performed, and it showed the greatest variance in the vertical direction. Hence, the vertical (z) coordinate is used here for the analysis. A graphical representation of the data preprocessing procedure is shown in Fig. 4.1a. The data has been windowed into IL, GL and TL (See Sec. 4.1). The force data that corresponds to IL (blue in Fig. 4.1a) is used as the input and the label corresponding to TL is used as the output (as shown in Fig. 4.1b). This way, the forecasting problem becomes a classification problem. The data contained in IL and the corresponding label form a training data sample. Here, the TL has been chosen to be 1. This ensures the prediction of the patients' status immediately after GL. This procedure is general enough to include various values of TL and make predictions considering various events in the TL time window. Window length (WL) is the total length of the data used to generate a

single sample, that is, the sum of IL, GL and TL. A sliding window of length WL (independently for training and testing data, as described in the cross-validation section Sec. 4.3) with an offset (See Fig. 4.1a) of OL is used to prepare multiple data samples for training and testing. This is done at the individual patient level so that cross-validation can be carried out on an individual basis. The mean and standard deviation of the quarter of cycle length of all the patients is 28.4 cs and 7.6 cs, respectively. Hence, the OL is chosen to be 28 cs (approximately a quarter of an average cycle length) for training and testing for all the patients. But this does not prevent one from using the tested classifier at a lower OL value to produce a higher temporal resolution in a real-time prediction scenario. The OL is chosen to be well below the cycle length to avoid stepping cycles getting missed while window length WL is slid with an offset OL.

4.2 Labelling

This subsection describes how the data labels are generated, which is considered as ground truth (ideal expected result) in the machine learning algorithms. The data is labelled into freezing and non-freezing using a modified version of the criteria provided in (Nantel, Solages and Bronte-Stewart, 2011). Modifications to the criteria are given here. For scaling, the average of the peaks is used in this work as it is closer to the body weight rather than the max of the peaks in contrast to (Nantel, Solages and Bronte-Stewart, 2011). This is done to account for the fact that the force exerted can be slightly more or less than the actual bodyweight of the subject due to the acceleration of the subject's movement. In Nantel, Solages and Bronte-Stewart, 2011 freezing intervals are defined as *abnormally long* intervals between peaks, where *abnormally long* is defined as 1.2 times the means of the periods of the previous three intervals or two times the mean period of the trial. In this work, *abnormally long* window length for detecting freezing is defined to be 1.5 times the average time-period of all the cycles across all the patients (mean cycle length). Selecting the *abnormally long* window to be larger could relatively aid in predicting freezing episodes that are comparatively longer and vice-versa. OL is also chosen to be lower than the

abnormally long window length to avoid missing any freezing regions. The method which uses the previous three cycles for computing the time-period as given in Nantel, Solages and Bronte-Stewart, 2011 is not used as it is not applicable in the case where freezing happens during the initiation (or before three steps are completed) and uniform criteria are needed to be used throughout. A visual examination has been conducted as suggested in Nantel, Solages and Bronte-Stewart, 2011 to assure the validity of the method. Moreover, video recordings were used to qualify FoG events in Young et al., 2016 and for trials analysed here, there were no discrepancies between FoG events detected by the algorithm and visual inspection. Furthermore, video based methodology is increasingly being recognized as the gold standard for assessing FoG (Gilat, 2019). Therefore, there is justification for assuming that the detection algorithms used here are, at least in the case of the current data, are valid for determining FoG events. This way, a binary label for every time point in the data as freezing ('1') or non-freezing ('0') is obtained. In this study, a correct prediction of FoG is considered to be a positive outcome as far as the performance of the ML algorithm is concerned. This is applicable when one refers to terms such as false positives and false negatives.

4.3 Cross Validation

The training, testing, and validation is carried out in the following manner. A version of leave one out cross-validation (LOOCV) is carried out by first leaving all samples of one patient out. That is $\{1...N-1\}$ patient data samples were chosen from N (number of patients each with a set of data) as *'model generation set'* and N^{th} one as the *'unseen set'*. $\{1...N-2\}$ patient data samples were chosen from the *'model generation set'* for training (*'training set'*) and $(N-1)^{th}$ one as the *'testing set'* generating a model to be tested on the *'unseen set'*. Then another subset of the *'model generation set'* of cardinality $N-2$ is chosen as *'training set'* leaving the rest as *'testing set'*. Then the process is repeated $N-1$ times, generating $N-1$ models. These models were then tested on the *'unseen set'* to generate $N-1$ performance scores. Successively, the process is repeated with another subset of the overall patient

data set chosen as the *'model generation set'* and the rest as *'unseen set'* resulting in $N(N-1)$ performance scores, that is, $N-1$ scores for each patient. F1 score is the harmonic mean of precision and recall. Precision is the ratio of true positives to the sum of true positives and false positives. Recall is the ratio of true positives to the sum of true positives and false negatives. F1 score (Opitz and Burst, 2019) is used to measure the performance, and the median of $N(N-1)$ performance scores (with $N=9$) were used to compare different classifiers. An advantage of using this method is the generation of an ensemble of models which could be combined in different ways to inform the design of patient-specific interventions.

4.3.1 Integrating the Classifier Outcomes

As described in the cross-validation section, once an ensemble of $N-1$ models is generated, one needs to combine their outcomes. A 'minority vote' is used for combining the outputs of $(N-1)$ models to test the *'unseen'* case. The minority vote is defined as a case where an 'or' gate is used to combine the binary classifier outputs. An 'or' gate produces a '0' for two inputs if and only if both the inputs are zeros, every other case results in '1'. This methodology is used in this work to reduce the chances of false negatives as the application demands safety.

'Majority vote' methodology is another alternative for combining the classifier outcomes, where an 'output' is selected when the majority of the classifiers produce that 'output'. This method is also tested for a subset of the parameters for all the subjects. Successively this is compared with the 'minority vote' technique.

4.3.2 Parameter Analysis Procedure

The methodology used for the analysis of the windowing parameters is described in this section. A set of F1-scores (Haghighi et al., 2018) (Opitz and Burst, 2019) is generated by different combinations of patients and windowing parameters. That is, when the impact of IL is investigated, scores are generated by fixing GL (to 0 cs) and classifier type (to one of Neural Network (NN), Naive Bayes (NB) or Random Forest (RF)), and varying IL and patient identification numbers. The

specific discrete values of IL chosen are [37, 56, 113, 226, 339, 452] and patient identification numbers are [0, 1, 2, 3, 4, 5, 6, 7, 8]. The average cycle length of the signals is approximately 113 cs forming the rationale for choosing the grid for IL. This produces a 2-dimensional array that corresponds to every patient and every IL. The median of these scores across the patient dimension is computed to generate a single performance measure for every IL. This procedure is carried out for all the classifier types to generate multiple 2-dimensional arrays. Similarly, when the impact of GL is investigated, scores are generated by fixing IL (to 226 cs) and classifier type (to one of NN, NB or RF), and, varying GL for all patients, successively computing the median across the patient dimension. GL part of the data is not given as an input to the classifier, but it rather forms a parameter to determine how early one can predict the event. The discrete grid used for GL is [0, 20, 40, 100, 200] for understanding the prediction accuracies closer to and away from the freezing event. This is also extended in a similar way to all classifier types. Class weights for the true-cases were varied from 1 to 100 for the RF classifier, with windowing parameters set as GL = 0 cs and IL = 113 cs. The models generated by varying class weights are tested to obtain the F1-scores corresponding to every patient. The median of the standard deviations of the F1-scores (across different models of varying class weights) and the corresponding median of the F1-scores (averaged across different models of varying class weights) are computed to understand the effect of class weights. Kruskal Wallis H test has been used for comparing the classifiers as normality is not assumed. The Spearman rank-order correlation coefficient is used for computing correlations.

4.3.3 Classifiers and Related Parameters

The following sections describe the details of the classifiers and the reason for choosing NB as the benchmark.

Naive Bayes (NB) as Benchmark

The NB classifier acts as the benchmark classifier for this study because of the following reasons. The classifier assumes conditional independence and is very fast for supervised learning (Zhang, 2004). That is, the predicted label $\tilde{y}$ is computed as follows,

$$\tilde{y} = P(y) \arg\max y \prod_{i=1}^{n} P(x_i|y) \tag{4.1}$$

where $P(x_i|y)$ (conditional probability of a feature x_i given label y) is computed by assuming a Gaussian distribution, where, the parameters are estimated using maximum likelihood estimation algorithm (MLE) (Myung, 2003). The proportionality constant $P(y)$ is the relative frequency of the label y.

Neural Network (NN) and Random Forest (RF) Classifiers

Neural networks are ubiquitous in the world of machine learning. The beginnings of the neural network architectures are inspired by the way in which human neurons work. A basic unit of a neural network is a perceptron which takes a vector $\mathbf{x}$ as input and produces an output y after a linear and a nonlinear transformation

$$y = \sigma(\mathbf{w}.\mathbf{x} + \mathbf{b}) \tag{4.2}$$

where $\mathbf{w}$ is the vector of weights, $\mathbf{b}$ the bias and $\sigma(\cdot)$ a nonlinear function such as $\tanh(\cdot)$ or $\max(0, \cdot)$. One could then define a layer of a neural network as a column of perceptrons, each receiving the input $\mathbf{x}$ and producing its own outputs. Successively, a deep neural network is a set of layers stacked one after the other, with each receiving input from the previous layer. In this architecture, the first layer receives the input $\mathbf{x}$, and the final layer produces a vector of outputs $\mathbf{y}$ depending on the number of neurons in the output layer. One then creates a loss function that compares the generated outputs with the labels one has from the data in a classification problem and generate a loss. This loss is successively used to train the weights and bias term using *back propagation* and optimization algorithms. NN classifiers can learn a

nonlinear function approximation and generate an appropriate decision boundary for the problem. Five hidden layers of 100 neurons are used for supervised learning. The solver used in NN is limited memory Broyden–Fletcher–Goldfarb–Shanno (LBFGS) for faster convergence (Zhu et al., 1997; Pedregosa et al., 2011; Liu and Nocedal, 1989). A lower number of layers deteriorated the performance, while a higher number did not improve it.

In decision-tree based classification, a decision tree is generated from labelled training data containing a set of features and corresponding labels. A threshold of the feature that partitions the data the best is chosen from the feature values to create a root node (Su and Zhang, 2006). This process is continued for a predefined depth until one ends up with a set of leaf nodes which contain data from the same class. This essentially splits the data into subsets, where every subset belong to a single class (Su and Zhang, 2006). An RF classifier is an estimator that fits a set of decision tree classifiers on sub-samples of the dataset and uses its average for prediction.

In this work, the maximum depth of the tree used is 200, with a class weight of 100 for the true cases and 1 for false, giving more weight to freezing prediction. The freezing phenomenon is episodic, and there is a lower number of freezing episodes when compared to the number of walking cycles in PD (Barthel et al., 2016). A higher class weight in RF is chosen for the true cases to address this imbalance and signify the relative importance of freezing prediction compared to predicting the normal stepping. To understand its impact, weights assigned to the true cases are varied from 1 to 100 with a spacing of 10 at IL = 113 and GL = 0. The RF classifier has a lesser chance of over-fitting compared to a single decision tree as it uses multiple trees (forest) and averaging.

4.3.4 Classifier Comparison

The performance of three well-established classifiers RF, NN and NB (Pedregosa et al., 2011) is compared. The NB classifier acted as a baseline for comparison. F1-scores can be calculated in multiple ways (Opitz and Burst, 2019). The averaged

F1-score version described in Opitz and Burst, 2019 is used as the 'F1-score' in this work. Median F1-Score across different patients is used as the performance measure for a classifier. The effect of the IL and GL on the performance measure is determined to understand the trends and optimal IL. The F1-scores claimed are after the application of 'minority-vote', while methodologies such as 'majority-vote' and 'minority-vote' are equally valid with their pros and cons. A short comparison of the 'minority-vote' technique with the 'majority-vote' methodology is also provided for a subset of parameter values for all the subjects combined. A detailed description of the parameters used for the comparison of classifiers is provided in Sec. 4.3.2

4.3.5 Procedure for Real-Time Prediction

This section presents the proposed methodology for real-time prediction. This is not to evaluate the performance of the algorithms. A real-time prediction scenario is illustrated for a single patient.

Moreover, to show the ability of the algorithm to control sensitivity/specificity by changing only the way of combining the models, the false positive and negative ratios are provided here for a particular patient using minority-vote and majority-vote methodology. To this end, mean false positives (MFP) and mean false negatives (MFN) of all classifiers (NN, NB, RF) combined is estimated for majority-vote, and minority-vote cases for the case shown here and their ratios are provided. False-positive and false-negative rates are also computed for all the patients for comparative purposes.

In the case demonstrated, an IL = 226 cs is used, and the data is supplied to the classifier by sliding the window over time. This sliding window with an OL = 10 cs replicates the real-time prediction scenario where prediction is made after every 10 cs. The classifier has to predict the immediate possibility of a freeze giving '1' in the case of a freeze and '0' otherwise. The output of the classifier is obtained over time and shown along with ground truth (GT). The label of TL in each sample form the ground truth for that sample. An ideal classifier matches GT. No prediction is possible until the first set of data points for the time defined by IL is available.

Therefore, this doesn't form part of the 'union of TL data'. After this point, there is a prediction that corresponds to every TL data.

Moreover, input data of length 226 cs has been tested for the time it takes for prediction using the methodology described in this chapter. Specifically, this is carried out by running the prediction algorithm (minority vote based - RF, NN and NB) 100 times in a single core on an HP Laptop (16 GB RAM, Intel(R) Core(TM) i7-9750H CPU) and finding the median. The computational time for prediction has been found to be less than 1 cs and therefore negligible for the use-case.

4.4 Results

The fraction of freezing episodes is approximately 34% of the overall data, the total number of freezing episodes in the whole data set consisting of 9 patients is 174, the average duration of freezing episodes is approximately 12.08 s (SD = 13.5 s), and the average number of freezing episodes per subject is 3 (SD = 1.6) per trial.
In this section, the following results are presented:

- The analysis of the performance of classifiers, by varying the windowing parameters IL and GL as discussed in Sec. 4.4.1.
- A demonstration of the online prediction as discussed in Sec. 4.4.2

4.4.1 Classification Performance

The performance of NN and RF is found to be superior compared to NB (Kruskal Wallis H test, $p < 0.05$ for both). This could be due to a more complex relationship between the features learned by NN and RF when compared to the NB classifier. The performance of NN and RF were not statistically different (Kruskal Wallis H test, $p \approxeq 0.276$). GL and the classifier performances are inversely correlated with the Spearman rank-order correlation coefficient of $\approxeq -0.99$ and $p < 0.01$. The best input lengths for NB, RF and NN were found to be 113 cs, 113 cs and 226 cs, respectively. The neural network performs well for a range of IL (113-339 cs) while the other classifiers deteriorate the performance beyond an input length of 113 cs. Fig. 4.3

(a) (b)

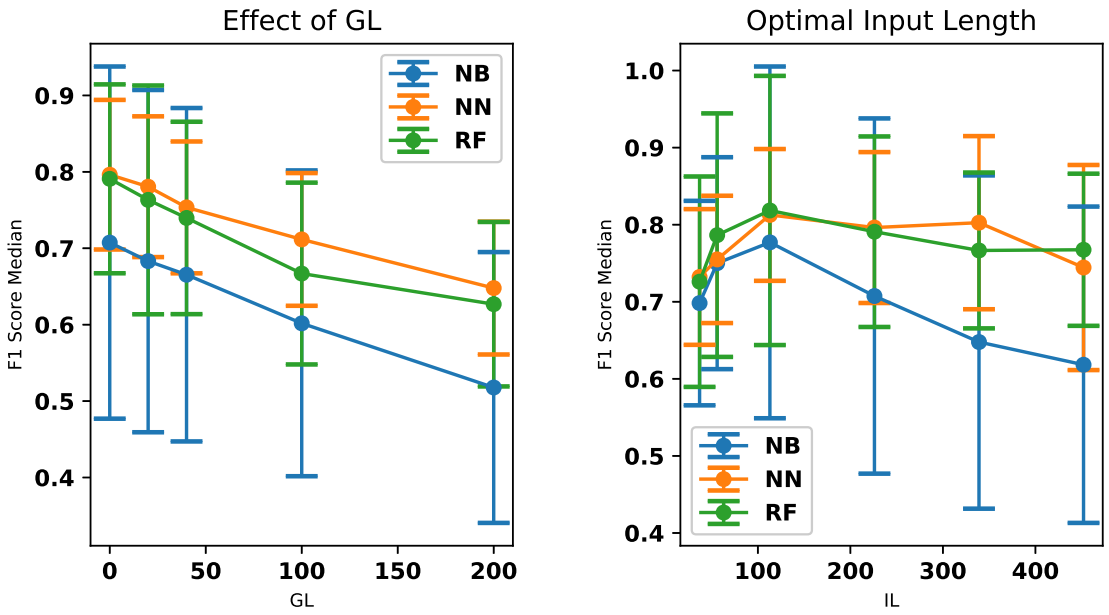

Figure 4.2: The effect of GL and IL on the median F1-scores. The standard deviation has also been provided as error bars. (a) The median F1-scores of NN, RF and NB classifiers are compared here. NN classifier outperforms all other classifiers in this aspect. The performance of the classifier decreases with respect to an increase in GL. Dots and the lines drawn indicate the computed data points and the linear interpolation between them, respectively. (b) F1 score (median over all the patients) is shown as a function of the IL. The accuracy is shown to be optimal at an input length of 113 cs This is particularly evident in the case of the NB and RF classifiers. Dots and the lines drawn indicate the computed data points and the linear interpolation between them, respectively.

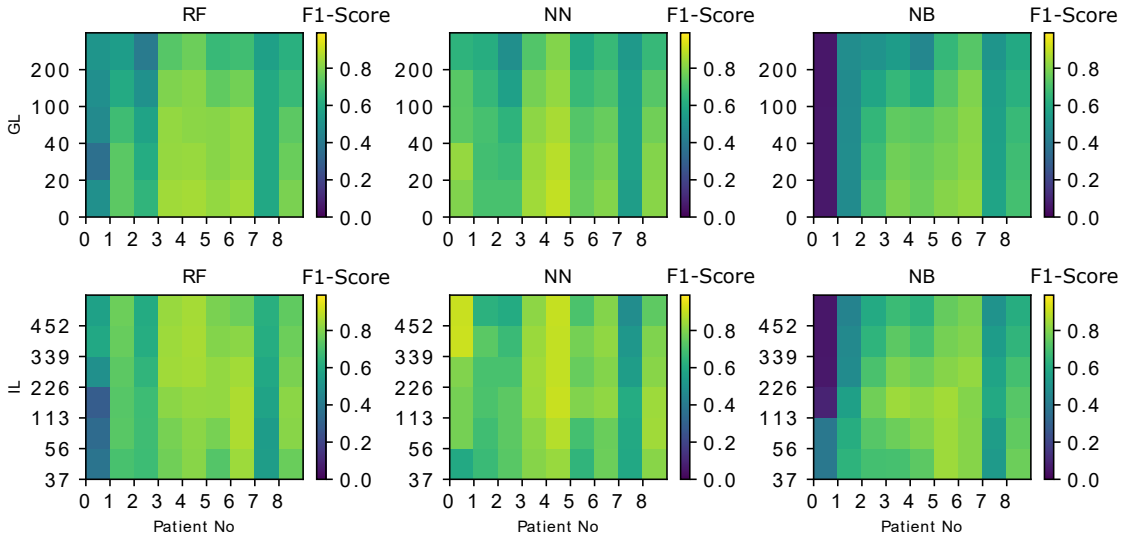

Figure 4.3: The effect of IL, GL on the F1-scores of the classifiers is demonstrated for every classifier and every patient. IL = 226 cs is chosen when GL is varied and GL = 0 is chosen when IL is varied. The patient-specific score variation can also be noted in every case (e.g. The accuracy of the first patient (patient No. '0') is lower for both RF and NB but NN performs better in that case). The metric used in the colour-bar for comparison is the F1-score.

shows the effect of IL and GL on the F1-scores of the classifiers for every patient. A constant value of IL (= 226 cs) is chosen when GL is varied, and GL = 0 cs is chosen when IL is varied. The scores are found to vary between patients. While Fig. 4.2a and Fig. 4.2b show an overall trend, there are individual differences between patients (see Fig. 4.3), which is typical in freezing studies (Mazilu et al., 2015). For example, patient no.0 revealed very low scores for the NB classifier, while patient no.5 revealed a higher score. Also, NN performs better for patient no.4 than RF and NB. For patient no. 6, RF performs better than the other two. There are, therefore, individual differences in the optimal IL estimates. Moreover, given the black-box nature of the classifiers, why one classifier performs better/worse for a particular patient is difficult to ascertain. This points to a need for personalisation and a larger data collection exercise to determine the individual patient's optimal parameter sets, categorising participants according to the emerging freezing 'sub-types' (Ehgoetz Martens et al., 2018).

For the RF classifier, the models corresponding to different class weights are

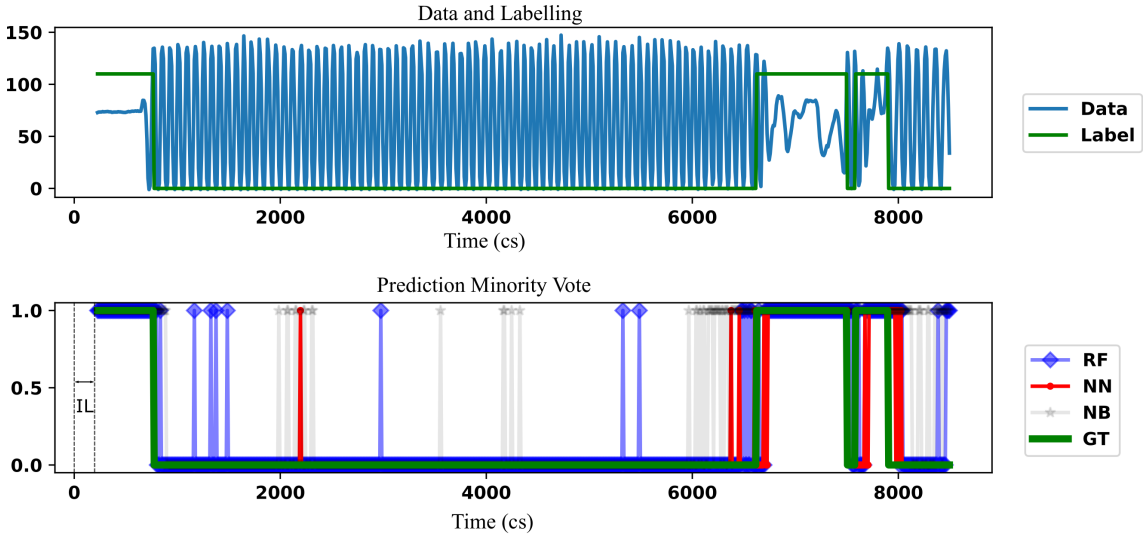

Figure 4.4: The comparison of the freezing prediction using NN, RF with the benchmark NB (using a lighter shade) is demonstrated. Data (Force in lbs) and the corresponding label for the time frame where the prediction is carried out is shown in the top figure. This is the union of the TL part of the data and corresponding label for a single patient. Label '110' is used instead of '1' to indicate freezing for clarity, that is, to keep the label well above the centre of the plot. The initial IL data cannot form target data, as there is not enough information for prediction before that. The bottom figure indicates the comparison of the classifiers against the ground truth (GT). The prediction is started only after a time defined by IL. Parameters used are IL = 226 cs and GL = 0 cs, OL = 10 cs. In this case, NN shows fewer false positives than RF, while both classifiers have less false positives than NB.

tested and used to obtain the F1-scores corresponding to every patient. The median of the standard deviations of the F1-scores (across models of varying class weights) is found to be 0.03. The corresponding median of the F1-scores (averaged across models of varying class weights) is found to be 0.82. Low standard deviation indicates the results presented are robust against the class weights used as the mean/median F1-scores are more than ten times higher than the standard deviations obtained. But, one could also argue that there is room for personalization by making use of the individual differences, which causes the dependence of the F1-scores on the weights.

4.4.2 Real-Time Prediction Demonstration

Minority vote based prediction of a single patient data is shown in Fig. 4.4 as an example. A machine learning model which has not previously seen this patient's data has been used for the purpose. The example is chosen not to indicate the performance of the classifiers but to show the ability to predict in real-time (once in every 10 cs). The prediction of different classifiers is indicated in different colours. A similar result is obtained at OL = 28 cs as well. In the demonstration, OL = 10 cs is chosen to show the ability of the classifier to be used at a higher temporal resolution than it is trained at. The NN prediction shows a lower number of false positives (a freeze or '1', even when there is no freeze) than RF. RF classifier shows a lower number of false positives than NB. Minority-vote method has lesser MFN than majority-vote method with their ratio being 0.36 : 1 (MFN for minority-vote method : MFN for majority-vote method). Minority-vote method has a higher MFP than majority-vote with the ratio being 1 : 0.3 (MFP for minority-vote method : MFP for majority method). False positive and negative rates for all patients (averaged over all classifiers in minority-vote case, IL = 113, GL = 0) is found to be 0.26 (SD = 0.25), 0.20 (SD = 0.16) respectively. False-positive and negative rates for all patients (averaged over all classifiers in majority-vote case, IL = 113, GL = 0) is found to be 0.16 (SD = 0.22), 0.29 (SD = 0.18) respectively.

4.5 Discussion

Our analysis demonstrated that it is possible to predict freezing events using vertical force data from stepping. Prediction of freezing events from stepping data is addressed as a classification problem. In doing so, the data is windowed using IL, GL, TL and OL as relevant parameters and generated the input data and output labels accordingly. Moreover, the impact of IL and GL on the F1 scores has also been studied.

F1-scores (> 0.8) obtained for the classification is found to be decreasing for an increased GL, and this score is subject dependent. This indicates that the earlier one tried to predict a freezing event, the less accurate the prediction became. The average natural time-period of the signals is found to be approximately 113 cs in this work. The optimal performance of the classifiers in this range indicates that, in the case of this stepping task, the physiological changes preceding a freeze take effect approximately one step before the freezing event. Despite including 174 freezing episodes, the modelling of freezes from relatively few participants is a limitation of the study, and future work aims to increase the sample size to improve the generalisability. The windowing paramters are explored by fixing other parameters to constant values. This way of studying the effect of parameters implicitely assumes that the 'trend in the result' (while varying one parameter e.g. GL) is not altered due the choice of the fixed parameter (e.g. IL)

Prediction and detection are different questions concerning the freezing of gait time series data. There are several attempts to detect freezing onset. The recent study by Aich et al., 2018 used accelerometer data where the authors show a detection accuracy of 88%. Whereas, this work aimed at prediction rather than detection of the freezing. The prediction accuracy depends heavily on the degradation of stepping (and its associated data) prior to freezing which is patient dependent (Mazilu et al., 2013). This dependence is also very evident in our study from Fig. 4.3 where the patient '0' has lower F1-scores compared to other patients for RF and NB classifiers. This highlights the necessity for a flexible, personalisable algorithm to meet patient needs. (Mazilu et al., 2013), have used accelerometer data and produced an F1 score

of 0.56 for prediction. (Mazilu et al., 2015) later show an accuracy of 71.3% using ECG and skin conductance. One can not directly compare these studies to our study because of the following reasons: 1) There are limitations with the step in place task as the spatial characteristics such as 'sequence effect' (Chee et al., 2009) can not be expressed in the current task. 2) The kinetic interactions between the feet and support surface are primarily responsible for the kinematic changes recorded and analysed in the previous work described above, particularly step length. As such, one could argue that an evaluation of kinetics (i.e. the dynamic loading and unloading of each limb) is likely to yield more accurate predictions of resultant kinetics. 3) Also, as this work aims at real-time prediction, a classification based on FoG/Pre-FoG states (Mazilu et al., 2013) may not be meaningful as the stream of data (in the moving window) may contain a mixture of these states. Moreover, in our work, training and testing the data from different attentional focus produces a model which can work more reliably in a real-life scenario where the patients are not restricted to one type of attentional focus.

In this work, the 'minority-vote' methodology is used for combining the output of the classifiers. Improving safety by way of minority-vote would result in higher false positives resulting in unnecessary cues being produced and hence diminished effectiveness. But false positives resulting in triggering a cue unnecessarily is not detrimental to the patient's life, but a false negative result while crossing the road can be. The fear of falling for a patient leads to immobilisation of the patient and further complications such as osteoporosis, constipation, reduced fitness, social isolation etc. (Bloem et al., 2004). Therefore, one could assume the benefit of avoiding a freeze far outweighs the risk of fatigue. Also, once trained, one can combine the model ensembles in different ways to suit the patient's needs. However, this trade-off forms one of the critical limitations of this work.

The algorithm's real-time prediction ability and flexibility in combining different models to enable further personalisation have been demonstrated. This flexibility becomes important in practical cases, as one would have to aim to adjust the sensitivity and specificity according to the patient needs. As the algorithm

developed here generates multiple models, one could personalise this according to the patient requirements by changing the way it is combined. The majority-vote and minority-vote based methodologies demonstrated in this work form two ends of the spectrum of possible ways of combining the model outcomes. Higher false positives of minority-vote method are justified by the reduction in false negatives, as the application necessitates more increased safety.

Spatial characteristics of gait such as "sequence effect" (Chee et al., 2009) cannot be observed by force data while stepping in place. Therefore, future endeavours could aim to evaluate predictions using gait data collected during forward-walking. The methods developed here (e.g. windowing, cross-validation procedure etc.) are also suitable for accelerometer data obtained from smartphones and other wearable devices. Furthermore, the training process developed here could directly be used with forward walking gait with minor modifications. The NN models could be reused in the walking scenario by transfer learning approaches. The proposed method could be extended to other signal features and parametrised cost functionals (Parakkal Unni et al., 2017) to potentially improve the prediction. Time series prediction, multilabel classification, and personalisation are future work.

In conclusion, the proposed method operating in conjunction with a sensory/visual/auditory cue (in a wearable device) could potentially help a PD patient walk more efficiently with less occurrence of FoG. It could be challenging to acquire force plate data in daily life settings. However, the rapid evolution of low-cost portable devices, such as wireless force-sensing insoles, provides a feasible solution to acquiring kinetic data (at least sufficient to calculate the proportion of body weight on each limb, as described here) in real-time. However, the conclusion implicitly assumes providing a cue 1-2 s before a freeze is sufficient to address freezing, which one could believe to be adequate for supplying cues such as the one presented in (Barthel et al., 2018). More studies have to be performed to understand 'how early' and 'what kind' of cue needs to be provided to reduce the chance of freezing.

5. Ankle Push-Off Based Mathematical Model for Freezing of Gait in Parkinson's Disease

There is a need for a model to explain the empirical observations in PD-Gait, such as the high coefficient of variability and freezing near narrow passages (Snijders et al., 2008). Plantar flexors provide the necessary push-off force to move the stance

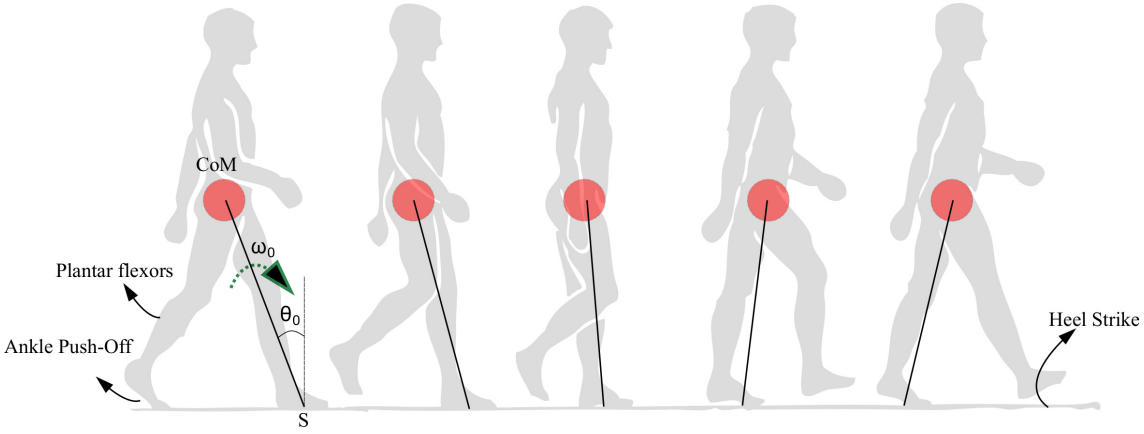

Figure 5.1: Anatomical representation of the stance phase for the left leg and swing phase for the right leg. The heel strike and ankle push-off is also indicated. The position of the centre of mass (CoM) is shown as a red circle which is assumed to be rotating with respect to a pivot point S. The location of the plantar flexors, approximate region generating ankle push-off force and heel strike region are noted. The initial angle and angular velocity are represented by θ_0 and ω_0 respectively.

leg forward. Subsequently, the muscles of the hip and knee moves the swing leg forward. An anatomical representation of the stance leg, under the action of the ankle, push-off force, is provided in Fig. 5.1. The effect of opposing forces generated by the plantar flexors observed in PD, as reported in (Nieuwboer et al., 2004), need

to be included in the gait model. Such a model will help understand the essential aspects of neural and mechanical systems contributing to PD-Gait, also shedding light on the future experimentations required. In this chapter, the relationships between the high variability and freezing will be studied by deriving a set of forces acting on the stance leg. They are driven by the Electromyogram (EMG) signals and, therefore, the activity of the CPGs. The kinetics of both swing leg and stance leg will be studied to understand their roles under the action of these forces.

In summary, the model in this chapter is built with two aims. The first aim is to explain the empirical observations seen in PD-Gait with a minimum number of variables. These include (1) a high coefficient of variation in PD subjects (Heremans, Nieuwboer and Vercruysse, 2013a), (2) a pattern of reduction of step lengths before freezing (Nutt et al., 2011), (3) the ability of sensory and visual cues to help reduce freezing (Young, Rodger and Craig, 2014; Rochester et al., 2005; Amini, Banitsas and Young, 2019), (4) the difficulty of freezing prediction, and (5) the occurrence of freezing near obstacles and narrow passages (Snijders et al., 2008). Secondly, the model aims to show the role of the swing leg as a supplier of ankle push of force and one that determines the time of heel strike. Hence, a bipedal model and a reduced low dimensional model resembling an inverted pendulum are studied upon the action of the ankle push-off force. The movement of the CoM under the action of the ankle push-off force is depicted in Fig. 5.1. Hence, the hypothesis investigated in this study is that the variability and the motor symptoms associated with PD (Heremans, Nieuwboer and Vercruysse, 2013a) can be explained by the experimentally observed premature activation of plantar flexors observed in PD (Nieuwboer et al., 2004). The work done in this chapter has been published in the following article.

- M. Parakkal Unni, P. P. Menon, M. R. Wilson and K. Tsaneva-Atanasova (2020c). 'Ankle Push-Off Based Mathematical Model for Freezing of Gait in Parkinson's Disease'. In:*Frontiers in Bioengineering and Biotechnology*, p. 1197.

The chapter is structured as follows. The methodology in Sec. 5.1 starts with the physiology of walking and ends with the derivation of the equations of motion and

rationale for using a reduced model. Further, the analysis procedure for the reduced system is described in Sec. 5.2. Subsequently, the results of the simulation and discussion are provided in Sec. 5.3 and 5.4 respectively.

5.1 Materials and Methods - Modeling

5.1.1 Physiology

Walking is a complex process that involves the interaction of the brain, spinal cord and musculoskeletal systems (Nutt et al., 2011). The typical gait cycle associated with walking involves '*stance*' and '*swing*' phases. The stance phase begins with a crucial heel strike phase, which is the initial contact that occurs instantaneously. As soon as the stance phase ends, the swing phase begins. The plantar flexor muscles of the trailing leg supply energy to 'push-off' the contra-lateral leading leg (Zelik and Adamczyk, 2016). Once the push-off occurs, the trailing leg enters the swing phase. The soleus and gastrocnemius muscles are the most notable plantar flexors, of which the significant role of the latter one in PD freezing/walking is established (Nieuwboer et al., 2004). Even though physiologically, there is a non-linear relationship between the EMG signals and the torques generated (Genadry, Kearney and Hunter, 1988), one can assume a linear relationship (Hof and Van Den Berg, 1977) between the envelope of the EMG (CPG firing) and the torques generated about the joint. Several other muscles are involved in walking, but the present study investigates only the effect of the plantar flexors, as these muscles supply most of the energy required for walking. In this work, the 'freezing step' is defined as the step at which the legs do not have sufficient angular momentum to progress walking forward. When the physiology is modelled as an inverted pendulum-like system, the freezing results in backward motion of the stance leg. In a real-life scenario, this implies the patient either falls or stops movement. The remark 2 provides the definition for freezing and related terms used in this work.

Remark 2 *In this study, 'freezing' or 'freezing event' is defined as the condition where there is no forward motion of the stance leg. 'Freezing episode' is defined as the*

events happening in the time interval between the heel strike phase and the freezing event. Hence, the 'start of the freeze' is defined to be at the heel strike phase after which a freezing event occurs.

Here, a systematic stability analysis is carried out, including unstable regimes, of the model in contrast to the stable limit cycle behaviour studied in robotics (Grizzle, Abba and Plestan, 2001) and passive walking dynamics literature (McGeer et al., 1990). Even though one can explain the complex freezing behaviour through several possible ways (Nutt et al., 2011) (some of them purely based on neural control), an attempt is made here to explain it in the simplest possible way and to understand the effect of neuromuscular inputs in producing unstable and chaotic walking behaviour as observed in PD (Heremans, Nieuwboer and Vercruysse, 2013a).

5.1.2 Dynamics of Walking

The dynamics of walking involves the coordinated action of neural input and muscles of the limbs. It consists of a continuous movement of the limbs as well as state reset at heel strike resulting in discrete dynamics (Sinnet et al., 2011). Plantar flexors of the swing leg supply the necessary torque to push the CoM forward. While walking, the CoM is supported by the leg in the stance phase for most of the time (80-90%). The double support phase is approximately 10-20% of the overall gait cycle (Kharb et al., 2011; Wahde and Pettersson, 2002). The motion of the CoM with single support under the action of the plantar flexors is modelled in this work. Though the double support phase is not explicitly modelled, its corresponding forces and resets are considered. The heel strike is modelled using discrete dynamics. Traditionally, the dynamics of walking is often modelled as biped model (Taga, 1995). In this section, a simplified biped model is presented. Further, a reduced, low dimensional, *inverted pendulum system* is considered as a special case relevant to PD. It is assumed that CoM is at the tip of the pendulum, and the links and the swing leg are massless. Therefore, the model generates the motion of the CoM of the human body. Running and jumping gaits are not considered in this model as the links are assumed to be rigid. It is also assumed that sufficient friction exists to avoid any slip.

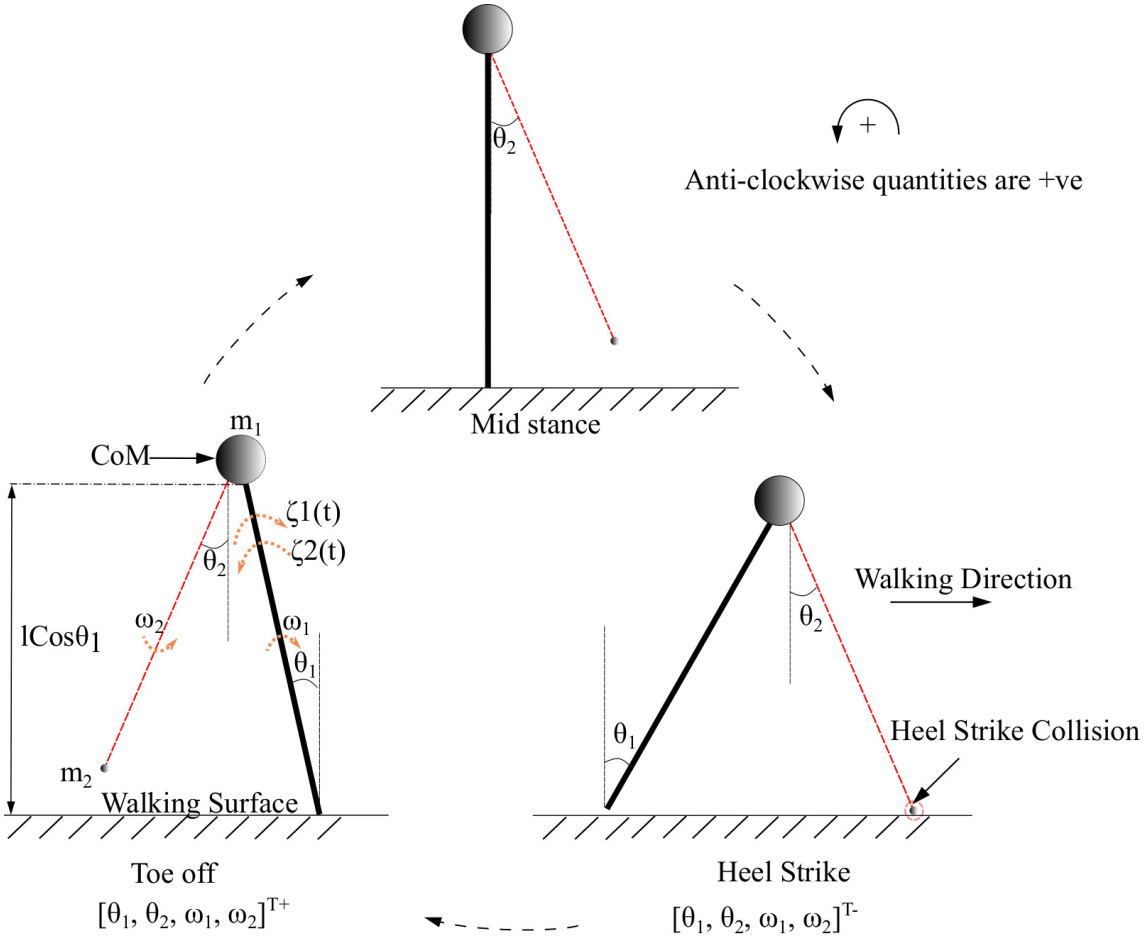

Figure 5.2: The toe-off, mid stance and heel strike instances of the two connected links of the biped with its CoM while walking in the forward direction. CoM indicated as a circle represents a point mass at the tip of the pendulum. The swing leg is indicated in red. The point of collision during a heel strike instance is circled in red. The terms θ_1 and θ_2 are the angles that the stance and swing legs subtend w.r.t. the vertical (in the inertial reference frame) respectively. The quantities ω_1, ω_2 and m_1, m_2 are the corresponding angular velocities and masses of the body and swing leg respectively. The torques that are acting on the stance leg are indicated as $\zeta_1(t)$ (ankle push-off force) and $\zeta_2(t)$ (torque due to the activation of the plantar flexors of the stance leg). States immediately before and after heel strike is indicated with '-' and '+' superscripts respectively.

The angular displacements are assumed to be small enough (< 0.5 rad.) (Polese et al., 2012; Ranavolo et al., 2011; Usherwood, 2005) to allow for first/second-order approximations during the stance phase. Kane's method (Kane and Levinson, 1985) is used to derive the equations of motion (EoM). Kane's dynamical equation is of the form $\bar{F}_r + \bar{F}_r^* = 0$, where $\bar{F}_r$ and $\bar{F}_r^*$ represents generalized active forces and generalized inertia forces respectively as described in (Kane and Levinson, 1985) (chapter 6, page 159). The equations in the form necessary for simulation is obtained using python libraries, the details of which are given in (Gede et al., 2013).

Symbols $m_1,\ m_2$ represent the mass of the body and swing leg respectively as shown in Fig. 5.2. The length of both the legs is represented by l. The variables associated with the system are the components of the vector $z = [\theta_1,\ \theta_2,\ \omega_1,\ \omega_2]^T$ which are the angles and angular velocities (w.r.t inertial frame for stance leg and w.r.t. stance leg frame for swing leg) as indicated in Fig. 5.2. There are two types of angular velocities. The one which corresponds to the rotation of the rigid body with respect to its centre of rotation is called spin angular velocity, and one which corresponds to the revolution of a point with respect to an origin is called orbital angular velocity. In this work, spin angular velocities with respect to the centre of rotation of the rigid links are considered as they rotate about the centre of rotation.

Hybrid systems (Lunze and Lamnabhi-Lagarrigue, 2009) are a class of dynamical systems, which exhibit both continuous states and discrete mode dynamics often associated with events such as resets, jumps, and switching. The continuous behaviour is typically governed by a system of differential equations (similar to Eq. 5.1) and the discrete part is governed by a vector-valued function (similar to Eq. 5.2) (Lunze and Lamnabhi-Lagarrigue, 2009)(chapter 1). The system's state determines the transition between the discrete and continuous governing equations in the overall phase space.

The dynamics in this work is governed by the general hybrid dynamical system of the form described in Sec. 3.2.5. The explicit dependence on t and λ given in the Sec. 3.2.5 is avoided here in the definition of the model (e.g. z is used instead

of $z(t)$).

$$\dot{z} = \mathcal{F}(z),\ z^- \notin S \tag{5.1}$$

$$z^+ = \Delta(z^-),\ z^- \in S \tag{5.2}$$

where,

$$S \ := \ \{z \in \chi \mid g_{reset}(z) = 0\} \tag{5.3}$$

where, $\mathcal{F}(z)$, $\Delta(z^-)$ and $g_{reset}(z)$ are continuous vector valued functions of z. In the absence of external torques acting on the leg, the term $\mathcal{F}(z)$ is,

$$\mathcal{F}(z) \ = \ \begin{bmatrix} \omega_1 \\ \omega_2 \\ \frac{1}{2l(m_1+m_2\sin^2(\theta_2))}\left(2gm_1\sin(\theta_1) - gm_2\sin(\theta_1+2\theta_2)\right. \\ \left.+gm_2\sin(\theta_1) + lm_2\omega_1^2\sin(2\theta_2) - 2lm_2\omega_2^2\sin(\theta_2)\right) \\ -\frac{\sin(\theta_2)}{l(m_1+m_2\sin^2(\theta_2))}\left(gm_1\cos(\theta_1) + gm_2\cos(\theta_1) - l\omega_1^2(m_1+m_2)\right. \\ \left.+lm_2\omega_2^2\cos(\theta_2)\right) \end{bmatrix} \tag{5.4}$$

The function, $\Delta(\cdot)$ is the reset map, $\chi \subset \mathbb{R}^4$ the state space, and $g_{reset}(\cdot)$ is the function that defines the heel strike. The set 'S' defines a surface where the heel strikes the ground and the states change abruptly according to the reset map. The z^- and z^+ indicate the states immediately before and after the heel strike respectively. The functions $\Delta(\cdot)$ and $g_{reset}(\cdot)$ are described in the subsequent sections.

As the body mass is considerably larger than the mass of the leg, the case where m_2 goes to 0 has only been considered. Further, small-angle approximation (valid for angles in the range $0 - 0.25\ rad.$ which is in the range in which the model is operating) leads to the following equation for $\dot{\omega}_1$ and $\dot{\omega}_2$

$$\dot{\omega}_1 \ = \ g\frac{\theta_1}{l} \tag{5.5}$$

$$\dot{\omega}_2 \;=\; -\frac{(g - l\omega_1^2)\theta_2}{l} \tag{5.6}$$

The ankle push-off forces of the stance leg supply the majority of the energy needed to propel the leg forward. When this neuromuscular forcing $\Gamma(t)$ is added to the stance leg, the Eq. 5.5 becomes,

$$\dot{\omega}_1 \;:=\; g\frac{\theta_1}{l} + \Gamma(t) \tag{5.7}$$

The forcing term $\Gamma(t)$ is derived in the following section.

5.1.3 Derivation of the Forcing Terms

The torques acting on the stance leg are derived in this section to generate the neuromuscular forcing term $\Gamma(t)$ for the stance leg. Torque produced by the plantar flexors on the trailing leg is defined as $G_r(t)$ and that on the leading leg as $G_l(t)$. These torques are assumed to be linearly related to the envelope of the EMG signals, which are positive functions of time (Nieuwboer et al., 2004). The torque $G_r(t)$ generates the ankle push-off force $F(t)$ and is assumed to be in phase with the heel strike. In the proposed model, the force $F(t)$ and the torque $G_l(t)$ are assumed to be

$$G_l(t) \;:=\; \tau_l(\sin(2\pi f_{r_1} t + \phi) + 1) \tag{5.8}$$

$$F(t) \;:=\; \tau_r(\sin(2\pi f_{r_2} t) + 1) \tag{5.9}$$

where τ_l and τ_r are constants. The variables, f_{r_1}, f_{r_2} and ϕ represent frequencies and the phase difference between torques on the leading and trailing leg respectively. Both frequencies are assumed to be unity. The ankle push off torque acting on the leading leg (in stance phase) can be calculated using the free body diagram shown in Fig. 5.3. The pivot points of the trailing leg and leading leg are 'O' and 'S' respectively. The effect of plantar flexor of the left and right legs on CoM, are opposite, while activated simultaneously. Trailing leg and leading leg subtends the same angle θ_1 w.r.t. the normal to the ground, as the trailing leg and leading leg

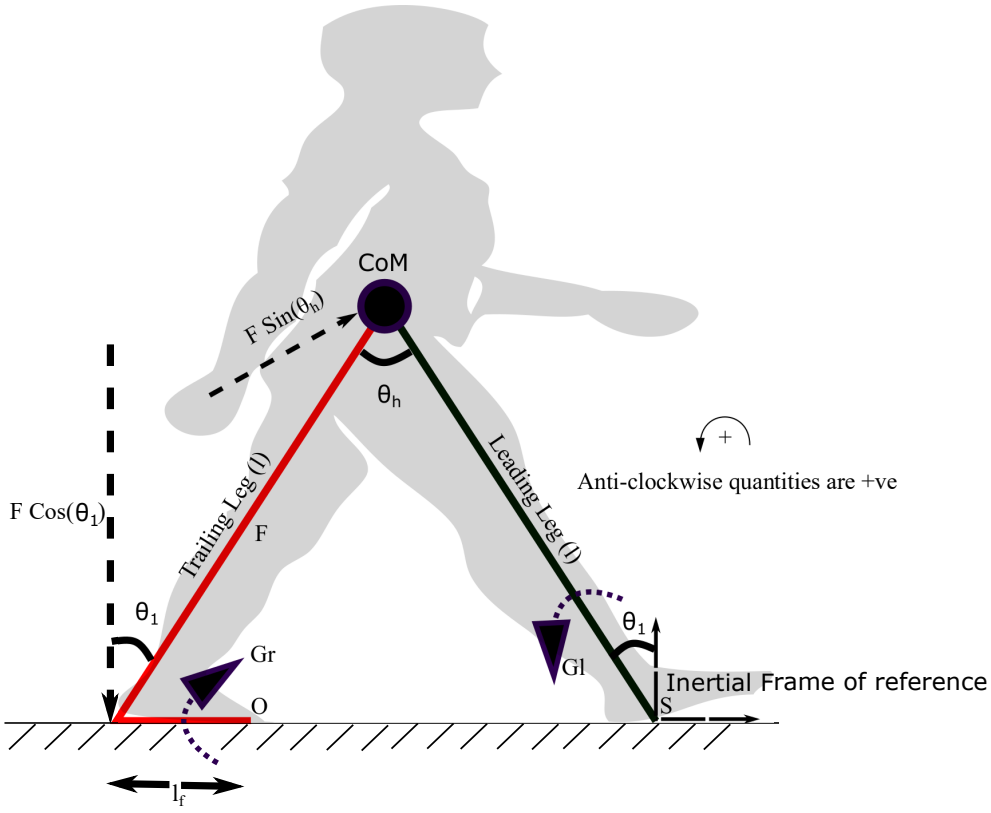

Figure 5.3: The diagram visualizes the forces and moments on leading and trailing leg that enable the movement of the centre of mass (CoM) forward. Symbols S and O indicate the points on leading and trailing leg about which the torques G_l and G_r are applied. G_r is the torque generated by the plantar flexors of the trailing leg, which results in a force F (ankle push-off) acting on the leading leg, about the point 'S'. The distance between the pivot point to the point of action of the force is l_f. The plantar flexors of the leading leg generate a torque G_l in the leading leg, in the opposite direction. The angle the leading leg subtends with the vertical axis at S is θ_1. θ_h represents the hip angle. The moments are balanced about 'S' to get the equations of motion (EoM). An approximate position of the starting stance phase is shown in the background in grey colour.

together with the ground is assumed to form an isosceles triangle. One could note that the double support phase is not explicitly modelled, and only forces acting parallel to the sagittal plane are considered. By balancing the moments about the point 'S' in Fig. 5.3 yields,

$$I\dot{\omega}_1 = G_l(t) - lF(t)\sin(\theta_h) + mgl\sin(\theta_1) \tag{5.10}$$

When angle θ_1 is small ($\sin(\theta) \approx \theta$) and since $I = m_1 l^2$, Eq. 5.10 is rewritten as,

$$m_1 l^2 \dot{\omega}_1 = G_l(t) - lF(t)\sin(\theta_h) + m_1 gl\theta_1 \tag{5.11}$$

Substituting $F(t)$ and $G_l(t)$ from Eq. 5.8 and Eq. 5.9 in Eq. 5.11, one obtains,

$$m_1 l^2 \dot{\omega}_1 = \tau_l(\sin(2\pi f_{r_1} t + \phi) + 1) - l\tau_r(\sin(2\pi f_{r_2} t) + 1)\sin(\theta_h) + m_1 gl\theta_1 \tag{5.12}$$

Rearranging Eq. 5.12, angular acceleration of the leading/stance leg is,

$$\dot{\omega}_1 = \frac{\overbrace{\tau_l(\sin(2\pi f_{r_1} t + \phi) + 1)}^{\text{Plantar flexors of the leading leg } (=\zeta_2(t))}}{l^2 m_1} - \frac{\overbrace{\tau_r l\sin(\theta_h)(\sin(2\pi f_{r_2} t) + 1)}^{\text{Ankle push off from trailing leg } (=\zeta_1(t))}}{l^2 m_1} + \overbrace{\frac{g\theta_1}{l}}^{Gravity} \tag{5.13}$$

$$:= \frac{\zeta_2(t) - \zeta_1(t)}{m_1 l^2} + \frac{g\theta_1}{l} \tag{5.14}$$

where $\Gamma(t) := \frac{(-\zeta_1(t)+\zeta_2(t))}{m_1 l^2}$ (as shown in Fig. 5.2) is the time varying neuromuscular forcing.

The initial velocity of the swing leg is assumed to be constant in every step. As the mass m_2 is assumed to be zero, the corresponding angular momentum is also equal to zero. Therefore, the angular velocity of the stance leg is reset to conserve its angular momentum and the initial angular velocity of the swing leg after reset is assumed to be a positive constant to account for the impulse during the ankle push-off. This is a valid assumption, as the definition of freezing in this work is independent of

the swing leg movement. A reset is carried out when $\theta_1 + \theta_2 = 0$ and $\theta_1 < 0$. Using Eq. 5.6 and Eq. 5.14, the equations of motion of a biped can be written as in Eq. 5.1 - 5.2, where the functions $\mathcal{F}(z)$, $\Delta(z)$, $g_{reset}(z)$ and the set S are written as follows,

$$\mathcal{F}(z) := \begin{bmatrix} \omega_1 \\ \omega_2 \\ \frac{\zeta_2(t)-\zeta_1(t)}{m_1 l^2} + \frac{g\theta_1}{l} \\ -\frac{(g-l\omega_1^2)\theta_2}{l} \end{bmatrix} \tag{5.15}$$

$$\begin{aligned} S &:= \left\{ \begin{bmatrix} \theta_1, & \theta_2, & \omega_1, & \omega_2 \end{bmatrix}^T \in \chi \mid g_{reset} \left(\begin{bmatrix} \theta_1, & \theta_2, & \omega_1, & \omega_2 \end{bmatrix}^T \right) = 0 \wedge \theta_1 < 0 \right\}, \\ g_{reset}(\cdot) &:= \theta_1 + \theta_2, \\ \Delta(\cdot) &:= \begin{bmatrix} -\theta_1, & -\theta_2, & \omega_1 \cos(\theta_h), & \omega_2^0 \end{bmatrix} \end{aligned} \tag{5.16}$$

with initial conditions $\omega_1(0) = \omega_1^0,\ \theta_1(0) = \theta_1^0,\ \omega_2(0) = \omega_2^0,\ \theta_2(0) = \theta_2^0$.

Remark 3 *It may be noted that the torque generated by the plantar flexors is assumed to act about the point 'O' as the pivot point. Balancing the moments due to the ankle push off force, $F(t)$ and $G_r(t)$ about the point O, the ankle push-off force can be determined in terms of $G_r(t)$ as,*

$$F(t) = \frac{G_r(t)}{l_f \cos(\theta_1)} \tag{5.17}$$

Here, the distance, l_f is taken between the heel to the pivot point on the foot for calculating the moments, as shown in Fig. 5.3. Therefore, implicitly, the following assumption has been made while prescribing $F(t)$.

$$\frac{G_r(t)}{l_f \cos(\theta_1)} := \tau_r(\sin(2\pi f_{r_2} t) + 1) \tag{5.18}$$

5.1.4 Rationale for Using a Low dimensional Model for Analysis

The angular velocity of the stance leg contributes directly to the angular acceleration of the swing leg. A higher absolute angular velocity of the stance leg leads to lower acceleration of the swing leg. However, the dynamics of the stance leg in Eq. 5.14 is uncoupled from the dynamics of the swing leg and hence resembles the dynamics of an '*inverted pendulum system*'. It may be noted that the term '$l\omega_1^2$' can be approximated to a constant as in the physiological range of low angular velocities (especially in PD patients) $g >> l\omega_1^2$ (typically quantity $l\omega_1^2 = 0.448$ m.rad^2.$s^{-2} = 0.7 \times 0.8^2$ is of order '0' while $g = 9.8$ m.s^{-2} is of order 1). This results in a condition where the swing leg acts independently of the stance leg, effectively determining the step length. Therefore, an inverted pendulum walking model for PD subjects is adequate when constant step length is assumed. Fig. 5.1 depicts the physical rationale behind the use of an inverted pendulum model. The constant step length assumption is general enough to explain the variability in stepping as this leads to variability in stepping angular velocities rather than step lengths. In summary, the analysis of the stance phase walking model in light of the PD walking behaviour at a constant step length is presented in the following sections. Physiologically, the hip applies torques on the swing leg and controls its initial angular velocity. The hip torques acting on the swing is not relevant in propelling the CoM forward, as most of the torque required for that is provided by the ankle (Zelik and Adamczyk, 2016). Therefore, an assumption made on the swing leg angular velocity will not affect the model's applicability to the freezing problem, as freezing is linked to the inability of the legs to propel the CoM forward in the case of walking. Hence, swing leg angular velocity is reset to ω_2^0 in every step. Furthermore, as there is no swing leg in the low dimensional model, one could avoid explicitly specifying the parameter ω_2^0 and any associated assumptions.

5.2 Analysis of the Reduced System

When considered independently of the swing leg, the dynamics has states corresponding only to the stance leg, i.e. $z = [\theta_1,\ \omega_1]^T$. The terms defining the Eq. 5.1 - 5.2 for the inverted pendulum case are given below.

$$q(\cdot) := \begin{bmatrix} \omega_1 \\ \frac{\zeta_2(t)-\zeta_1(t)}{m_1 l^2} + \frac{g\theta_1}{l} \end{bmatrix} \tag{5.19}$$

$$S := \left\{ \begin{bmatrix} \theta_1, \omega_1 \end{bmatrix}^T \in \chi \mid g_{reset}\left(\begin{bmatrix} \theta_1, \omega_1 \end{bmatrix}^T \right) = 0 \right\} \tag{5.20}$$

$$g_{reset}(\cdot) := \theta_1 - \theta_{reset} \tag{5.21}$$

$$\Delta(\cdot) := \begin{bmatrix} -\theta_1, \omega_1 \cos(\theta_h) \end{bmatrix}^T \tag{5.22}$$

As the inverted pendulum model is analysed independently, θ_1, m_1, θ_1^0 and ω_1^0 will be referred here as θ, m, θ_0 and ω_0 respectively. These equations are solved to produce the motion trajectory during the stance phase of the stepping cycle. The sequence of model evolution is depicted in Fig. 5.4, with the beginning and end of the stance positions, initial angular position (θ_0), initial angular velocity (ω_0) and the angle at reset (θ_{reset}). Step length is defined to be equal to $|\theta_{reset}|$ where $|.|$ denotes the absolute value. This definition of steplength is valid as the leg length is assumed constant in the model. As the physical meaning of θ_{reset} is the angle subtended by the stance leg during a heel strike, one could note that its value can vary when one walks with a different stride length or when the ground is not uniform. Moreover, θ_{reset} determines the initial angle for every step except the first step (as the first step can start from any arbitrary physiologically meaningful angle). In a biped model, the θ_{reset} is implicitly determined, but in the case of the inverted pendulum, it is not, as the model does have a swing leg.

5.2.1 Gait Cycle

The proposed model explicitly considers only the single support period of the *'stance'* phase of the gait cycle. However, the forces and reset happening at double support

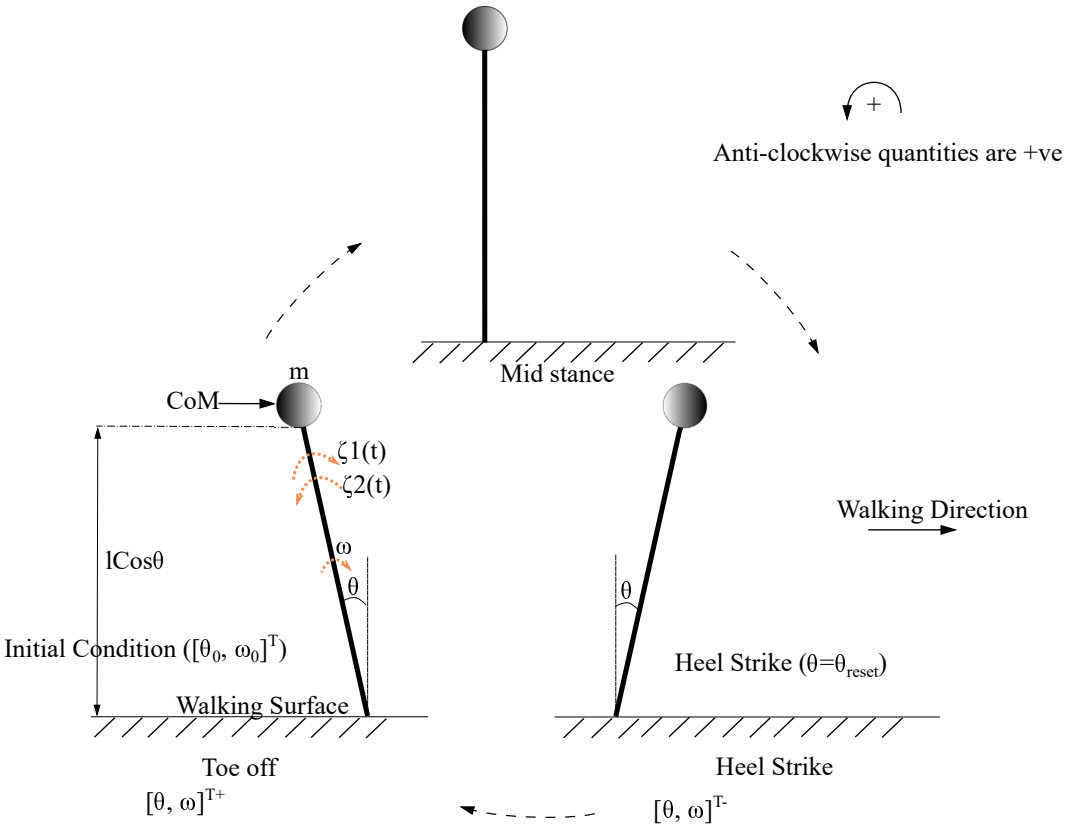

Figure 5.4: Gait cycle for the low dimensional (*inverted pendulum system*) system is shown. Terms $[\theta_0, \omega_0]^T$ and $[\theta_0, \omega_0]^{T-}$ indicate the initial and final angular position and velocity of the leading/stance leg respectively at the beginning and end of the stance phase. θ_{reset} is the angular displacement at which the angle is reset. The CoM (centre of mass) which is assumed to be acting as a point mass at the tip of the inverted pendulum is shown as a circle. States before and after heel strike is indicated with '-' and '+' superscripts respectively.

period are accounted for. Therefore, 'gait cycle' in this study has been defined as the process where the model states evolve from an initial condition of a step (end of 'double support phase') until the reset condition (where the heel of the swing leg is assumed to collide with the ground or 'heel strike condition') is met and the initial condition of the next step is computed. Here, the state of the system moves through three different states (end of 'double support phase' (this is defined as the beginning of the stance in this model as the double support phase is not explicitly modelled), end of the *'stance'* (before the collision of the contra-lateral leg) and heel strike (after the collision of the contra-lateral leg)) whose notations are given below

(Eq. 5.23) [1], [2].

$$[\theta_0,\ \omega_0]^T \mapsto \underbrace{[\theta_0^-,\ \omega_0^-]^T}_{\text{Before collision}} \mapsto \underbrace{[\theta_0^+,\ \omega_0^+]^T}_{\text{After collision}} = [\theta_1,\ \omega_1]^T \tag{5.23}$$

Here $[\theta_0,\ \omega_0]^T$, $[\theta_0^-,\ \omega_0^-]^T$, $[\theta_0^+,\ \omega_0^+]^T$ correspond to the states at the initiation of the step, states at the end of the flow 'immediately' before collision, and states 'immediately' after collision respectively. The states immediately after collision form the initial condition for the next step $[\theta_1,\ \omega_1]^T$. The superscripts ('-', '+') need not indicate the relative sizes of the states but the sequential order in which they appear that is '-' superscript represents before collision variables, and '+' represents after the collision. But it should be noted that the transformation from $[\theta_0^-,\ \omega_0^-]^T$ to $[\theta_0^+,\ \omega_0^+]^T$ happens instantaneously in the model. Counterclockwise angles are defined as positive. In a typical walking simulation, this results in $\theta^- < 0 < \theta^+$. That is, the stance phase ends at a negative value for the angle and resets to a positive value before beginning the next stance phase.

When step number is not relevant, subscripts indicating the step number will be dropped, from before and after collision state symbols for the derivation of the Eq. 5.24. The same superscript will be used while referring to other parameters which change during collision [3].

The states $[\theta,\ \omega]^T$ evolve as a function of time except at the collision point, where the same time point maps to two different state values. [4]

$$[\theta_n,\ \omega_n]^T \mapsto \underbrace{[\theta^-,\ \omega^-]^T}_{\text{Before collision}} \mapsto \underbrace{[\theta^+,\ \omega^+]^T}_{\text{After collision}} = [\theta_{n+1},\ \omega_{n+1}]^T \tag{5.24}$$

5.2.2 Heel Strike Condition

A heel strike is defined as the state at which the swing leg (trailing leg) collides with the ground. This is modelled using an appropriate reset condition. At heel

[1] Here $a \mapsto b$ indicates state a 'maps to' state b after some time t where $t \geq 0$

[2] $[z_1^-,\ z_2^-]^T$ and $[z_1,\ z_2]^{T-}$ are used interchangeably, where, z_1 and z_2 are components of some vector

[3] p^- and p^+ refers to any parameter p before and after collision respectively in a particular step cycle.

[4] $\theta(t)$ and $\omega(t)$ are multi-valued functions at the point of collision.

strike, both the angle and angular velocity are reset from the 'before collision' to 'after collision' state as described in Eq. 5.24. The collision of the swing leg (trailing leg) at heel strike is modelled to be inelastic with angular momentum conserved. Therefore, the magnitudes of the angular momentum about the point of collision after and before collision are equated in the following way to create the transition rule for angular velocity

$$lm(v^{+}\sin(\pi/2)) = lm(v^{-}\sin(\pi/2+\theta_h)) \tag{5.25}$$

$$lm(l\omega^{+}) = lm(l\omega^{-})\cos(\theta_h) \tag{5.26}$$

$$\omega^{+} = \omega^{-}\cos(\theta_h) \tag{5.27}$$

at the n^{th} iteration(step)

$$\omega_{n+1} = \omega_n^{+} = \omega_n^{-}\cos(\theta_h) \tag{5.28}$$

where θ_h is the hip angle. The angle, on the other hand, will be reset from θ^{-} to $-\theta^{-}$. This results in the following transition rules at $\theta^{-} = \theta_{reset}$

$$\omega_n^{+} = \omega_n^{-}\cos(\theta_h) \tag{5.29}$$

$$\theta_n^{+} = -\theta_n^{-} \tag{5.30}$$

Rearranging one obtains $\Delta(\cdot)$ as

$$\Delta\left(\left[\theta,\ \dot{\theta}\right]^{T-}\right) = \left[-\theta,\ \dot{\theta}\cos(\theta_h)\right]^{T} \tag{5.31}$$

5.2.3 Analytical and Numerical Solution of the Equations of Motion

The differential equation Eq. 5.1, was solved using the definition of the vector field given in Eq. 5.19 analytically to obtain the flows given below.

$$\begin{aligned}\theta(t) &= f_\theta(t,\ \omega_0,\ \theta_0) := N_1/D_1 \\ \omega(t) &= f_\omega(t,\ \omega_0,\ \theta_0) = \frac{d}{dt}(f_\theta) := N_2/D_2\end{aligned} \tag{5.32}$$

where the terms N_1, D_1, N_2 and D_2 of the analytical solution are given below.

$$\begin{aligned}N_1 = {} & l(\Psi_N^2+\Omega_1^2)(lm(\Psi_N^2+\Omega_2^2)(\theta_0\sqrt{l}\Psi_N^2(e^{2t\Psi_N}+1)+\omega_0\sqrt{l\Psi_N^2}(e^{2t\Psi_N}-1)) \\ & -\tau_r\sin(\theta_h)(\Omega_2(e^{t\Psi_N}-1)(\sqrt{l}\Omega_2(e^{t\Psi_N}-1)+\sqrt{l\Psi_N^2}(e^{t\Psi_N}+1))+ \\ & \sqrt{l}\Psi_N^2((e^{t\Psi_N}-1)^2-2e^{t\Psi_N}\sin(t\Omega_2)))+\tau_l(\Psi_N^2+\Omega_2^2) \\ & (\sqrt{l}\Psi_N^2((e^{t\Psi_N}-1)^2-2e^{t\Psi_N}\sin(t\Omega_1+\phi)+\sin(\phi)(e^{2t\Psi_N}+1)) \\ & +\Omega_1(e^{t\Psi_N}-1)(\sqrt{l}\Omega_1(e^{t\Psi_N}-1)+\cos(\phi)\sqrt{l\Psi_N^2}(e^{t\Psi_N}+1)))\end{aligned} \tag{5.33}$$

$$D_1 = 2l^{5/2}m\Psi_N^2e^{t\Psi_N}\left(\Psi_N^2+\Omega_1^2\right)\left(\Psi_N^2+\Omega_2^2\right)$$

$$\begin{aligned}N_2 = {} & l(\Psi_N^2+\Omega_1^2)(lm(\Psi_N^2+\Omega_2^2)(\theta_0\sqrt{l}\Psi_N^2(e^{2t\Psi_N}-1)+\omega_0\sqrt{l\Psi_N^2}(e^{2t\Psi_N}+1)) \\ & -\tau_r\sin(\theta_h)(\Omega_2(\sqrt{l}\Omega_2(e^{2t\Psi_N}-1)+ \\ & \sqrt{l\Psi_N^2}(e^{2t\Psi_N}+1))-2\sqrt{l}\Omega_2\Psi_Ne^{t\Psi_N}\cos(t\Omega_2)+\sqrt{l}\Psi_N^2(e^{2t\Psi_N}-1))) \\ & +\tau_l(\Psi_N^2+\Omega_2^2)(-2\sqrt{l}\Omega_1\Psi_Ne^{t\Psi_N}\cos(t\Omega_1+\phi) \\ & +\Omega_1(\sqrt{l}\Omega_1(e^{2t\Psi_N}-1)+\cos(\phi)\sqrt{l\Psi_N^2}(e^{2t\Psi_N}+1)) \\ & +\sqrt{l}\Psi_N^2(\sin(\phi)+1)(e^{2t\Psi_N}-1))\end{aligned} \tag{5.34}$$

$$D_2 = 2l^{5/2}m\Psi_Ne^{t\Psi_N}\left(\Psi_N^2+\Omega_1^2\right)\left(\Psi_N^2+\Omega_2^2\right)$$

where,

$$\begin{aligned} \Omega_1 &= 2\pi f r_1 \\ \Omega_2 &= 2\pi f r_2 \\ \Psi_N &= \sqrt{g/l} \end{aligned} \tag{5.35}$$

The analytical solution is intended to be used for the bifurcation analysis as numerical solutions may not always be able to detect the chaotic behaviour (Lozi, 2013). Therefore, a discrete map governing the motion will be derived using the analytical solution in the following sections. A numerical solution of the Eq. 5.1 - 5.2 using definitions given in Eq. 5.19 - 5.22 with the appropriate reset conditions (in the physiological range) are solved to show the freezing behaviour and dynamics in the phase plane. PD subjects are known to freeze intermittently. Therefore, the time the subject walks until the freeze could be considered an important measure to quantify transient walking behaviour. A simulation for a 10 s window is carried out for different values of the parameters τ_l and τ_r (for a constant initial condition). The total time for which transient walking behaviour occurred is computed numerically as a function of the parameters τ_l and τ_r. Numerical methods are also used in solving boundary value problems to gain further insights into the system, as given in the remark 4.

Remark 4 *The parameters τ_l and τ_r determine the amount of energy supplied to the system apart from gravity. To understand how they influence the kinetic energy of the system, the difference in speed between the initial and final states are compared for the boundary value problem with boundary conditions $\theta_0 = 0$ rad. and $\theta_{0.5} = -0.1$ rad. with definitions given in Eq. 5.19 - 5.22 unchanged. Here, the boundary conditions are chosen from the physiological range.*

The quantities $\tau_l,\ \tau_r,\ \omega,\ \phi,\ \theta_{reset}$ and step length have units N m, N, rad. s^{-1}, rad., rad. and rad. respectively, when not specified.

5.2.4 Derivation of a Map to Describe Successive Stance Phases

The evolution of the flow (given by Eq. 5.32) is terminated when the swing leg meets the ground. In other words, when there is sufficient energy in the system for forward motion, there exists a 'reset time' $T(\theta_0,\ \omega_0)$ such that $f_\theta(T(\theta_0,\ \omega_0),\ \omega_0,\ \theta_0) = A_{reset}(\theta_0)$. Here, $A_{reset}(\cdot)$ is a function of the joint angle and the ground that determines the angle of the stance leg while the foot strikes the ground. The arguments associated with the reset time $T(\theta_0,\ \omega_0)$ will be dropped and will be referred to as T from here on. Accounting the transition rules in Eq. 5.29 for reset and conservation of angular momentum,
one defines[5]

$$\theta_1 = \theta^+(T) := -f_\theta(T,\ \omega_0,\ \theta_0) \tag{5.36}$$

$$\omega_1 = \omega^+(T) := f_\omega(T,\ \omega_0,\ \theta_0)\cos(\theta_h) \tag{5.37}$$

Following an induction hypothesis, for an arbitrary initial condition $(\theta_n,\ \omega_n)$ the map is

$$\theta_{n+1} = -f_\theta(T,\ \omega_n,\ \theta_n) \tag{5.38}$$

$$\omega_{n+1} = f_\omega(T,\ \omega_n,\ \theta_n)\cos(\theta_h) \tag{5.39}$$

The following definitions are made to make the notations compact for further analysis

$$\theta_{n+1} = \tilde{f}_\theta(T,\ \omega_n,\ \theta_n) := -f_\theta(T,\ \omega_n,\ \theta_n) \tag{5.40}$$

$$\omega_{n+1} = \tilde{f}_\omega(T,\ \omega_n,\ \theta_n) := f_\omega(T,\ \omega_n,\ \theta_n)\cos(\theta_h) \tag{5.41}$$

where $\tilde{f}_\omega(T,\ \omega_n,\ \theta_n,\ \phi)$ and $\tilde{f}_\theta(T,\ \omega_n,\ \theta_n,\ \phi)$ are T parametrized family of maps for $(\omega_n,\ \theta_n) \mapsto (\omega_{n+1},\ \theta_{n+1})$.

[5]Even though the symbol $\theta(T)$ is used at the point of collision, it may be noted that this is a one to many mapping and therefore is not a single valued function in the traditional sense of the word.

To investigate the condition of same step lengths and to generate a 1D map for further evaluation, $A_{reset}(\theta, t)$ is set to be θ_{reset}. Here θ_{reset} is an arbitrary angle in the physiological range at which the swing leg meets the ground. Then for an intermediate step, (when there is sufficient energy to move forward) there exists a $\tilde{T}$ s.t. $\tilde{f}_\theta(\tilde{T}(\theta_n,\ \omega_n),\ \omega_n,\ \theta_n) = \theta_n = -\theta_{reset}$. When there is not enough energy and therefore momentum to move forward, the model behaviour is defined as freezing.

To find the $\tilde{T}$ at which θ_n maps to itself, the following minimization problem is solved [6] using Newton's method (*Mathematica, Version 12.0*). This detects implicitly the time at which the swing leg collides with the ground.

$$\tilde{T}(\theta_n,\ \omega_n) := \arg\min_{T}(\tilde{f}_\theta(T,\ \omega_n,\ \theta_n,\ \phi) - \theta_n) \tag{5.42}$$

Substituting $\tilde{T}$ from Eq. 5.42 in Eq. 5.41 the following map is obtained.

$$\begin{aligned} \omega_{n+1} &= \tilde{f}_\omega(\tilde{T}(\theta_n,\ \omega_n),\ \omega_n,\ \theta_n) \\ &:= H(\omega_n) \text{ when } \theta_n = \theta_0\ \forall n \in \mathbb{N} \end{aligned}$$

When used as a 1D map,

$$\omega_{n+1} := \tilde{f}_\omega(\omega_n) \tag{5.43}$$

The argument $\tilde{T}$ in the function will be dropped from here-on. The function $\tilde{T}$ acts on the same input ω_n and $\theta_n = \theta_0$. This map has been analysed to show the freezing behaviour and variabilities associated with PD walking. The map has been studied for a particular parameter value to show the presence of horseshoe in the Sec. 5.2.5.

Remark 5 *Eq. 5.1 - 5.2 represent a general hybrid system. When the hybrid bipedal system's solution is sought these equations are solved using the definitions given in Eq. 5.15 - 5.16 ; and, Eq. 5.19 - 5.22 are used for hybrid inverted pendulum system.*

[6] The objective function is appropriately constrained to the positive real numbers such that the solution of the minimization problem forms the root of the equation $\tilde{f}_\theta(T,\ \omega_n,\ \theta_n,\ \phi) - \theta_n = 0$.

5.2.5 Graphical Analysis of the Map Between Stance Phases

A horseshoe is a characteristic of a map which indicates chaos under iteration. Here, the presence of a horseshoe has been shown for a set of parameter values in the physiological range for the map developed ($\tilde{f}_\omega$). Using the conditions for horseshoe and therefore chaos, given in (Glendinning, 1994), the presence of the same could be shown for $\tilde{f}_\omega^n$ (the function $\tilde{f}_\omega$ composed n times).

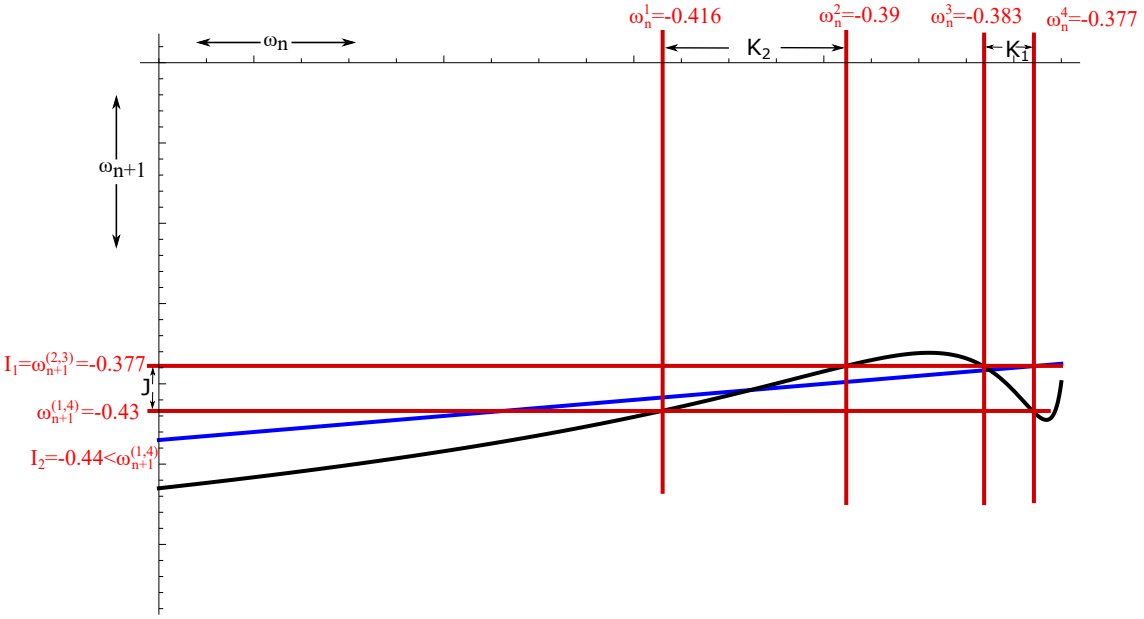

Figure 5.5: There is a horseshoe in the interval between I_1 and I_2 for the map $\tilde{f}_\omega$. The proof is given in Sec. 5.2.5. An unstable equilibrium is formed in the interval K_2 ($|\dot{\tilde{f}}_\omega| > 1$) and an outward spiralling equilibrium in the interval $K_1(|\dot{\tilde{f}}_\omega| < -1)$. Blue line is the identity, the black curve is the map $\tilde{f}_\omega$. A set of red lines are drawn perpendicular to the axis to indicate that the intervals K_1 and K_2 maps to J.

Proposition 5.2.1 *For the map $\tilde{f}_\omega$ a horseshoe exists in the interval $I = [I_1,\ I_2] = [-0.377,\ -0.44]$. The parameters used are $\tau_l = 5$, $\tau_r = 35$, $l = 0.6\ m$, $g = 9.8\ m\ s^{-1}$, $m = 70Kg$.*

Proof Let $\omega_n^4 = -0.377,\ \omega_n^3 = -0.383,\ \omega_n^2 = -0.39,\ \omega_n^1 = -0.416,\ \omega_{n+1}^{(2,\ 3)} = -0.377,\ \omega_{n+1}^{(1,\ 4)} = -0.43,\ -0.44 = I_2 < \omega_{n+1}^{(1,\ 4)}$. Let the intervals be chosen in the following manner $I = [I_1,\ I_2],\ J = [\omega_{n+1}^{(2,\ 3)},\ \omega_{n+1}^{(1,\ 4)}]$ and $\omega_n^4 = \omega_{n+1}^{(2,\ 3)}$. One also has, $K_1 = [\omega_n^4,\ \omega_n^3],\ K_2 = [\omega_n^2,\ \omega_n^1]$. $\tilde{f}_\omega(K_2) \mapsto \tilde{f}_\omega(K_1) \mapsto [\omega_{n+1}^{(2,\ 3)},\ \omega_{n+1}^{(1,\ 4)}] = epJ$ (end

point preserved J). $K_1 \subset J,\ K_2 \subset J,\ \ J \subset I,\ \ K_1 \cap K_2 = \varnothing$ and $\tilde{f_\omega} \in C^0(I,\ \mathbb{R})$. Therefore, there is a horseshoe in the interval.

5.3 Results

Numerical simulation of the PD-Gait and associated freezing behaviour is described in this section. The change in the angular velocity from negative to zero is a property of any solution containing freezing by definition. Typically, in this model, the angular velocity changes to a positive value under the action of gravity during a freeze. The effect of variation of the parameters $\tau_l,\ \tau_r,\ \phi,\ \theta_{reset}$ are also investigated. The work in this chapter shows that the two opposing torques produced from the plantar flexors could elicit freezing and chaotic behaviour. The ability of these torques to cause freezing behaviour has been shown first in a simplified biped model described using Eq. 5.15 - 5.16, and then in the inverted pendulum model generated by Eq. 5.19 - 5.22. As argued previously, the inverted pendulum dynamics sufficiently captures the PD walking scenario. The results are presented in the sequel to support this hypothesis. Also, walking is the process of moving the CoM by pushing the stance leg forward, and the inverted pendulum model helps to study the effect of the stance leg independent of other variables. A range of values for the parameters $\tau_l,\ \tau_r,$ and ϕ have been analysed to clarify the trend in behaviour. The range in which the behaviour of the map $\tilde{f_\omega}$ changes the number of periodic orbits from 'zero' to 'more than one' in the lower absolute value of angular velocity conditions, is given in Table 5.1. Simulations are carried out to understand the behaviour of the system over and above this range. But it may be noted that the maximum value of the torque for $l = 0.6$ m., $\theta_{reset} = -0.1$ rad. is approximately $0.23|\tau_r|$ N m and $2|\tau_l|$ N m in forward and backward directions respectively. Hence, in this case, forward pushing plantar flexors has to generate 8.7 times the 'premature activation of plantar flexors' to cancel the effect if the phase is exactly matched. Physiologically, the minimum value of these torques is zero, and the maximum is subject-specific.

5.3.1 Freezing in a Biped Model

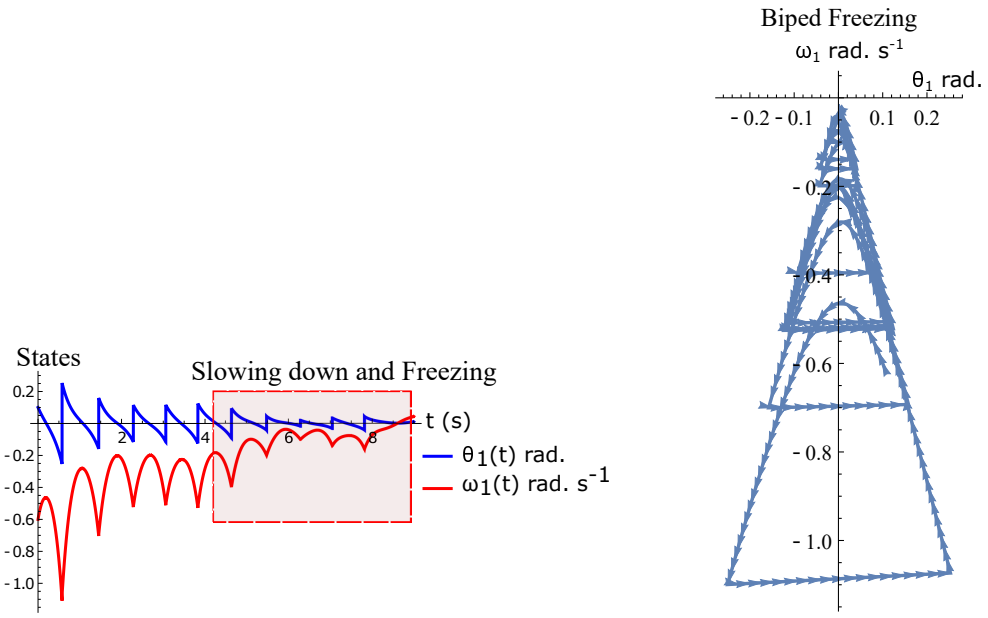

(a) (b)

Figure 5.6: Results of numerical simulation of the biped during freezing. Parameters are chosen to be $\tau_l = 2.3$ N m, $\tau_r = 15.74$ N, $\phi = -\pi/2$ rad. and initial conditions $\theta_2(0) = -0.1$ rad., $\theta_1(0) = 0.1$ rad., $\omega_2(0) = 2$ rad. s^{-1}, $\omega_1(0) = -0.6$ rad. s^{-1}. The change in the θ_{reset} in every step and gradual reduction in θ_1 nearer to a freezing event is evident. (a) Simulated time series of the states θ_1 and ω_1. Region of slowing down and freezing is highlighted (b) Shows numerical simulation of biped in the phase plane.

The hybrid system (Eq. 5.1 - 5.2) defined by the Eq. 5.15 - 5.16 are simulated numerically, and the results are shown in Fig. 5.6a - 5.6b. The figure indicates normal walking for the first few steps and then freezing thereafter(highlighted). The gradual reduction in step length observed experimentally prior to freezing (Nutt et al., 2011) is also observed in the model.

There are two dissipative forces in this model: the opposing torques due to the plantar flexors and the dissipation at the heel strike. Long-range walking will be achieved when the speed gain in every step compensates for these two effects. The neuromuscular system cannot control the dissipative effect of the heel strike, but the effect of plantar flexors can. Fig. 5.7a - 5.7b illustrates the effect of the plantar flexors in this regard.

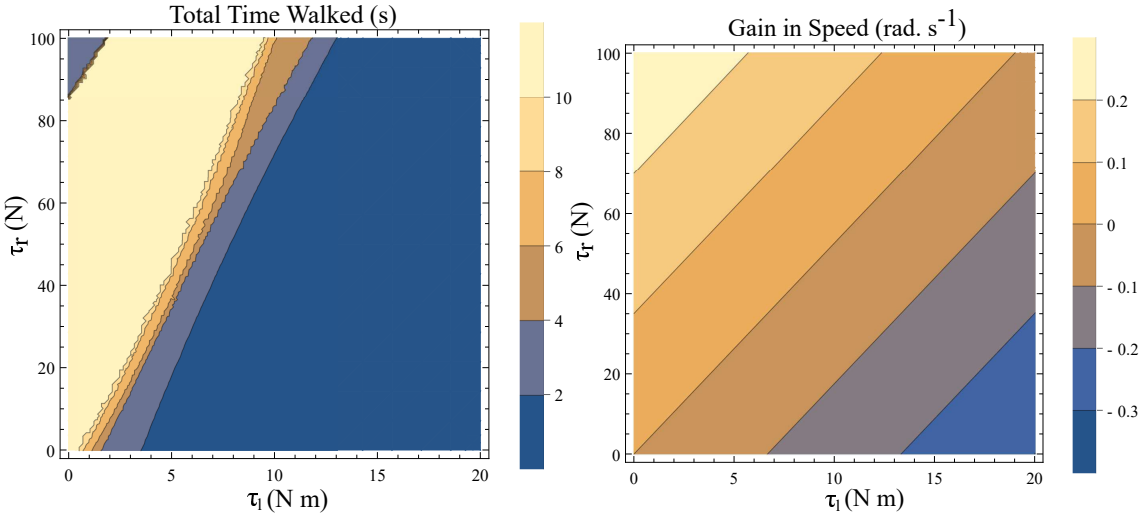

(a) (b)

Figure 5.7: (a) A simulation was carried out for a time window of 10 s, and the total time walked before freezing was computed. This time is plotted as a function of τ_l and τ_r. The initial conditions are set to be $\theta_2(0) = -0.1$ rad., $\theta_1(0) = 0.1$ rad., $\omega_2(0) = 1$ rad. s^{-1}, $\omega_1(0) = -0.6$ rad. s^{-1} and $\phi = -\pi/2$ rad. The yellow region forms the optimal region of the parameters τ_l, τ_r where walking is achieved. (b) Contour plot of the difference in speed($|\omega(0)| - |\omega(0.5)|$) as a function of τ_l and τ_r determined by solving a BVP numerically with $\theta_0^0 = 0$ and $\theta_1^{0.5} = -0.1$ rad. for the biped model with the other initial conditions being $\theta_2^0 = -0.1$ rad., $\omega_2^0 = 1$ (and $\phi = -\pi/2$ rad.). This illustrates a decrease in the speed and therefore kinetic energy when there is an increase in τ_l and a decrease in τ_r.

A simulation was carried out for a 10 s window and computed the time difference between the start of the simulation and the time of the last heel strike before the freezing event (as defined in remark 2). This is shown as a function of the parameters τ_l and τ_r in Fig. 5.7a. The blue shades indicate eventual freezing and shorter walking time, and the yellow region is the safer non-freezing region. Moreover, there is an intermediate region of parameter τ_l and τ_r in which the walking happens without freezing in the 10 s window. A higher value of τ_l necessitates a higher τ_r for walking. Nevertheless, a very high τ_r does not necessarily exhibit balanced walking, as it can result in a lack of coordination between the swing leg and the stance leg. Although the initial value problem (IVP) in Fig. 5.7a and boundary value problem (BVP) in Fig. 5.7b cannot be directly compared, they show analogous qualitative results. That is, to achieve the same speed gain (or kinetic energy (KE) gain), a higher τ_l demands a higher τ_r. Therefore, a key aspect of PD freezing is the inability of the two plantar flexors to coordinate to produce the required energy. From an energy point of view, the role of the swing leg is essentially in the generation of ankle push of force. In the following sections, the dynamics of the stance leg is studied independently using an inverted pendulum model, reducing the role of the swing only as a supplier of the ankle push-off force.

5.3.2 Freezing in an Inverted Pendulum Model

Freezing is a condition where there is no more forward motion of the leg. Numerical simulation of such a scenario in the inverted pendulum model is shown in Fig. 5.8a where there is a freezing episode after 18 s. A gradual reduction in step length observed in the biped model translates to the increased time taken to make the final few steps before freezing. The simulation in the phase plane for the last three steps is shown in Fig. 5.8b. The dissipative torques due to the opposing plantar flexors act in the same way in the inverted pendulum model. Fig. 5.9a - 5.9b illustrate this similarity, where an increased τ_r generates higher speed gains and an elevated τ_l results in lower speed gains and lower total walk times. This is because increasing parameter τ_r strengthens the forward ankle push-off while larger τ_l amplifies the

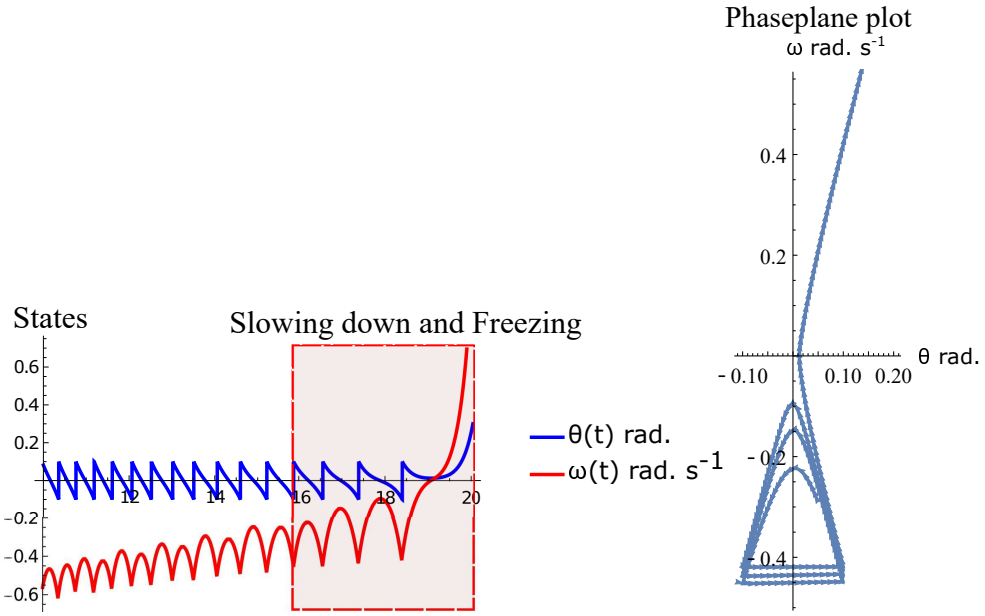

(a) (b)

Figure 5.8: Simulation of the inverted pendulum dynamics for the parameter values $\phi = -\pi/2$ rad., $\omega_0 = -1$ rad. s^{-1}, $\tau_l = 2$ N m, $\tau_r = 11$ N. Freezing occurs after 18s (a) States θ and ω as a function of time (10-20 s). Region of slowing down and freezing is highlighted (b) Numerical simulation of the inverted pendulum states in the phase plane for 16-20 s

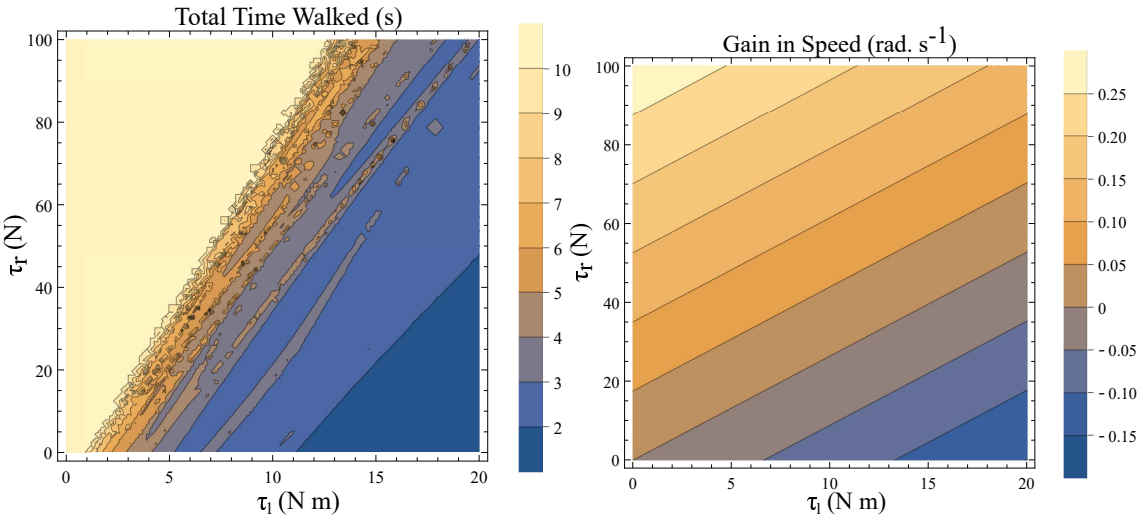

(a) (b)

Figure 5.9: (a) A simulation was carried out for a time window of 10 s, and the total time of walking before freezing was computed. This time is plotted as a function of τ_l and τ_r. The angle is reset when $\theta(t) = -0.1$ rad. and $\phi = -\pi/2$ rad. The colours indicate the duration of the walk (see the legend)(b) Contour plot of difference in speed ($|\omega(0)| - |\omega(0.5)|$) as a function of τ_l and τ_r determined by solving a BVP with $\theta_0 = 0$ rad. and $\theta_{0.5} = -0.1$ rad. (and $\phi = -\pi/2$ rad.) in Eq. 5.1 - 5.2 using definitions in Eq. 5.19 - 5.22. This illustrates a decrease in the speed and therefore KE when there is an increase in τ_l and a decrease in τ_r.

dissipative torque. A critical difference between the inverted pendulum model and the biped model is that a higher τ_r will not result in an imbalance in the former as there is no swing leg in that model, while there is a lack of balance in the latter. The contour plot of the speed differences as a function of τ_l and τ_r is shown in Fig. 5.9b. The figure shows that a higher value of τ_l and a lower value of τ_r result in negative speed gain (reduction in KE). Numerical simulation of the total time of the walk, defined as the difference between the time in which the first step is taken, and the last step before freezing in 10 s, is shown in Fig. 5.9a. More than 9 s of walking indicates that there is no freezing in that parameter range in that time frame. A higher τ_r and lower τ_l results in better walking performance as in the case of a biped. Therefore, energetically, PD related behaviour that is of interest is analogous in the inverted pendulum and biped model. Therefore, the analytical solution of the inverted pendulum model is investigated further to understand the consequence of the change in parameters τ_l, τ_r and ϕ. These parameters are controlled by the neural system, while others, such as the mass of the body and length of the legs are not. The quantity θ_{reset} distinguishes the inverted pendulum model from the biped model. Hence, the effect of this parameter is also studied.

5.3.3 Parameter Exploration of Inverted Pendulum: Study of the Map $\tilde{f}_\omega$

The neural control on the muscles modifies the magnitude and the phase of the control signals. Investigation of the parameters τ_l, τ_r and ϕ, therefore, reveals the effect of the neural control on walking dynamics. One of the hypotheses investigated through the model is the generation of variability through the premature activation of the plantar flexors. The phase difference of the 'premature' activation is quantified using the parameter ϕ in the model. Fig. 5.10 shows the bifurcation diagram of the parameter ϕ in the range 0 to -2π for constant values of τ_l and τ_r. A period-doubling route to chaos can be observed when ϕ is varied between -5π/8 to $-\pi/4$. The map $\tilde{f}_\omega$ is iterated for 500 walking cycles, and the last 50 walking cycles are used to compute the equilibrium points. The Feigenbaum bound is found to be at $\phi = -1.37$

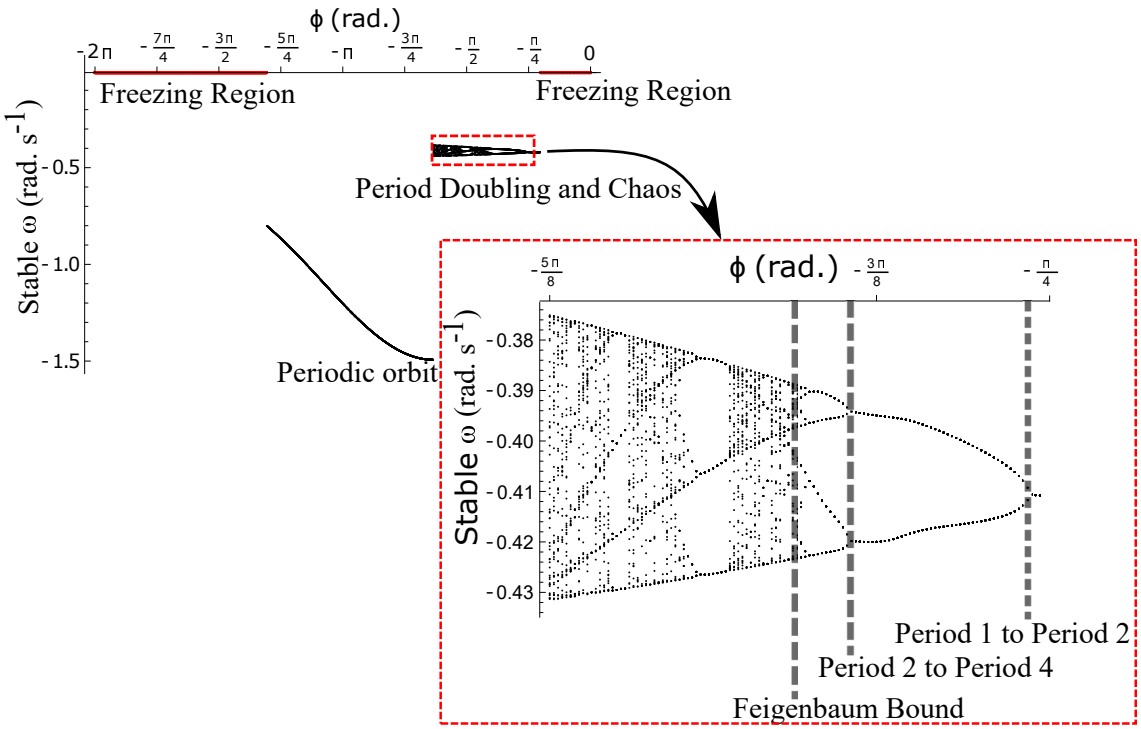

Figure 5.10: Stable ω is shown as a function of the parameter ϕ for $\omega_0 = -0.433$ rad.s^{-1}, $\tau_l = 5$ N m, $\tau_r = 35$ N. The Feigenbaum bound was found to be at $\phi = -1.37$ rad. where walking becomes fully chaotic. The period-doubling cascade has been highlighted and enlarged. This chaotic region forms only a small part of the overall parameter space of ϕ. This region is sandwiched between the walking and the freezing regions indicated in red.

rad. at which walking becomes fully chaotic. This indicates that the premature activation (or lack of coordination between the muscles) can generate highly irregular behaviour in the system despite deterministic neural signals. The region of chaotic ϕ is sandwiched between the periodic orbits and freezing region. This suggests a higher variability in walking, likely arising from a shift in ϕ (early activation of plantar flexors), must be treated cautiously. Fig. 5.10 shows the presence of chaos in the system for carefully selected parameter values. Its presence and stability are illustrated for other parameters values and initial conditions using a set of maps in Fig. 5.11 - 5.13b and bifurcation diagrams in Fig. 5.14a - 5.14d. A summary of the insights gained from the maps is given in the Table. 5.1. The presence of a period three orbit in a one-dimensional map is indicative of other periodic orbits and chaos. The presence of horseshoe in any of the period 1, 2, ...,n maps also indicates chaos.

An illustration of the presence of a horseshoe for a set of parameter values is given in Sec. 5.2.5. The intersection of the $\tilde{f}^1_\omega$, $\tilde{f}^2_\omega$, $\tilde{f}^3_\omega$ maps with $\omega_n = \omega_{n+1}$ indicate period 1, 2, 3 orbits respectively. Fig. 5.11 - 5.13b illustrate how the maps change with respect to the variation of parameters.

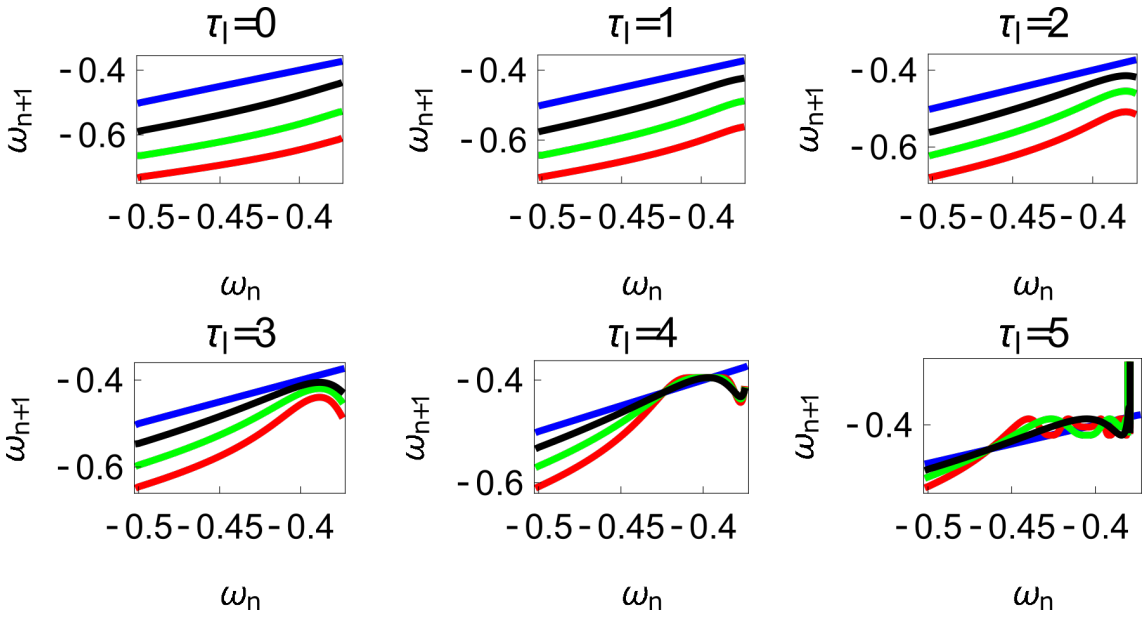

Figure 5.11: Maps obtained by varying the parameter τ_l and fixing $\tau_r = 35$ N, $\phi = -1.57$ rad., $\theta_{reset} = -0.1$ rad. The black, green and red curves represent $\tilde{f}^1_\omega$, $\tilde{f}^2_\omega$, $\tilde{f}^3_\omega$ respectively and the $\omega_n = \omega_{n+1}$ is shown in blue. The curves intersect the blue line at a higher absolute value of angular velocity forming an attractor, this is not shown in the figure. There are no periodic orbits for the low velocity regimes for $\tau_l = 0 - 2$ N m but they appear afterwards. Units: τ_l, τ_r, ω, ϕ, θ_{reset} and step length has units N m, N, rad. s^{-1}, rad., rad., and rad. respectively, when not specified.

Variation of the parameter τ_l or the magnitude of premature activation (as ϕ is set to -1.57 rad.) results in a set of rich, dynamic behaviours as shown in Fig. 5.11. The presence of the periodic orbits starts approximately around $\tau_l \approx 3$ N m, where the maps tangentially intersect the $\omega_n = \omega_{n+1}$ line. The intermittency thus created could elicit a period of slow walking (as ω_n and ω_{n+1} are less than -0.5 rad. s^{-1}) as observed in PD. The period three orbits are exhibited upon a further increase in τ_l. As can be seen from the maps in Fig. 5.11 - 5.13b, a higher initial value of $|\omega_n|$ (e.g. $|\omega_n| > 0.45$ rad. s^{-1} for $\tau_l \approx 3$ N m) results in a further increase in ω_{n+1} and gets attracted towards the periodic orbit of the higher absolute value

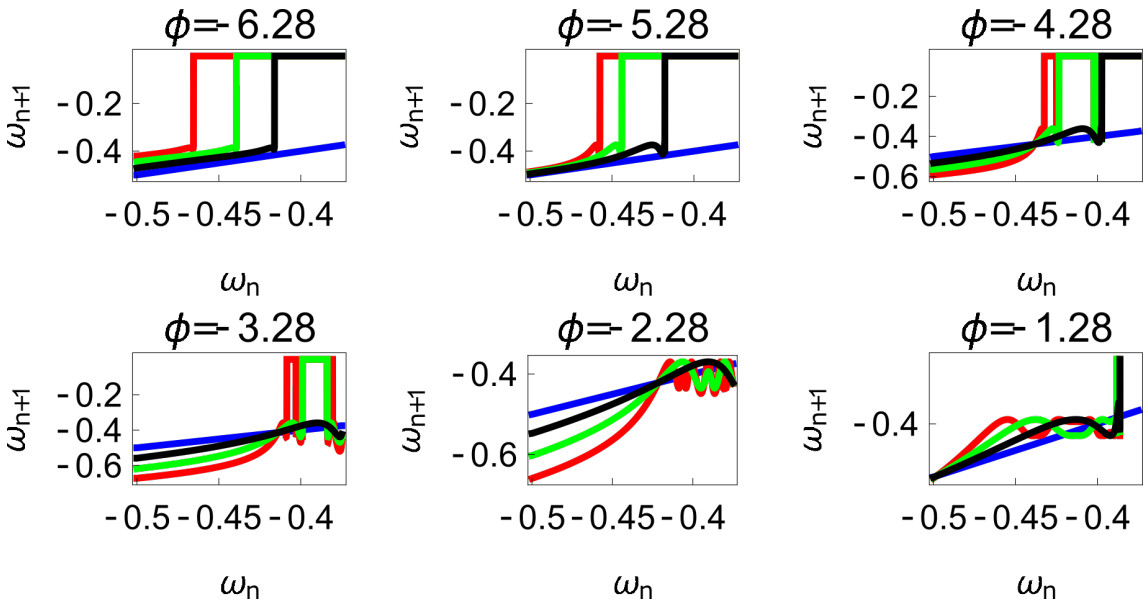

Figure 5.12: Varying the parameter ϕ and fixing $\tau_r = 35$ N, $\tau_l = 5$ N m, $\theta_{reset} = -0.1$ rad. The black, green and red curves represent $\tilde{f}^1_\omega$, $\tilde{f}^2_\omega$, $\tilde{f}^3_\omega$ respectively and the $\omega_n = \omega_{n+1}$ is shown in blue. The curves intersect the blue line at a higher absolute value of angular velocity forming an attractor, this is not shown in the figure. Creation of the periodic orbits and its coexistence is observed. Units: τ_l, τ_r, ω, ϕ, θ_{reset} and step length has units N m, N, rad. s^{-1}, rad., rad., and rad. respectively, when not specified.

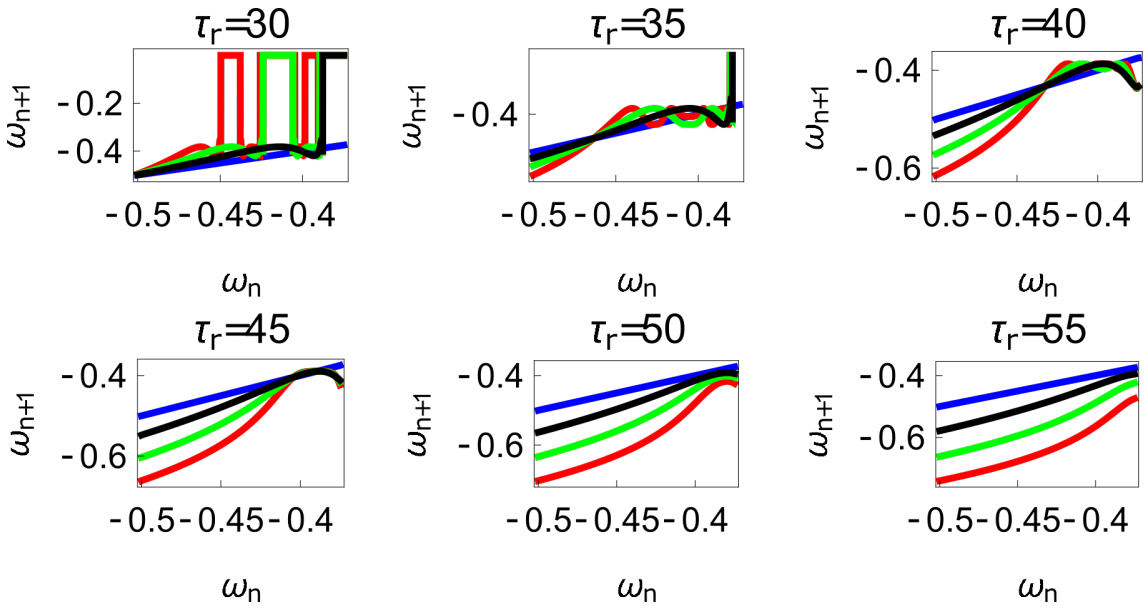

(a) Varying the parameter τ_r keeping $\tau_l = 5$ N m, $\phi = -1.57$ rad., $\theta_{reset} = -0.1$ rad. fixed. The black, green and red curves represent $\tilde{f}^1_\omega$, $\tilde{f}^2_\omega$, $\tilde{f}^3_\omega$ respectively and the $\omega_n = \omega_{n+1}$ is shown in blue. The curves intersect the blue line at a higher absolute value of angular velocity forming an attractor, this is not shown in the figure. Increasing τ_r has an analogous behaviour as decreasing τ_l.

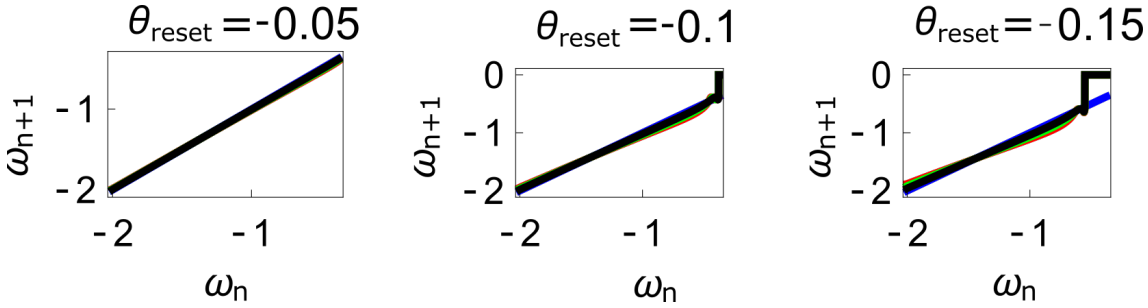

(b) Varying the parameter θ_{reset} keeping $\tau_r = 35$ N, $\phi = -1.57$ rad., $\tau_l = 0.5$ N m. The black, green and red curves (overlapped) represent $\tilde{f}^1_\omega$, $\tilde{f}^2_\omega$, $\tilde{f}^3_\omega$ respectively and the $\omega_n = \omega_{n+1}$ is shown in blue. The curves intersect at a high absolute value of angular velocity. The unstable region moving to the higher absolute value of angular velocities (moving to the left) can be observed while $|\theta_{reset}|$ is increased. Physiologically, different values of θ_{reset} could correspond to different step lengths.

Figure 5.13: Variations of the parameters τ_r and θ_{reset} are depicted in Fig. 5.13a and 5.13b respectively. Units: τ_l, τ_r, ω, ϕ, θ_{reset} and step length has units N m, N, rad. s^{-1}, rad., rad., and rad. respectively, when not specified.

of angular velocity; revealing how swaying back and forth helps the PD patients in getting out of a freeze. Increasing τ_r results in almost opposite behaviour as that of τ_l (Fig. 5.13a). Varying ϕ can result in chaotic behaviour as shown in Fig. 5.10, and, Fig. 5.12 indicates the variation in the maps which leads to this behaviour. The neural control of the activity of plantar flexors is not explicitly modelled here. However, coming out of freeze could be the result of an increase of τ_r or decrease τ_l or increased initial absolute angular velocity produced by swaying. A low absolute value of angular velocity (voluntary or involuntary) or decrease of τ_r or increase of τ_l results in freezing (angular velocity moving to the region where $\omega_n = 0$ rad. s^{-1}). This explains the higher chances of freezing episodes even when the subject reduces the velocity (voluntarily/involuntarily) near narrow passages. An increase in the step length or $|\theta_{reset}|$ results in freezing at relatively higher absolute angular velocities (Fig. 5.13b). However, it may be noted that an increased step length is typically associated with an increased absolute angular velocity due to inertia and, consequently, could be beneficial. There is likely an optimum step length for every subject as there is a trade-off between fatigue and initial angular velocity, which warrants further study.

5.3.4 Bifurcations of the One Dimensional System for the Inverted Pendulum Model

Even though for most of the regions, the slope of the map in relation to the $\omega_n = \omega_{n+1}$ line can be identified visually, the stability of the system is not explicitly studied in the previous section. The contour of $\tilde{f}^n_\omega(x,\ \tau_l,\ \tau_r, \phi) = x$ for n=1 and 3 are plotted for variation in parameters in Fig. 5.14 and 5.15 respectively. The stability is computed by taking the derivatives (numerically) for the maps described in Fig. 5.11 - 5.13b. These contours show how the points of intersection with the $\omega_n = \omega_{n+1}$ line for the maps shown in Fig. 5.11 - 5.13b change upon parameter variations.

Period one orbits are the normal walking cycles. The existence of these orbits in both low and high angular velocity conditions and different parameter variations are displayed in Fig. 5.14. In Fig. 5.14a two fixed points come closer to each other

and completely vanish for high values of τ_l resulting in a complete lack of periodic solutions. Typically, walking could be ascribed to the stable region for periodic orbits, but when ω_0 is lower, and τ_l is non-zero, another periodic point emerges in the low-velocity regimes. This, therefore, results in slow-walking regions, which under perturbations could lead to freezing. Also, at low-velocity regimes, the region is discontinuous and unstable for small perturbations of the values of parameters or initial conditions. The stable periodic orbit moves to the lower absolute value of angular velocities as τ_l increases and eventually disappears. The behaviour observed while decreasing τ_r is analogous to an increase in τ_l. Fig. 5.14b shows how changing τ_r and ω_0 results in creation/destruction of the periodic orbits. It can be discerned that at a sufficiently low value of τ_r, the periodic orbit disappears. A higher value of τ_r results in the separation of the periodic orbits resulting in higher stable walking angular speeds. A comparable behaviour could be observed while decreasing τ_l in Fig. 5.14a.

Initial angular velocity plays a major role in the behaviour of the system. The effect of neural control parameters τ_l and τ_r in generating periodic behaviour has been illustrated for lower and higher absolute angular velocity conditions in Fig. 5.14c and 5.14d respectively. In Fig. 5.14c the periodic orbit appears stable only for a small fraction of the parameters space. This is due to the highly discontinuous map shown previously. Conversely, at higher initial angular speeds, the period one orbit is stable, as shown in Fig. 5.14d. One could see that an increase in τ_l moves the periodic orbit into an unstable region, resulting in the possibility of a freeze. The presence of these orbits could only be seen in the low-velocity regions of the maps.

Orbits of minimal period three indicate chaos and the presence of every other periodic orbits (Glendinning, 1994). The period 3 orbits for the variation of the parameters τ_l and τ_r is shown in the Fig. 5.15. The Period 3 orbit is shown in blue and the period one in yellow.

Table 5.1: Summary of qualitative behaviour of the map

No	Parameter	Range Simulated	Figure No	Consequence of increasing the parameter
1	τ_l	[0, 5]	5.11	Increased τ_l results in the appearance of period 1-2-3 and higher orbits. This results in freezing at lower absolute angular velocity conditions
2	ϕ	[-6.28, -1.28]	5.12	Increase in ϕ results in the period doubling bifurcations as described in the Fig. 5.10. When everything else remains constant a variation in ϕ results in freezing and high variability in walking.
3	τ_r	[30, 55]	5.13a	Increased τ_r results in disappearance of period 1-2-3 and higher orbits. This is one of the ways in which the patients get out of a freeze
4	θ_{reset}	[0.05, 0.15]	5.13b	Increased step length results in freezing region change its location on the map, from low initial absolute angular velocity to a higher absolute angular velocity initial conditions.

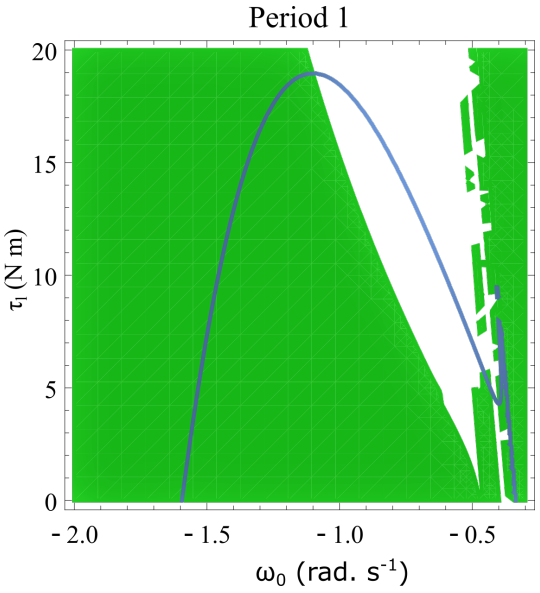

(a) $\phi = -\pi/2$ rad., $\tau_r = 40$ N, $\theta_{reset} = -0.1$ rad.

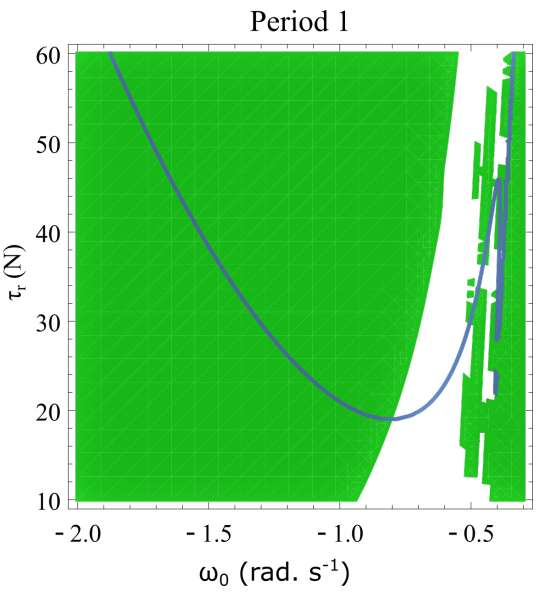

(b) $\phi = -\pi/2$ rad., $\tau_l = 5$ N m, $\theta_{reset} = -0.1$ rad.

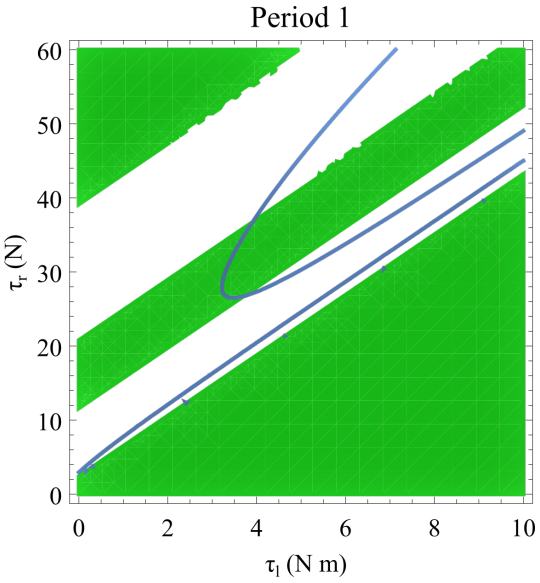

(c) $\phi = -\pi/2$ rad., $\omega_0 = -0.4$ rad. s^{-1}, $\theta_{reset} = -0.1$ rad.

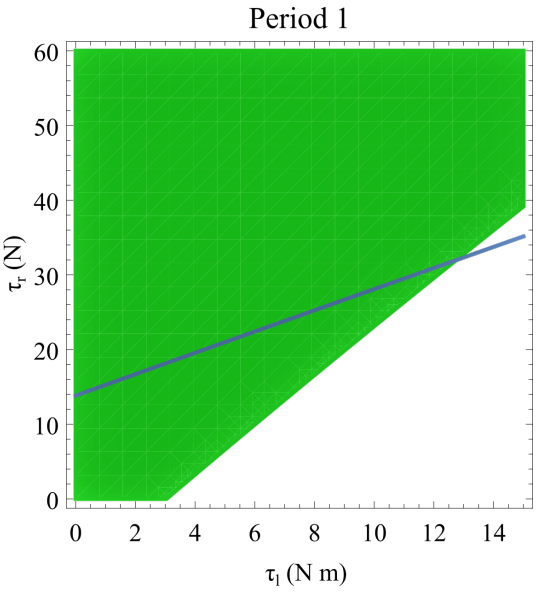

(d) $\phi = -\pi/2$ rad., $\omega_0 = -1$ rad. s^{-1}, $\theta_{reset} = -0.1$ rad.

Figure 5.14: Period one orbits are shown by varying τ_l and τ_r for two different values of initial angular velocities in Figs. 5.14c and 5.14d. Period one orbits found by varying τ_l and ω_0 is shown in Fig. 5.14a. Period one orbits found by varying τ_r and ω_0 is shown in Fig. 5.14b. The parameter values used are given in the respective figures. The green region shows the stable region where $\dot{\tilde{f}}_\omega < 1$. The stable periodic regions are the ones where the green region overlap the curves of the periodic orbits. Units: τ_l, τ_r, ω, ϕ, θ_{reset} and step length has units N m, N, rad. s^{-1}, rad., rad., and rad. respectively when not specified.

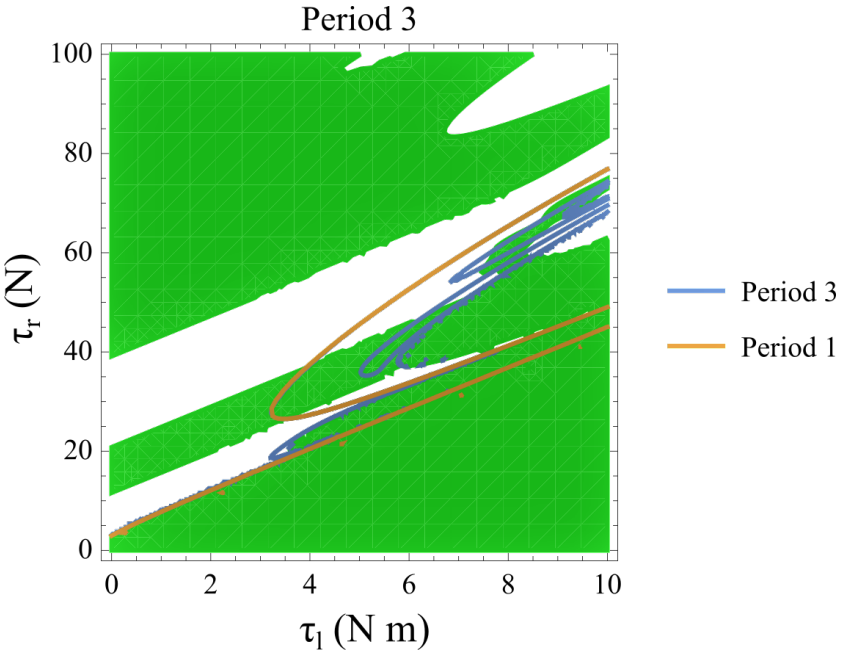

Figure 5.15: Constant parameters used are $\phi = -\pi/2$ rad., $\omega_0 = -0.4$ rad. s^{-1} and $\theta_{reset} = -0.1$ rad. The stable period 3 region is shown in green. The intersection of the period 3 orbits (in blue) and the stable regions form the region of stable period three orbits. The presence of period 3 orbits implies orbits of all other periods and therefore chaos.

5.4 Discussion

Freezing of gait results from an intricate set of interacting physiological systems, which consist of the brain, spinal cord, musculoskeletal system and external disturbances (Nutt et al., 2011). The model developed in this chapter explains how a lack of coordination between central pattern generators of the plantar flexors of the leading leg and trailing leg (Nieuwboer et al., 2004) could lead to freezing and variability of walking.

In this chapter, a model of the torques generated by the plantar flexors acting on the stance leg has been proposed; and its effect on a biped and a reduced inverted pendulum model is studied. The pattern of freezing observed in the model matches well with the behaviour observed experimentally [7] in (Nutt et al., 2011) and Fig. 5.6a. The equilibrium point description (Feldman, 1986; Sainburg, 2015) of the control of the muscles is avoided here, and instead, an explicit control signal has been

[7]The Fig. 1 in Nutt et al. (2011) is referred here. Source of the figure :`https://pubmed.ncbi.nlm.nih.gov/21777828/#&gid=article-figures&pid=figure-1-uid-0`

opted. However, variabilities in the 'torque-length characteristics' (Feldman, 1986) for a particular (set of) equilibrium point (points) can generate torques required for motion. Therefore, a parallel between the equilibrium point hypothesis of postural balance and our model can be drawn if the torques prescribed in the model are assumed to be the result of variabilities in the 'torque-length-characteristics'.

Chaotic regions are observed to be closer to those regions where freezing occurs. In the inverted pendulum model, these regions show up only at low absolute angular velocity initial conditions, explaining why freezing is a 'rarely' occurring intermittent condition. Moreover, this also may explain why freezing happens near obstacles or narrow paths where the subject voluntarily slows down to reduce the chance of collision. Obstacles could be either perceived or real. Hence, even though the pattern of freeze remains the same, the causes could be varied. It might even be possible that the control of τ_l is driven by perceived obstacles or anxiety about the consequence of freezing (Ehgoetz Martens, Ellard and Almeida, 2014; Martens et al., 2016). An increase in τ_l, therefore, could be thought to be indirectly influenced by anxiety and perceived obstacles. However, this hypothesis warrants further experimentation.

Varying the parameter step length that controls the stride length is observed to affect the maps and the freezing regions. The results indicated that keeping the steps closer to each other such that $|\theta_{reset}|$ is minimized is safer for the PD patient. The stability of the period two and three orbits are highly sensitive to minor variations of parameters ($\phi,\ \tau_r,\ \tau_l$) which are proposed to be the reason for sporadic variabilities in gait seen in PD subjects. One could also hypothesize that stable low absolute angular velocity regions of the state space for some parameter values form a 'cantor set' and necessitates further study.

One could speculate that one reason for the observed help of auditory/sensory cues (Young, Rodger and Craig, 2014; Rochester et al., 2005; Amini, Banitsas and Young, 2019) in reducing instances of freezing is by indirectly forcing PD patients to make shorter steps with lesser variability, thus reducing the possibility of moving into the freezing region of walking. Variability in the walking times observed in

the inverted pendulum model translates to variability in step lengths in the biped model. The biped model shows a more complicated dependence on the parameters to eventual freezing (Fig. 5.7a).

Feedback mechanisms regulate the CPG activity with delays, noise and input from the brain (which in turn is affected by different factors, including emotional state). The age, ground and environmental conditions also play a role in walking. These variabilities are not accounted for in our model, which represents a limitation of the study. Furthermore, The forces arising due to the motion of swing leg mass on the stance leg during the swing phase is assumed to be negligible compared to the ankle push-off forces. This is justified as the primary force governing gait is ankle push off from the plantar flexors. The lack of explicit modelling of the double support phase also can result in minor changes in the time to take a step. The quantitative variations due to the lack of swing leg and an explicit model of the double support are assumed not to alter the results or conclusions qualitatively. Like any other studies based on a mathematical model and numerical simulations, our results and conclusions also might not necessarily represent the entire spectrum of patients. Further extensive patient-based studies are to be performed prior to using these ideas to treat PD-Gait. In future chapters, a more detailed model is planned to include these variabilities. The key aspects explained using the proposed model can be summarized as follows:

1. The higher variability in PD patients could result from parameters being closer to the point of chaos. A further change of the parameters can result in freezing. Therefore, increased variability should be looked at cautiously (clinically) and should be treated to reduce it. Moreover, the difficulty in the prediction of freezing also owes to the horseshoe near the freezing regions.

2. The pattern of reducing the step-sizes before freezing is the result of slowing down (Fig. 5.6a). Voluntary/involuntary decrease in angular velocity (in absolute terms) near the obstacles makes the subject more susceptible to freezing and irregular walking.

3. One plausible reason for sensory cues such as auditory or visual cues help

in freezing is by reducing step lengths. The proposed model shows that the decrease in step length helps in reducing freezing episodes at the lower absolute value of angular velocity conditions as it moves the patient away from the freezing region. A further experimental study is needed to understand the clinical applicability.

6. Central Pattern Generator Based Extension of the Freezing of Gait Model

Currently, there is no mathematical model (up to the author's knowledge) describing the freezing of gait (FoG) as well as variability in the gait with a focus on limb mechanics and CPG. Also, freezing like behaviour could be the transient behaviours of the dynamical system leading into a steady normal walking. Therefore, there is a need for a study to analyse a finite horizon problem (few steps forward in time) rather than the long term behaviour. Moreover, biological feedback and its effect on FoG also needs careful consideration. The augmented feedback is shown to have positive implications for PD patients, this also needs an explanation from the modelling perspective.

In this chapter, we combine a CPG model and the model of limb mechanics. The limb model focuses on the ankle push-off forces given in chapter 5 making it relevant to PD. Only single support phase of the stance leg is explicitely modelled in this chapter. A state dependent, event-driven feedback is provided to account for the impulse signal occurring at the heel strike. The mathematical description of such a system becomes a nonlinear-hybrid-dynamical system. The *orbital* stability of gait in this model is studied using a Poincare based approach, since the Jacobian associated with the model is singular. The effect of the feedback on gait variability is studied from the perspective of the neuromechanical system and the synchronisation properties of the CPG. The intermittent transition of the gait from walking to freezing and back has also been demonstrated.

The work done for this chapter has been submitted for peer review as follows:

- M. Parakkal Unni, P. P. Menon. 'Modeling and Analysis of Parkinsonian Gait' In:*Nonlinear Dynamics (Submitted in Sept 2021, Status: In Review).*

The chapter is structured as follows. The Sec. 6.1 provides the physiology and the assumptions relevant to CPG-based modelling of gait. The mathematical modelling procedure is described in Sec. 6.2. Further, the numerical simulation results and stability analysis is provided in Sec. 6.3 and Sec. 6.4 respectively. Subsequently, the effect of the external feedback in the absence of proprioceptive feedback (in Sec. 6.5), the effect of feedback on the neuromechanical system (in Sec. 6.6) are presented. Finally, the chapter ends with the discussion in Sec. 6.7.

6.1 Background

One could refer to Sec. 3.2.5 for the definitions used to describe the hybrid system such as the Poincaré section, time to reset and the switching surface.

One gait cycle constitutes two steps since the left and right leg acts as a stance leg. Henceforth, a gait cycle is the composition of $\mathcal{F}_R \circ \Delta_{L\to R} \circ \mathcal{F}_L \circ \Delta_{R\to L}$ where $\mathcal{F}_L$ and $\mathcal{F}_R$ denotes the flow corresponding to the left and right leg as the stance legs respectively, and '$\circ$' represents the composition. Symbols $\Delta_{L\to R}$ and $\Delta_{R\to L}$ represents the reset corresponding to the left leg to the right leg and vice-versa.

Consequently, it is convenient to study the composition of the Poincare map with itself ($P(P(.)) := \tilde{P}(.)$) for understanding the stability properties of the gait cycle. The stability of this map is numerically studied. The Jacobian that corresponds to the vector field and the *Poincaré map* are denoted by $D\mathcal{F}$, and DP respectively. A non-singular $D\mathcal{F}$ is essential to the contraction analysis of the system based on variational methods of analysis of the differential dynamics (Lohmiller and Slotine, 1998; Tang and Manchester, 2014). A lack thereof leaves only the possibility of Poincaré based analysis of P or its iterates.

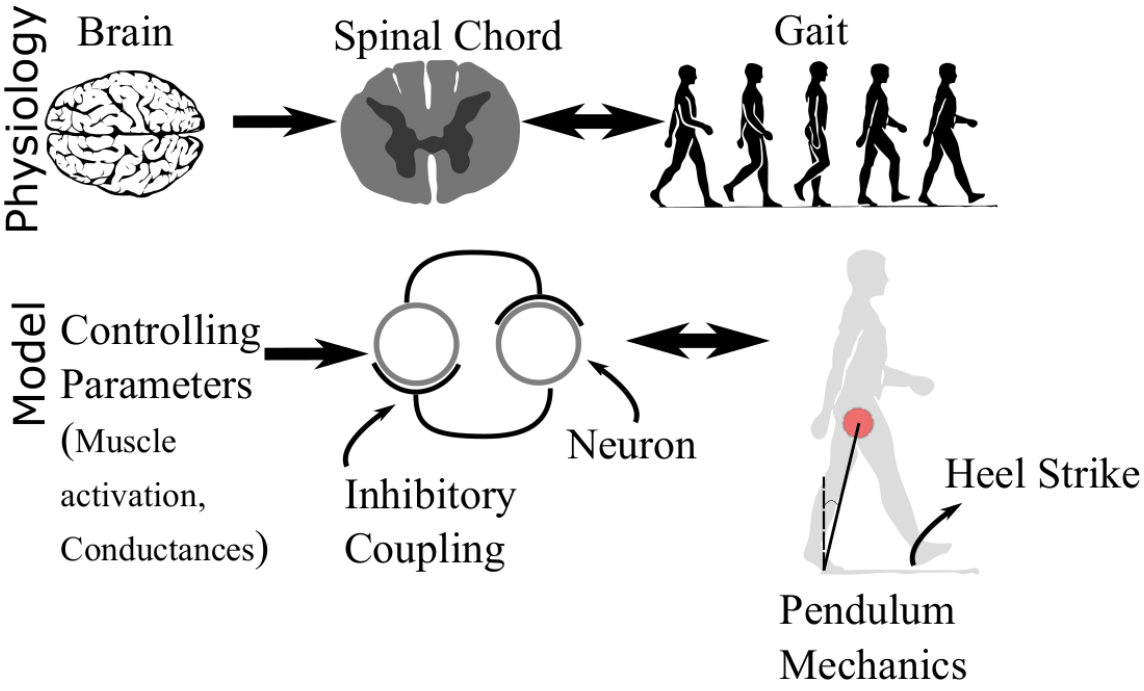

Figure 6.1: The physiology and the associated modelling assumptions are depicted here. The brain (basal ganglia, cortical and subcortical areas) control the spinal cord which in turn control gait. CPG is modelled as coupled oscillators (representing neurons). The walking dynamics are represented by a simple pendulum model.

6.1.1 Physiology

The relevant physiology is briefed here. Central pattern generators (CPG) are neuronal circuits in the spinal cord that can generate oscillatory activity without being forced rhythmically (Ijspeert, 2008). There is evidence in the literature for the presence of CPG in quadrupeds, (Grillner et al., 2001; Dietz, 2003) and indirect evidence (Dietz, 2003; Taub, Uswatte and Elbert, 2002) for its existence in humans. The brain modulates the CPG dynamics in the spinal-chord, (Dietz, 2003; Snijders et al., 2016) which in turn coordinates the leg-muscles using feedback inputs from the brain (Minassian et al., 2017; Berger, Dietz and Quintern, 1984). A simplified physiology of gait and the corresponding modelling aspects are depicted in Fig. 6.1.

A bursting dynamical state of a neuron/neuronal population is associated with the excitation of a group/bursts of action potentials in succession. The spinal CPG neurons are known to elicit bursting behaviour, (Grillner et al., 1995; Izhikevich, 2007) which control the torque generated by the muscles. While there are multiple spikes in a burst, the torque produced can be assumed to be resulting from the

'equivalent membrane potential' (Izhikevich, 2003; Genadry, Kearney and Hunter, 1988) of the bursting dynamics. The torques are generated during the bursting region of the dynamics. Almost very-low, or zero, torque is generated during the non-bursting region (Cresswell, Löscher and Thorstensson, 1995; Hof and Van Den Berg, 1977; Clancy, Bida and Rancourt, 2006). Consequently the neuromechanical dynamics is controlled by the equivalent voltage of the motor neuron (neuronal population) bursts (Grillner et al., 1995; Izhikevich, 2007) rather than individual spikes.

The role of sensory feedback inputs through afferent nerves in walking rhythm generation is now well-recognised (Dietz, 2003; Cheung et al., 2005; Tuthill and Azim, 2018). Transmission of these signals requires a finite amount of time to reach the destination. Hence, it occurs with a delay. However, this delay is known to be negligibly small (<50 ms.) (Malcolm, 1951) when compared with the stepping times (Bachlin et al., 2009). Hence, the feedback is modelled and studied as event-driven instantaneous inputs to the neuronal system. A defective utilization of these afferent feedback inputs has been suggested in PD in (Dietz and Colombo, 1998) resulting in defective electromyogram (EMG) traces (Dietz and Colombo, 1998; Nieuwboer et al., 2004) making feedback relevant in the study of PD-Gait.

6.2 Mathematical Modelling

The dynamics of the neuromechanical system governing PD physiology is explained in this section. The section starts with the complete equations of motion, the underlying assumptions and the description of the subsystems successively follow.

6.2.1 Equations of Motion

A hybrid system formulation of the Equations of Motion (EoM), as in Eq. 3.1 and Eq. 3.2, has three components: (1) continuous dynamics ($\mathcal{F}(z(t),\ \lambda)$), (2) a discrete part ($\Delta(z(t)^{-}, \lambda)$) and (3) a definition for the *switching surface* ($\mathcal{S}$). In this study, the continuous part of the dynamics ($\mathcal{F}(z(t),\ \lambda)$) comprise of two interacting subsystems, of which, one is a neuronal CPG part (Σ_{n_i}), modelled as two coupled oscillators and

the other corresponds to mechanical dynamics (Σ_m). Fig. 6.2 shows the interaction between the neuronal and mechanical systems and the external input received by the CPG.

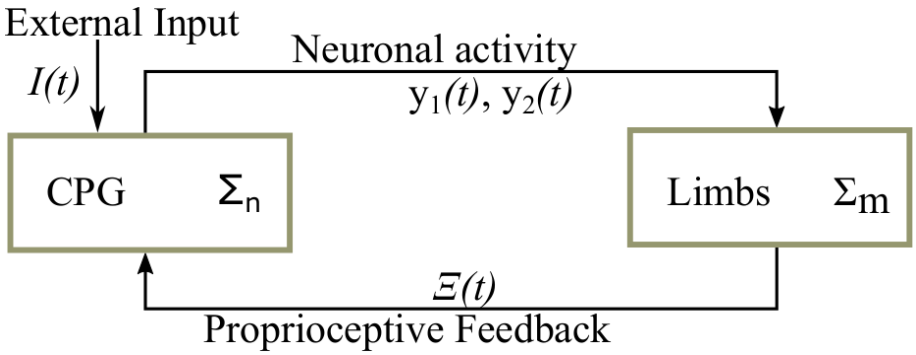

Figure 6.2: A block diagram showing the feedback interaction between the neural and mechanical components of the system. While the signals $y_1(t)$ and $y_2(t)$ become the inputs to the limbs, the proprioceptive feedback signal $\Xi(t)$ modulates the CPG. The term $I(t)$ represents external input signal received by the CPG.

The overall system is described using Eq. 3.1 and Eq. 3.2 with the following characterisation:

$$z = \left[y_1,\ x_1,\ y_2,\ x_2,\ \theta,\ \omega,\ \Xi \right]^T \ , \tag{6.1}$$

$$\mathcal{F}(z,\lambda) := \left[\ \Sigma_{n_1}^T\ \Sigma_{n_2}^T \ \middle|\ \Sigma_m^T\ \right]^T \ , \tag{6.2}$$

$$g_r\left(z\right) = \theta - \theta_{reset} \ , \tag{6.3}$$

$$\Delta\left(z^-,\lambda\right) = \left[y_1,\ x_1,\ y_2,\ x_2, -\theta,\ \omega\cos(\theta_h),\ -\Xi \right] . \tag{6.4}$$

The dependency on time in the equations is absent for brevity. The variables x_i and y_i represent the states of the CPG, with y_i indicating the activity of the i^{th} neuron. The oscillators in this model phenomenologically represent the collective activity of a neuronal population. In Eq. 6.2, the dynamics of the neuronal CPG is written as follows:

$$\Sigma_{n_i} := \begin{bmatrix} \frac{1}{\tau}\Bigg(\overbrace{\frac{-\alpha y_i\left(x_i^2+y_i^2-e\right)}{e} - x_i}^{\text{Intrinsic CPG Dynamics}} + \underbrace{\Xi\Phi_i}_{\text{Feedback}} + \underbrace{\sum_{j=1}^{2} w_{i,j}y_j}_{\text{Neuronal Coupling}} - \underbrace{aI_i(t)}_{\text{Ext. Input}} \Bigg) \\ \\ \frac{y_i}{\tau} \end{bmatrix},$$

$$i = 1, 2. \tag{6.5}$$

where,

$$\Phi := [-f_b,\ f_b]^T, \tag{6.6}$$

$$w := \begin{bmatrix} 0 & S_t \\ S_t & 0 \end{bmatrix}. \tag{6.7}$$

The term $w_{i,j}$, which controls the mutual inhibition through the synaptic strength S_t is an element of the matrix $w \in \mathbb{R}^{2\times 2}$. The neurons modelled are assumed to be mutually inhibiting (one inhibiting the other) and not directly influencing its own activity ($w_{1,1} = w_{2,2} = 0$). The element Φ_i of the vector $\Phi \in \mathbb{R}^2$ represents the positive or negative feedback strength (f_b). The term Ξ corresponds to the proprioceptive feedback from the limbs modulating the CPG dynamics. The constants $e,\ \alpha$ and τ govern the intrinsic CPG oscillator dynamics (Ijspeert, Crespi and Cabelguen, 2005) and discussed more in the sequel.

In Eq. 6.5, the effect of periodic auditory/sensory cues (Dietz, 2003; Cheung et al., 2005; Tuthill and Azim, 2018) is represented as a scaled periodic external input $aI_i(t)$ where

$$I(t) := \big[-u_s(t),\ u_s(t)\big]^T, \tag{6.8}$$

and

$$u_s(t) = \begin{cases} +1,\ \sin(2\pi\Omega_f t) \geq 0\ , \\ -1,\ \sin(2\pi\Omega_f t) < 0\ . \end{cases} \tag{6.9}$$

The variable a scales the amplitude of the external input, when present, and Ω_f represents the frequency of the input.

In Eq. 6.1, the states $\theta,\ \omega$, and Ξ represent the angle subtended w.r.t. the horizontal, angular velocity, and 'proprioceptive feedback' respectively. The 'proprioceptive feedback' state $\Xi \in \{-1,\ +1\}$ indicates which leg is on the ground at time t to generate an event-driven-feedback signal. When Ξ changes the state from -1 to 1 the sign of the feedback received by the oscillator changes. In this formulation, the proprioceptive feedback is sent from the limbs to the neural system. In Eq. 6.2, the mechanics of the limbs (Σ_m) are described using the following set of equations,

$$\Sigma_m = \begin{bmatrix} \omega \\ \frac{1}{\theta}\left(\Xi \max(0,\ \theta)\left(\frac{p(\theta,\ -\Xi)\tau_l \max(0,\ y_1)}{l^2 m} - \frac{p(\theta,\ \Xi)\tau_r \max(0,\ y_2)}{l^2 m}\right)\right) + \frac{g\theta}{l} - q(\theta) \\ 0 \end{bmatrix}\ , \tag{6.10}$$

where,

$$p(\theta,\ \Xi) := \begin{cases} l\sin(2\theta) & \text{when } \Xi = +1\ , \\ 1 & \text{when } \Xi = -1\ , \end{cases} \tag{6.11}$$

$$q(\theta) := \begin{cases} 0 & \text{if } \quad \theta < -\theta_{reset} + \epsilon\ , \\ K\theta & \text{if } \theta \geq -\theta_{reset} + \epsilon\ , \end{cases} \tag{6.12}$$

and $l,\ m,\ g$, and K are length, mass, acceleration due to gravity and the stiffness constant of the trailing leg, respectively. The parameters τ_l and τ_r scale the neuronal

activity signals y_1 and y_2 . The term $q(\theta)$ is introduced in this chapter to constrain the motion of the stance leg. It further helps to capture the transition from freezing to walking. The stiffness constant of the trailing leg (K) models the angular stiffness and ϵ is a small positive scalar. The hip angle (θ_h) in Eq. 6.4 is considered as twice the reset angle θ_{reset} since the step angle is assumed constant in every step. The step length is defined to be equal to $|\theta_{reset}|$ where $|.|$ denotes the absolute value.

6.2.2 Neuronal Dynamics as Locomotion Control

The CPG is assumed to control the movement of the limb dynamics (Dimitrijevic, Gerasimenko and Pinter, 1998) while simultaneously affected by feedback with a negligible delay (Malcolm, 1951). The 'equivalent membrane potential' (Izhikevich, 2003) of the bursting dynamics is assumed to control the torques generated in the muscles. Moreover, the activity of those neurons is directly proportional to the torques generated in the muscles.

In this work, the CPG is modelled as two interconnected oscillators effectively modelling the 'equivalent membrane potential'. The intrinsic CPG dynamics part in Eq. 6.5 is inspired from (Ijspeert, Crespi and Cabelguen, 2005) and in the absence of the external inputs and the feedback signal, the CPG exhibits *limit cycle*. Plantar flexors innervated by the neurons from the CPG supply the necessary torques to the limbs. The activation by the CPG occurs only for the positive neuronal activity, i.e., when $y_1 > 0$, or $y_2 > 0$. Hence, this representation effectively models muscle contraction.

The parameter e in the intrinsic CPG dynamics in Eq. 6.5 increases the amplitude of the *limit cycle*. Here, the limit cycle refers to that of a single oscillator. An increase in the amplitude of the limit cycle models the increased neuronal activity. The positive constants e and $\tau > 0$ together control the total energy in every stepping cycle. While the system is on the limit cycle, the term $x_i^2 + y_i^2$ is e, and thus there is no influence for the parameter α. Henceforth, the positive parameter α can be interpreted as a scaling of the perturbation from the limit cycle. The feedback $\Xi\Phi_i$, the neuronal coupling $\sum_{j=1}^{2} w_{i,j} y_j$ and the external input $I(t)$ in Eq. 6.5 can change

the phase of the oscillator. The perturbations to the phase of the oscillator have influence on the synchronisation (Izhikevich, 2003).

6.2.3 Mechanical model and Definition of Freezing

It has been shown in (Parakkal Unni et al., 2020a) that an inverted pendulum based model adequately represents the freezing and irregular walking motion of the centre of mass of the body having PD. The torque generated due to the plantar flexors' activity alone provides the ankle push-off forces to propel the leg forward. Inspired by this, the lower limb mechanics is modelled here as a hybrid inverted pendulum (inverted pendulum with a reset). The reset map and the differential part of the dynamics (Eq. 6.4 and Eq. 6.10 - 6.12) are derived by balancing the torques and the angular-momentum, respectively. The stiffness of the trailing leg is triggered when the angular displacement θ increases beyond $-\theta_{reset} + \epsilon$ in the counter direction to walking. In this study, ϵ is fixed at 0.02 (chosen arbitrarily, does not affect the dynamics qualitatively). The negative sign associated with the term θ_{reset} represents this convention. The stiffness term in Eq. 6.12 takes into account the opposing force exerted by the trailing leg preventing a fall; at this moment, the subject is assumed to freeze. This opposing stiffness force is necessary to model the shift from freezing to walking. The impulsive mechanics at 'heel strike' (when the swing leg hits the ground) is modelled using a reset, effectively making the dynamics belong to the class of hybrid system. At every instance the flow of the dynamics reaches the *switching surface* $\mathcal{S}$ in Eq. 3.3, the reset map given in Eq. 6.4 is applied. The function $g_r(z)$ in Eq. 6.3 defined the identity of the switching surface. The state representing the proprioceptive feedback Ξ is reset at every step accounting for the change in the stance leg loaded with the weight of body. The angular velocity is also reset to account for the conservation of angular momentum. Furthermore, the angle (θ) is reset to account for the alternation between limbs as given in (Parakkal Unni et al., 2020a).

By convention, a negative angular velocity indicates limbs moving forward. At every point in the phase space, a finite amount of energy is necessary to keep the direction of the angular velocity negative ($\omega < 0$). During a freezing episode,

the limbs receive insufficient net torque to move forward. Consequently, the angular velocity ω becomes positive, which leads to the following definition.

Definition 6.2.1 *Let $z_{t_0} \in \mathcal{S}$ be the state at time t_0 and $t_s - t_0$ be the time to impact (or reset).* Freezing trajectory *is defined as the set $\mathcal{C} := \{\zeta(t,\ z_{t_0}) \mid z_{t_0} \in \mathcal{S},\ \omega(t) > 0$ for any $t \in\ (t_0,\ t_s)\}$.*

The *freezing fraction* for a discrete simulation is determined by finding the fraction of time points where $\omega(t) > 0$ and satisfies Def. 6.2.1. The finite time simulation results are sampled uniformly, and the number of data points with $\omega(t) > 0$ is divided by the total number of points in the simulation to compute *freezing fraction*. From a physiological perspective, whenever the premature activation prevails upon the normal activation, the stance leg momentarily moves backwards, resulting in $\omega > 0$. Consequently, freezing fraction gauges the effect of premature activation of the muscles in the stance leg. According to Nieuwboer et al., 2004 premature activation of plantar flexors is a charecteristic of PD making *freezing fraction* very relevant for PD.

6.3 Numerical Simulation of Freezing and Normal Gait

The overall model described using Eq.3.1 and Eq. 3.2 with the characterisation given in Eq. 6.1 - Eq. 6.4 is simulated. Unless specified otherwise, values of the parameters and initial conditions used in the model have been listed in Table 6.1. The parameters are chosen to achieve physiologicaly meaningful walking. And, the neuronal system parameters are varied to understand their effect on FoG. The evolution of the states for a short duration of time is shown in Fig. 6.3. In simulations, high and low values of the feedback strength (f_b) are considered.

(i) Normal gait: In this simulation, no external input $I(t)$ is considered. Fig. 6.3a and Fig. 6.3b show the states of the CPG dynamics and the mechanical system during normal walking. The value of the feedback gain (f_b) used in the simulation is 1.

Table 6.1: The values of different parameters of the model and initial conditions

Mechanical system	
Parameters	Value (units)
l	0.6 m
g	9.8 ms^{-2}
m	70 Kg
τ_l	20
τ_r	20
θ_{reset}	-0.1 rad.
K	50
ϵ	0.02
Initial condition	Value (units)
θ_0	-0.05 rad.
ω_0	-0.5 rad. s $^{-1}$
Neuronal system	
Par.	Value (units)
e	0.5
τ	0.1
α	0.1
f_b	1 (normal gait), 0.1 (freezing gait)
S_t	1
a	0
Initial condition	Value (units)
y_{10}	1
y_{20}	2
x_{10}	1
x_{20}	1

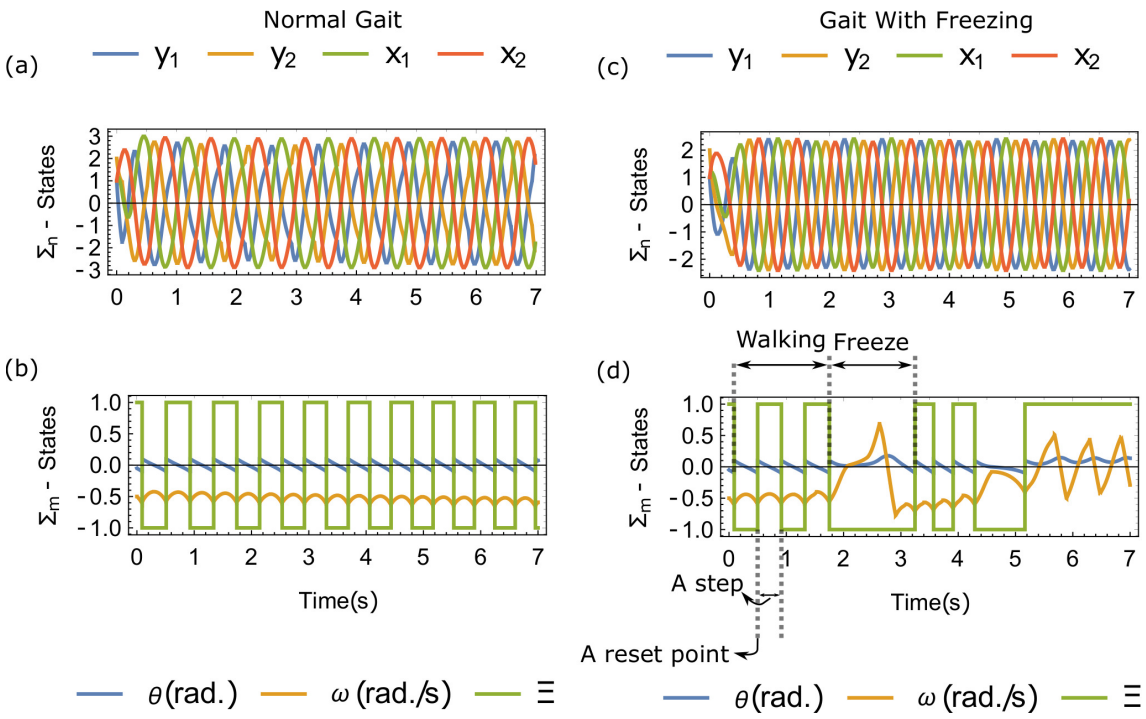

Figure 6.3: (a) The states of the neural system (y_1, y_2, x_1, x_2) at high value of feedback strength ($f_b = 1$). (b) States of the mechanical system (θ, ω, Ξ) at high value of feedback strength ($f_b = 1$).(c) The states of the neural system at a low value of feedback strength ($f_b = 0.1$) (d) States of the mechanical system at a low value of feedback strength ($f_b = 0.1$). Phases of Walking and Freezing, single step and one reset point are indicated.

(ii) Freezing of gait: The states of the neural and the mechanical system are indicated in (Fig. 6.3c) and (Fig. 6.3d) respectively. When compared with the results of normal gait, the freezing of gait is obtained by decreasing the value of the single parameter, the feedback gain (f_b), to a lower value of 0.1 from 1. The oscillations in the four neuronal state variables of the CPG can be noticed in Fig. 6.3c. Among the states, the signals y_1 and y_2 control the mechanical part of the system. In this simulation, the chosen low value of feedback strength ($f_b = 0.1$) is insufficient to synchronise the neural (Σ_{n_i}) and mechanical (Σ_m) systems. This aspect is evident from the resultant intermittent walking and freezing behaviour observed in Fig. 6.3d. The proprioceptive feedback state Ξ, indicating which leg is on the ground, changes the sign on reset as indicated in Fig. 6.3d, since $\Xi \in \{1, +1\}$ and $\dot{\Xi} = 0$. From Fig. 6.3d, it can also be observed that at the reset point, the state θ is reset to $-\theta$ as well.

The trajectory from an initial condition till the reset is defined to be a 'step'.

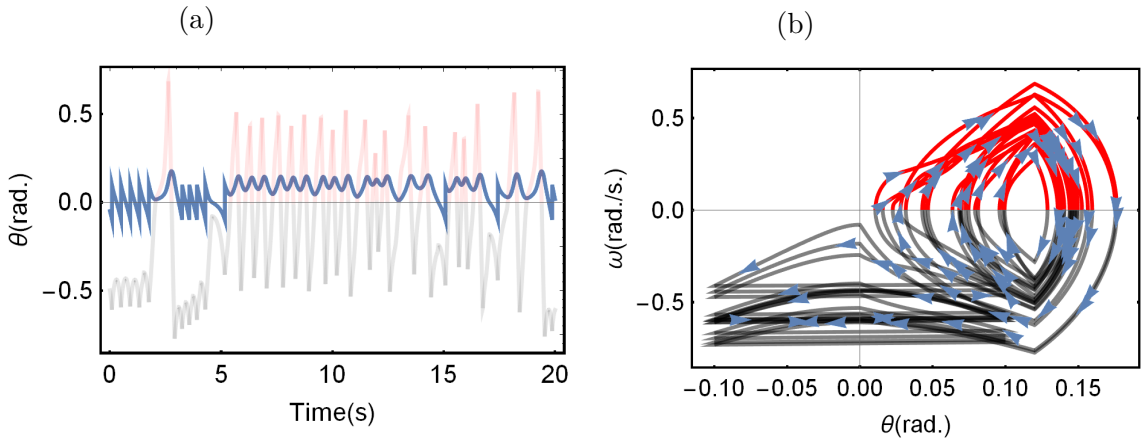

Figure 6.4: (a) Time series of $\theta(t)$ and $\omega(t)$ (in the background) for a low value of feedback gain ($f_b = 0.1$); (b) θ - ω phase plane diagram; the regions in red colour show part of the data exhibiting *freezing* behaviour where ω is positive.

A 'freeze' as defined in Def. 6.2.1 is indicated in Fig. 6.3d where ω crosses zero and reaches a positive value generating a longer 'pause' in walking. Multiple steps without an intermediate freeze are indicated as walking. One could note that, from the hybrid systems point of view, the 'pause' in walking owes to the relatively higher *time to reset*.

The sharp changes in angular velocity owe to two aspects of the model: (i) the reset accounting for the conservation of angular momentum, and (ii) the effect of the piecewise linear characteristics of $q(\theta)$ in Eq. 6.12 as the angle θ crosses the condition $-\theta_{reset} + 0.02 = 0.12$. The latter aspect contributes to the rapid changes to the angular velocity during the freezing episode shown in Fig. 6.3d.

Fig. 6.4a shows the time series of states θ and ω from 20 seconds of simulation. In the simulation, the feedback gain is fixed at 0.1. The regions where freezing occurs are indicated in red colour. The intermittent episodes of walking and freezing can be observed. A plot of the trajectories in the θ - ω phase plane is shown in Fig. 6.4b. In the phase plot, the segment of trajectories in the first quadrant shown in red colour reflects freezing behaviour, since angular velocity is positive. (iii) *In the presence of external input:* An external input $I(t)$ as in Eq. 6.8 is applied to the model ($f_b = 0.1$) which exhibited the intermittent freezing behaviour as shown in Fig. 6.3 c and 6.3 d.

The frequency of the external input Ω_f is 1.2 and the parameter a equals 2.5. Fig. 6.5 shows the effect of the external input, which converts an otherwise freezing gait into a normal gait. The external input is shown to influence the neuromechanical system resulting in a gait without freezing. In addition, short-time Fourier transform (STFT) of the filtered angular acceleration signal ($\dot{\omega}(t)$) is computed. A Gaussian filter of kernel radius ten is utilised for filtering the ($\dot{\omega}(t)$) signal. A window size of 0.32 sec and a sampling rate of 100Hz is adopted for the STFT calculation (*Mathematica, Version 12.0*). The STFT analysis indicated that the frequency content of the signal increases in the model during a freeze, which is in line with the experimental evidence (San-Segundo et al., 2019; Bachlin et al., 2009). The parameters are chosen such that the resolutions of the time and frequency are adequate to understand the behaviour.

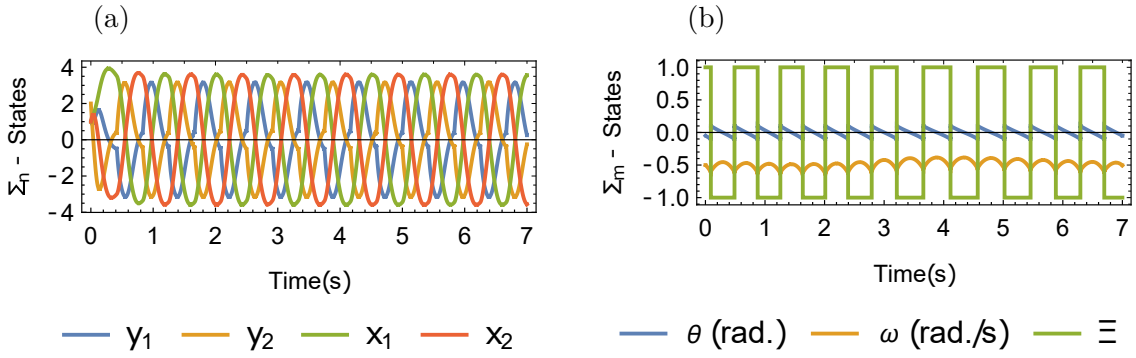

Figure 6.5: Recovery of normal gait for a low value of feedback gain ($f_b = 0.1$) in the presence of an external input $I(t)$. The parameters that correspond to the external input are $a = 2.5,\ \Omega_f = 1.2$.

6.4 Stability

Human locomotion is generally stable in the presence of a certain class of perturbations Iosa et al., 2014. The stability of the overall model in Eq.3.1 and Eq. 3.2 with the characterisation as given in Eq. 6.1 - Eq. 6.4 is analysed in this section. The CPG model considered in this work is phenomenological. Three parameters of the CPG model - the constant e governing the intrinsic CPG oscillator dynamics, the feedback gain f_b and the synaptic strength S_t - are of physiological significance (Ijspeert, Crespi and Cabelguen, 2005). For the purpose of the stability analysis, the perturbation

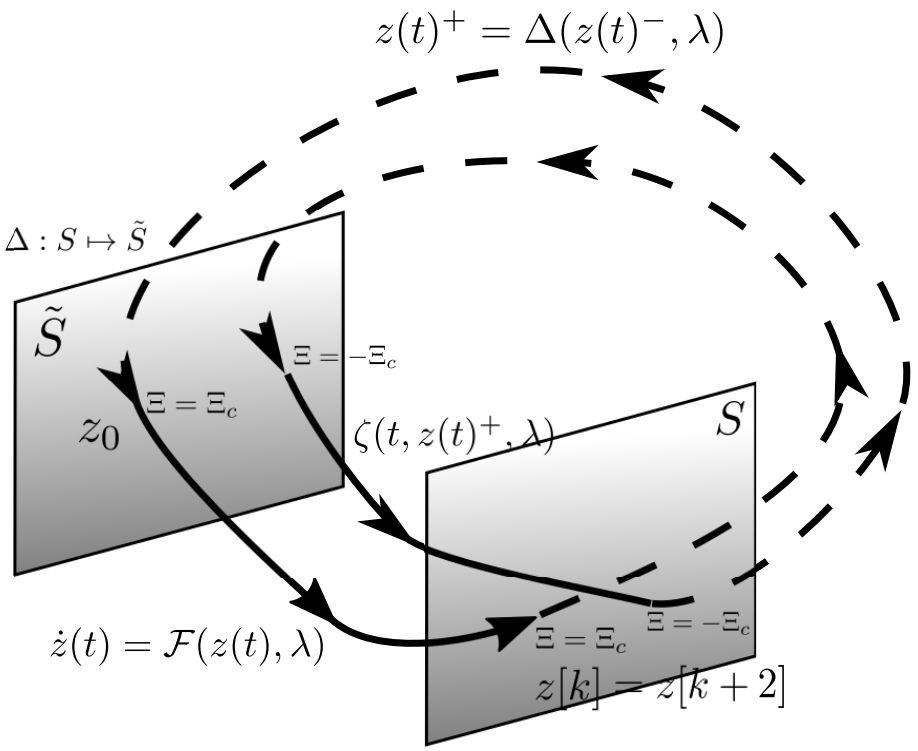

Figure 6.6: The value of Ξ as it changes between S and $\tilde{S}$ has been shown. The dashed lines represent the discrete dynamics governed by $\Delta(.)$ and the solid lines represent the smooth dynamics governed by $\mathcal{F}(.)$. The map $\tilde{P}(.)$ formed by iterating $P(.)$ two times, is also indicated.

to these parameters is assumed to occur within the range $e \in (0.1,\ 1), S_t \in (0,\ 6)$, and $f_b \in (0,\ 2)$ where relevant walking and freezing behaviours are exhibited. Demonstration of orbital stability of the *hybrid walking model* in the presence of the perturbations is vital.

For the stability analysis, the surface defined by the set $\mathcal{S}$ is considered for constructing the Poincare section. The discrete map $\Delta(.)$ maps the points from $\mathcal{S}$ to $\tilde{\mathcal{S}}$ which is again mapped back to $\mathcal{S}$ by the differential dynamics. The Poincare map P is defined as a composition of these maps taking a point $z[k] \in \mathcal{S}$ to $z[k+1] \in \mathcal{S}$. Since proprioceptive feedback state Ξ switches in every reset (as shown in Fig. 6.6), the map $\tilde{P}$ is formed by iterating P twice, which is considered for the stability analysis.

Out of the seven state variables, only five (excluding θ and Ξ as they remain constant during the evolution due to the differential part of the dynamics) are

considered for the computation of the Jacobian. This results in the definition of a new map, denoted by $\tilde{P}_c$, where the parameters θ and Ξ remain constant. Hence, the map $\tilde{P}_c$ is defined as follows,

$$\tilde{z}[k+2] = \tilde{P}_c(\tilde{z}[k]) \ , \tag{6.13}$$

where $\tilde{z}[k] := z[k] \setminus \{\theta[k],\ \Xi[k]\} \in \mathbb{R}^5$ is the state vector of the overall system excluding $\theta,\ \Xi$ at the k^{th} step. The Jacobian associated with this system is denoted by $D\tilde{P}_c \in \mathbb{R}^{5\times5}$.

A Taylor series based methodology, adapted from Goswami, Thuilot and Espiau, 1996a, is used for the computation of the Jacobian matrix of the map $\tilde{P}_c$. The eigenvalues of the Jacobian matrix $\mathcal{D}\tilde{P}_c$ determine the stability of the system (Devaney, 2018). Following the approach in Goswami, Thuilot and Espiau, 1996a, at the periodic point $\tilde{z}^*$ of the map $\tilde{P}_c$, the perturbation vectors $\delta\tilde{z}_i^*$s are applied. The vector $\delta\tilde{z}_i^*$ has only one small non-zero term ($= 10^{-3}$), such that, the perturbations are applied to each state independently. Hence, a diagonal matrix $\boldsymbol{\gamma} \in \mathbb{R}^{5\times5}$ is defined constituting the perturbation vectors $\delta\tilde{z}_i^*$ associated with each states as its columns. For the perturbation vector $\delta\tilde{z}_i^*$ associated with each individual state, the corresponding $(\tilde{P}_c(\tilde{z}^* + \delta\tilde{z}_i^*) - \tilde{z}^*) \in \mathbb{R}^{1\times5}$ is computed, yielding the matrix $\boldsymbol{\Omega} \in \mathbb{R}^{5\times5}$. Since $\boldsymbol{\gamma}$ is a diagonal matrix and $\boldsymbol{\Omega}$ is determined as described above using the map $\tilde{P}_c$, it is possible to write the Jacobian of $\tilde{P}_c$ as:

$$D\tilde{P}_c = \boldsymbol{\Omega}\boldsymbol{\gamma}^{-1} \tag{6.14}$$

The sequence $\{\tilde{z}_n\}$ is obtained by iterating the map $\tilde{P}_c$ in Eq. 6.13 starting from an initial condition $\tilde{z}_0 := (y_{1_0}, y_{2_0}, x_{1_0}, x_{2_0}, \theta_0, \omega_0)^T = (0.29, -0.29, 5.53, -5.53,$ $0.1, -0.7)^T$. Fifty iterations of the map $\tilde{P}_c$ are computed. The Jacobian matrix $D\tilde{P}_c$ is determined using the last iterate. One could note that this method cannot find unstable period - 1 orbits. The maximum absolute value of the eigenvalues (MAE) of the Jacobian matrix $D\tilde{P}_c$ determines the stability, and the system is stable whenever this value is less than 1. The condition (MAE < 1) can also include possible, stable,

intermittent freezing behaviour of the dynamics. Normal gait responses are associated with the Period-1 orbits. Hence, in addition to the MAE condition, an additional term based on the return map information is used to identify the Period - 1 orbits. The additional metric introduced ensures the convergence to Period-1 orbit over a finite period of simulation time.

The convergence of the orbits to a limit cycle during a finite time simulation is tested by generating a vector $\mathcal{C}_p$. The vector $\mathcal{C}_p$ is generated by computing the norm of the differences between consecutive iterates of states for the last 20 iterations in the following way,

$$\mathcal{C}_p := \{ \ \|(\tilde{z}[r] - \tilde{z}[r-1])\|_2 \ , \ \forall r \in \{N-n, \ N\}\} \ . \tag{6.15}$$

Here, N $(= 50)$ is the total number of iterations simulated, n $(= 20)$ is the number of consecutive iterations used for convergence estimation and r is the iteration number. The l_2 norm of the resulting vector $\mathcal{C}_p$ is computed as a measure of convergence. When $\|\mathcal{C}_p\|_2 < 10^{-4}$ the orbit is assumed to converge to a limit cycle. The procedure described addresses the Period - 1 orbits (stability of normal walking) of the map $\tilde{P}_c$. Period - 1 orbit of the map $\tilde{P}_c$ which in turn is formed by the iteration of the map P twice as explained in Fig. 6.6, hence when $N = 50$ a total of 100 steps are simulated. A Monte-Carlo stability analysis was performed. For this, the system in Eq. 6.1 - Eq. 6.4 is simulated using 1000 randomly initiated $(e, \ S_t, \ f_b)$ parameter vectors. For each $(e, \ S_t, \ f_b)$ parameter vector, the procedure discussed above is followed, and the MAE and $\|\mathcal{C}_p\|_2$ are computed to classify the stability of the walking regime of the system. The Fig. 6.7 show the results of the Monte-Carlo simulation. Here the green points indicate the stable period - 1 orbit, i.e., MAE < 1 and $\|\mathcal{C}_p\|_2 \leq 10^{-4}$. The analysis reveals the existence of stable periodic orbits for a subset of the parameter space considered. As evident in the Fig. 6.7 while a higher value of e and s_t are beneficial for walking, the key distinguishing factor is f_b. A higher value of f_b is necessary for the system to be in a stable periodic orbit. The median and standard deviation (given in brackets) of the parameter f_b, e and S_t in the stable periodic region (green) is found to be 1.34 ($\pm$ 0.37), 0.64 ($\pm$0.23), and 3.5 ($\pm$1.57) respectively.

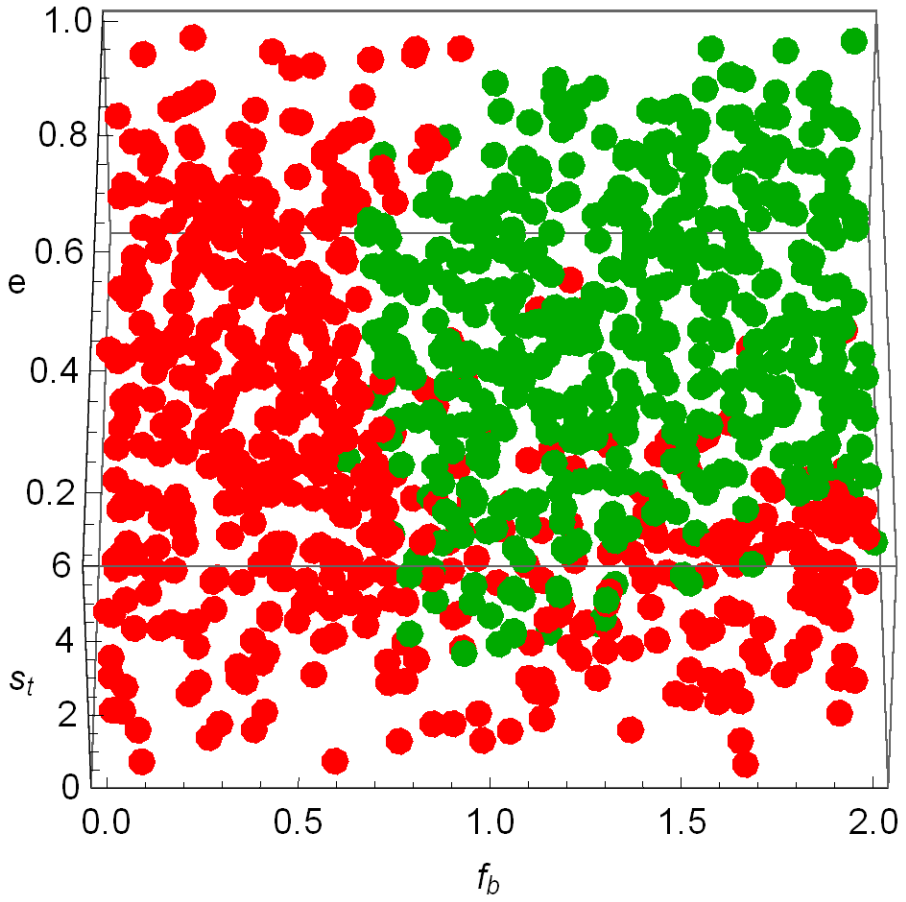

Figure 6.7: Results of the 1000 point Monte - Carlo simulation showing stable periodic region and the rest. The region with MAE < 1 and $\|\mathcal{C}_p\|_2 < 10^{-4}$ is shown in green. The rest of the region indicated in red. In the boundaries of the stability region the value $\|\mathcal{C}_p\|_2$ crosses 10^{-4}. The purpose of this figure is only to illustrate the ability of the model to generate stable walking in a subset of the parameter range.

The distribution of the parameters f_b, e and S_t in the stable region are significantly different ($p < 10^{-6}$ Mann-Whitney test) from that in the rest (red region).

Further analysis of the freezing fraction and coefficient of variation are aimed to study the possibility of a possible freezing episode during the iterations of the map.

6.5 Effect of External Input in the Absence of Proprioceptive Feedback

This section details the effect of periodic sensory signals such as auditory inputs and STN (subthalamic nucleus) stimulation given to PD patients for alleviating FoG. The external input $I(t)$ shown in Fig. 6.2 alters the phase and thereby influences the synchronisation as discussed in Sec. 6.2.2. In this section, the effects of varying the amplitude and the frequency of the external input $I(t)$ on states defining the neuronal activity $(y_1(t), y_2(t))$ and the angular velocity state of the limbs (Σ_m) in the absence of the proprioceptive feedback $\Xi(t)$ in Fig 6.2 are studied. This helps to understand qualitative differences in the region of synchronous behaviour of CPG and the non-freezing regime under the action of external periodic input for the overall system in the absence of proprioceptive feedback. The analysis is done in two sub-sections as follows:

6.5.1 Effect of external input on neuronal activity

The system in Eq. 6.1 - Eq. 6.4 under the influence of external input, with $a \neq 0$ and $f_b = 0$, possibly resulting from sensory or auditory cues (Dietz, 2003; Cheung et al., 2005; Tuthill and Azim, 2018), is studied. By forcing the feedback term to zero, the effect of external input on the CPG neural part of the system only is considered here. The amplitude scaling parameter a and the frequency Ω_f of the external input, in Eqs. 6.5, 6.8 and 6.9 are varied from 0 to 3 in steps of 0.1 and from 0 to 2 in steps of 0.025, respectively. The range and steps are chosen such that the trend is revealed in the physiologically acceptable range. The frequency range is chosen to be a representative range of the walking frequencies (Hausdorff et al., 2003). The effect of variations on the CPG is quantified in the following manner.

The system in Eq. 6.1 - Eq. 6.4 is simulated for 30 seconds using two sets of initial conditions - (a) Nominal initial conditions as given in Table 6.1, and (b) Perturbed initial conditions with $y_{10} = 2$ instead of $y_{10} = 1$ and the remaining as listed in Table 6.1. The perturbation to state y_1 alone causes desynchronisation.

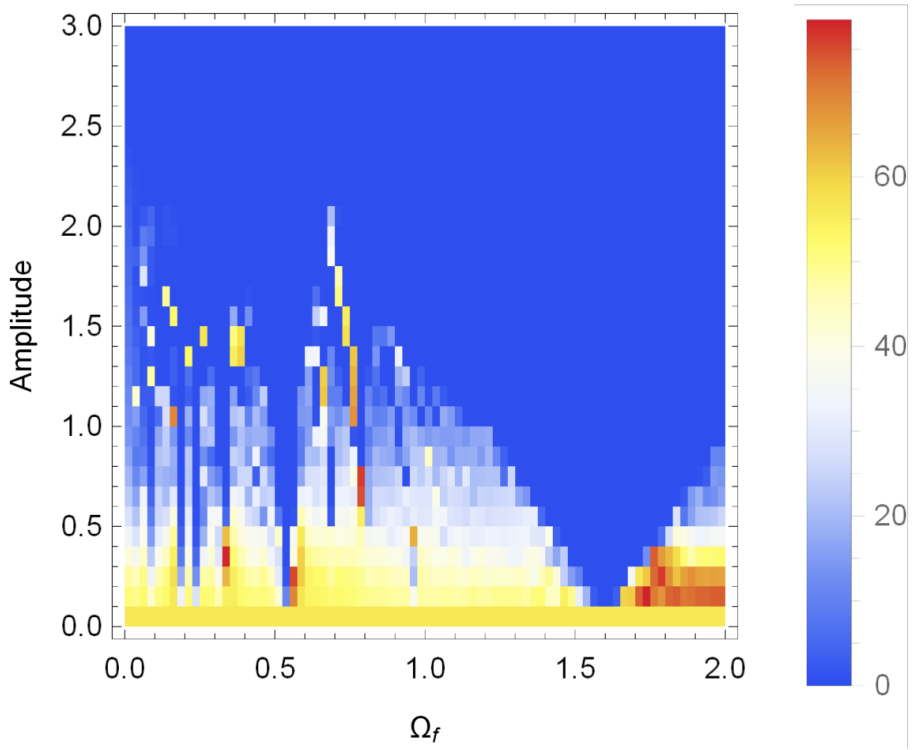

Figure 6.8: The l_2 norm of the difference trajectories, $\|\mathcal{E}\|_2$, for different values of frequency Ω_f in Eq. 6.9 and for different values of amplitude scaling parameter in Σ_{n_i} (with 0.1-0.025 grid). $\|\mathcal{E}\|_2$ calculated for time duration from $t_1 = 27$ to $t_2 = 30s$ with initial conditions (a) $y_{10} = 1$ and (b) $y_{10} = 2$. The highly synchronised regions are in blue with low value for the norm.

The chosen perturbed initial condition corresponds to a point chosen outside the limit cycle of the oscillator. Let the subscripts 'a' and 'b' in sequel correspond to the two cases of initial conditions for the 30 seconds finite time simulation of the system as described above. Let $\mathcal{Y}_a^{[t_1,\ t_2]}$ and $\mathcal{Y}_b^{[t_1,\ t_2]}$ represent the CPG neuronal activity state vectors $(y_1(t),\ y_2(t))$ during the time period $[t_1,\ t_2]$ starting at two different initial conditions. While synchronisation is achieved, $\mathcal{Y}_a^{[t_1,\ t_2]}$ and $\mathcal{Y}_b^{[t_1,\ t_2]}$ must be close in both phase and amplitude, in a non-trivial manner. Further, let $\|\mathcal{E}\|_2 := \|\mathcal{Y}_a^{[t_1,\ t_2]} - \mathcal{Y}_b^{[t_1,\ t_2]}\|_2$ be the l_2 norm of the difference between the neuronal activity trajectories from $t_1 = 27$ to $t_2 = 30s$. When two trajectories $\mathcal{Y}_a^{[t_1,\ t_2]}$ and $\mathcal{Y}_b^{[t_1,\ t_2]}$ are close in both phase and amplitude the $\|\mathcal{E}\|_2$ reaches a very small value ($\|\mathcal{E}\|_2 <= 10^{-4}$) indicating here synchronisation of neuronal states. The term $\|\mathcal{E}\|_2$ for different values of frequency Ω_f in Eq. 6.9 and for different values of scaling of amplitude a in Σ_{n_i} is plotted in Fig. 6.8.

External cueing is a highly relevant treatment option for PD (Spaulding et al., 2013; Ghai et al., 2018; Willems et al., 2006; Nieuwboer, 2008). Moreover, orbitally stable walking requires synchronised neuronal activity at the level of CPG. In Fig. 6.8 a region of synchronised behaviour (blue region) can be observed for a higher amplitude of external input.

Even though one could see synchronised neural activity at a low amplitude of external input, synchronised neural behaviour is observed for a relatively broad range of frequencies at a higher amplitude of external input.

6.5.2 Effect of External-Input on the *Freezing Fraction*

The neuromechanical system described in Eq. 6.1 - Eq. 6.4 under the influence of external input (with $a \neq 0$ and $f_b = 0$) is studied in this section for its effect on *freezing fraction* defined in Sec. 6.2.3. The parameters a and Ω_f of the state independent exogenous input term $aI(t)$ in Eq. 6.5 are varied. The frequency Ω_f and the amplitude a of the external input are plotted against the *freezing fraction* in Fig. 6.9. The simulation is executed for 30 s, and the fraction of freezing events is computed from the simulated data. The result is plotted in Fig. 6.9 where the

blue and red region indicates the region of the low and high number of freezing episodes, respectively. A blue region is observed with a low freezing fraction when the external input frequency (Ω_f) is between 1 to 1.5 Hz. In this region, the neural and mechanical systems synchronise to generate a normal gait pattern. Figures 6.5a and 6.5b demonstrate the effect of external input on otherwise freezing neuromechanical model with a very low feedback ($f_b = 0.1$), as fully evident from the present analysis in Fig. 6.9.

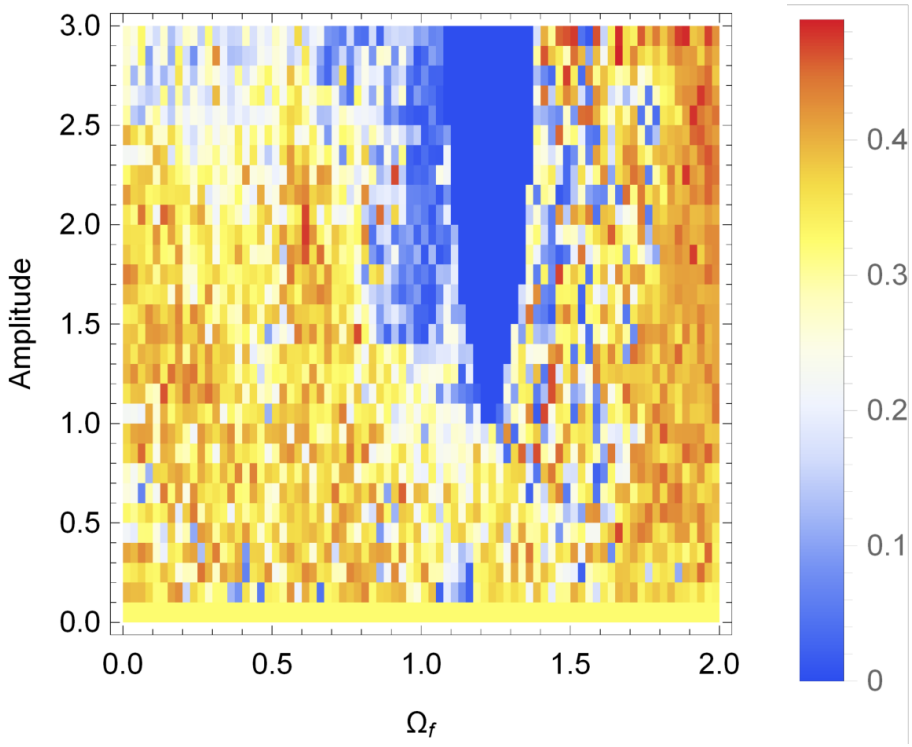

Figure 6.9: The effect of external input is studied here on a system with no feedback ($f_b = 0$). The amplitude of the input a and frequency of stimulation Ω_f are plotted against the *freezing fraction*. The simulation is done for 30 s. and the corresponding fraction of freezing events are computed. The blue region has a low, and the red region has a high fraction of freezing events. For the parameter set chosen, the appropriate frequency to achieve walking is between 1-1.5 Hz.

6.6 Effect of feedback on the overall system

The sensitivity of the parameters f_b and e in CPG dynamics has been studied to understand gait variability. The coefficient of variation (CV) (Ospina and Marmolejo-

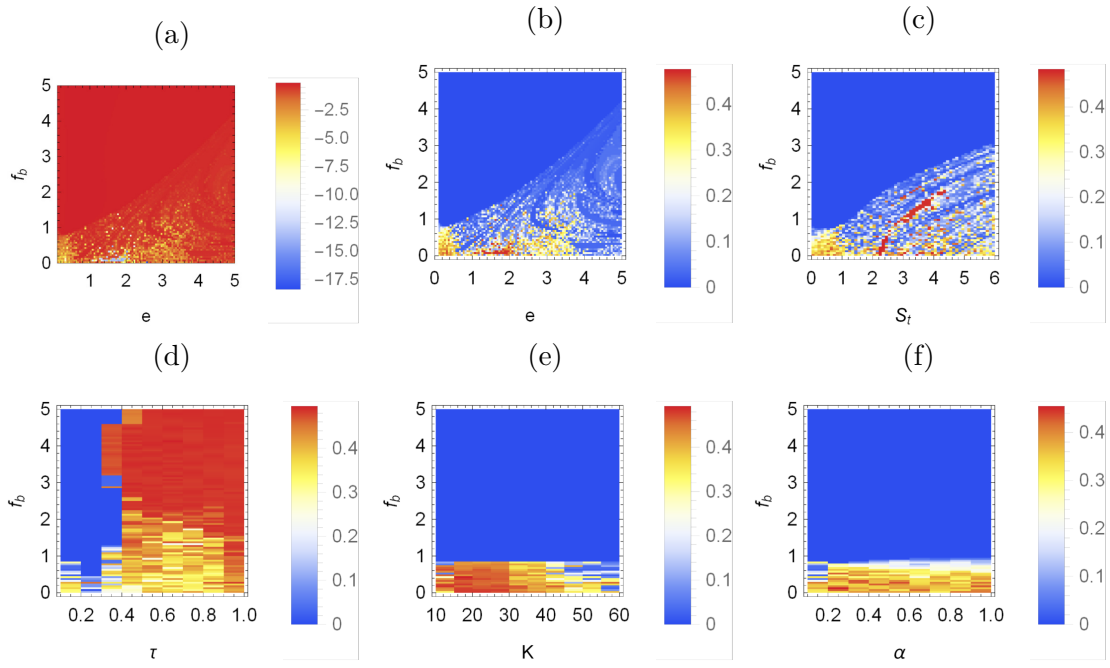

Figure 6.10: The parameters e, f_b, α, τ, K, S_t are studied here to understand its effect on the *freezing fraction*. The effect e and f_b on CV is also provided. While freezing depends on every parameter in the model, its dependence on S_t, τ and e are qualitatively different from α and K when simultaneously varied with f_b. The effect of f_b on synchronisation is not altered by the other parameters, and an increase in τ results in freezing even at high f_b. (a) CV of a 30 s. simulation while varying e and f_b has been plotted. A low value of f_b and e result in a higher absolute value of CV and vice-versa. (b) *Freezing fraction* in 30 s. simulation; while varying e and f_b has been plotted. A low value of f_b and e result in higher *freezing fraction* and vice-versa. Qualitatively region of high *freezing fraction* also can have high CV (c) The effect of S_t and f_b on the *freezing fraction* is indicated (d) The effect of τ and f_b on the *freezing fraction* is considered. (e) The effect of K and f_b on the *freezing fraction* is studied. (f) The effect of α and f_b on the *freezing fraction* is plotted.

Ramos, 2019) is used as the metric for this study. The coefficient of variation is calculated as the ratio of the standard deviation to the mean of the angular velocity ω in simulations. The static parameters f_b and e are varied, and the *hybrid walking model* is simulated for a duration of 30 s. The CV of the ω is presented as a function of the parameters e and f_b in Fig. 6.10a. Lower f_b generates high variability. A very low value of e results in a lower energy supply to the mechanical system and results in higher variability. A region of appropriate f_b and e (the red region in Fig. 6.10a) results in low variability and low freezing. The freezing fraction (see Fig. 6.10b) also has a qualitatively identical pattern as that of Fig. 6.10a. This helps to explain the higher variability seen in PD patients (Heremans, Nieuwboer and Vercruysse, 2013a).

6.6.1 Parameters $\alpha,\ \tau,\ K,\ S_t$

A set of figures are provided here which study the effect of parameters $\alpha,\ \tau,\ K,\ S_t$. The parameters are explored while varying simultaneously with f_b. The parameters $\alpha,\ \tau,\ K,$ and S_t (Fig. 6.10) are also studied to understand its effect on the *freezing fraction* while varied simultaneously with the parameter f_b. Increasing α and K from 0 to 1 and 10 to 60 respectively showed qualitative changes in behaviour only at lower f_b ($f_b < 1$). Increasing τ resulted in higher freezing fractions even at higher f_b values. Varying S_t with f_b showed different regions of walking and freezing behaviour is higher f_b resulting in lower freezing fractions.

6.7 Discussion

Freezing of gait (FoG) is a neuro-mechanical phenomenon emerging from the hybrid interactions between the neural and impulsive mechanical systems. This work sheds light on the physiological underpinnings from which this phenomenon emerge.

In this chapter, a mathematical model has been developed, taking into account the CPG based control, state-dependent proprioceptive feedback and limb mechanics. The proposed model exhibits normal gait with *orbital stability*, Freezing of gait (FoG) and transitions between the walking and freezing behaviour. The

proposed model explains freezing from the perspective of proprioceptive feedback (Sec. 6.6) and has relatively lower dimensional complexity than existing detailed biophysical models such as the one by Taga, 1995; Aoi et al., 2019. The analysis of the multiple parameters of the model together with feedback strength f_b revealed the importance of individual parameters on the freezing fraction.

The effect of sensory feedback on normal gait has been studied previously by several authors (Taga, 1995; Aoi and Tsuchiya, 2006; Tamura et al., 2020). It is also hypothesised that subjects with PD show a lack of adequate feedback (Spaulding et al., 2013; Ghai et al., 2018). The results in Sec. 6.6 articulates the role of feedback in freezing, primarily how the reduced feedback generates a lack of synchrony and consequently the FoG. The synchronisation of non-linear systems using external inputs is well established (Izhikevich, 2007). This study, specifically the results in Sec. 6.5.2, reveals how the synchronisation gets induced in PD-Gait to avoid FoG. Moreover, the results indicate that the external input ($I(t)$) helps to reduce the freezing incidences in this case for inputs of a range of frequencies (1 - 1.5 Hz) and amplitudes (greater than 1.2). Hence, there is potential for the use in real-life scenario with appropriate personalised adaptation of the model. One could validate the model by varying sensory/auditory cue amplitudes and frequencies provided to manage freezing. The model predicts that there will be a region of synchronized walking. One could note that this region could vary for different patients as the parameters could vary between subjects.

The external input models the auditory/sensory cueing in a phenomenological way, the frequency of which is vital (Willems et al., 2006). Cueing at low and very high frequency are not considered appropriate for managing FoG (Willems et al., 2006; Nieuwboer, 2008). Moreover, an STN stimulation study by Fischer et. al. (Fischer et al., 2020) also show entrainment in stepping in place for PD patients. Results in Sec. 6.5.1 and 6.5.2 indicates the plausible physiological mechanism underlying this frequency-dependent behaviour in PD. The 'region of synchrony' of oscillators shown in Fig. 6.8 is larger than the non-freezing areas shown in Fig. 6.9. Therefore, synchrony in CPG does not necessarily imply normal walking, and

walking in humans is essentially a result of synergistic neuromechanical interaction of the limbs and CPG.

The physiology of walking is still not well understood. NRGc (nucleus reticularis gigantocellularis), NRMc (nucleus reticularis magnocellularis), LC/RN (locus coeruleus / raphe nuclei) and Corticospinal tract (form motor cortex) send inputs to the CPG. Inhibitory NRGc input is modulated by the inputs from the pontine reticular formation (PRF) which is in turn regulated by the inputs from PPN (pedunculopontine nucleus). PPN, an area that controls posture and regulates muscle tone, receives projections from globus pallidus and substantia nigra pars reticulata (GPi and SNr), the input to which is defective in PD (Snijders et al., 2016). There is growing evidence on the role of PPN in PD-Gait (Magrinelli et al., 2016). In the model, the muscles' increased overall tonicity can be attributed to the parameter e for the limited region of parameter space investigated. Lowering e is beneficial in generating rhythmic walking in the model in some region of the parameter space with appropriate value for f_b. The generation of locomotor pattern upon stimulation of the region between ventral CNF (Cuniform Nucleus) and PPN could be explained this way.

Other parameters of the model are also analysed jointly with f_b. A high value of the parameter τ which slows down the CPG oscillators, resulted in freezing. For the higher value of τ, even a relatively higher value of feedback did not synchronise the system in the parameter range explored. The period of oscillations are driven by the neuromodulators and can vary within a range. A more detailed study of the variations in the oscillator's time period, its stochastic nature, and the variations in the phase responses of the neural system is future work. Varying connection strength (S_t) along with f_b also delineate the importance of higher feedback in the system with higher f_b resulting in lower chances of freezing.

The connection strength relates to the homeostatic plasticity of the CPG neurons (Northcutt and Schulz, 2020) and further experimental study is needed to understand its implication in PD. The parameter exploration points to the relatively complex ways of generating FoG and the possible reasons one treatment method

does not work for all. Furthermore, finding the exact physiological correlates of the model-parameters needs further study. An experimental study on human/animals under the influence of auditory inputs while simultaneously monitoring the CPG activity and the proprioceptive feedback input to the CPG would better understand the physiology.

Muscle synergy and the uncontrolled manifold hypotheses by Latash, Scholz and Schöner, 2002 puts forth a theory of coordinated action of a set of muscles such that motor redundancies are avoided. The proposed model shows that violation of this coordinated action hypothesis could lead to pathological behaviour such as freezing. Hence, this model and the muscle synergy hypothesis stay compatible. In the language used by Latash et al. (Latash, Scholz and Schöner, 2002), the 'bad region of variability' could very well be the cause of the pathological gait observed in PD. One could conclude that CPG and limb mechanics' dynamics are sufficient to explain many of the gait abnormalities, and a more focused study of the spinal cord changes and PPN in PD will shed more light on the matter.

7. Phase Reset Curve Based Generalization of the Freezing of Gait Model

This chapter aims to develop a simplified discrete model-based framework for studying gait using the learnings from the previously described models in chapters 5 and 6. The role of oscillators is simplified using the ideas of the phase reset curves (PRC), and the mechanics are further simplified using an energy argument. While this is a simple framework to study gait, the use of the PRC curves is general enough to study different types of neuronal oscillators or neuronal ensembles

Abnormal neural inputs counteract inertia and result in the sudden stoppage of gait, while generating high gait variability between freezing events (Barbe et al., 2014). Studies show activations of several regions of the brain correlate with seemingly disparate symptoms related to freezing of gait (Pozzi et al., 2019; Heremans, Nieuwboer and Vercruysse, 2013b). Therefore, it is unclear if the gait abnormalities (freezing, highly variable stepping) in PD are the manifestations of the same underlying cause or the result of several plausible pathologies.

In summary, the variability and freezing observed in PD-Gait necessitate a mathematical explanation. While there are several attempts to address this question, there is a need to develop a simple mathematical model which addresses this problem. Moreover, the model is required to accommodate the effect of PPN stimulation and the influence of oscillator time-period. There is also a demand for modularisation of the different systems governing the walking model, such that one could study different types of perturbations to the CPG system.

The chapter is structured as follows. The PRC based mathematical modelling procedure is described in the Sec. 7.1 with the relevant functions and quantification of freezing fraction in Sec. 7.2. Subsequently, the results and discussion are presented in Sec. 7.3 and Sec. 7.4 respectively.

7.1 Modelling

The section describes the assumptions and modelling approach used to generate maps governing PD walking dynamics.

7.1.1 Neural oscillators and phase

CPG are assumed to be controlling walking dynamics (Minassian et al., 2007), which can in turn be represented as oscillators. Sec. 3.2.6 provides a more detailed description of PRC and its relationship with oscillator dynamics. The following definition of phase is repeated for clarity.

Definition 7.1.1 *For each point x in the basin of attraction of the periodic orbit $\tilde{\varphi}(t)$ of the oscillator, there exists a unique function $\phi(x)$ such that*

$$\lim_{t\to\infty} |x(t) - \tilde{\varphi}(t + \phi(x))| = 0, \tag{7.1}$$

where $x(t)$ is a trajectory (solution) of the dynamical system starting with the initial point x. The value $\phi(x)$ is called the asymptotic phase *or* phase *of x (Josic, Shea-Brown and Moehlis, 2006).*

When the oscillator's trajectory is in the basin of attraction of the limit cycle, a function $\phi(\cdot)$ as defined in Def. 7.1.1 could be used to determine its *phase*.

PRC in Gait: One could assume the torques supplied to the legs as a function of the *phase*. Another key aspect is the effect of the perturbation on neural oscillators due to input from the limbs or the brain. This is modelled as perturbations to the *phase* of these oscillators. Perturbation of the oscillator of state x with phase $v := \phi(x)$ results in shifting the oscillator to a new state $\bar{x}$ with

phase $\bar{v}$. Then $\bar{v} := v + PRC(v,\ a)$. After time T_q the *phase* would be equal to $(v + PRC(v,\ a) + T_q\ )$ mod T where T is the time period of the oscillator and a is the amplitude of the feedback. It may also be noted that the continuous inputs for a longer duration can also be approximated as impulses (Izhikevich, 2007).

7.1.2 Mechanics

A linearised inverted pendulum model of the form $\dot{z} = \mathbf{A}z$ is used to approximate the limb dynamics, where the states $z = [\theta,\ \omega]^T$ and the system matrix $\mathbf{A}$ is

$$\mathbf{A} := \begin{bmatrix} 0 & 1 \\ g/l & 0 \end{bmatrix} \tag{7.2}$$

where, g is the acceleration due to gravity and l the length. The time required to

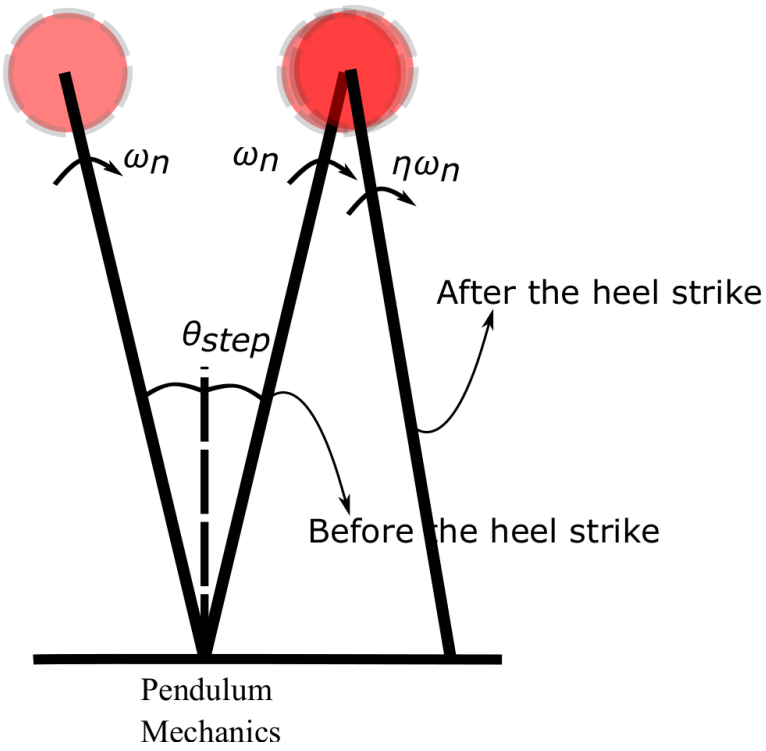

Figure 7.1: Inverted pendulum dynamics relevant to the PRC based discrete EoM. The angular velocity changes from ω_n to $\eta\omega_n$ after the heel strike.

reach the state z_e starting from the state z_s can then be computed for the cases where it is physically possible by finding the t_q s.t. $e^{\mathbf{A}t_q}z_s = z_e$ in terms of the elements of the matrix $\mathbf{A}$ and the initial conditions. Let the states $z_s = [\theta_{step},\ \omega_n]^T$

and $z_e = [-\theta_{step},\ \omega_n]^T$ represent the starting position and the end position of an inverted pendulum immediately before the heel strike. As indicated in Fig. 7.1, a constant angular velocity is assumed at the end of the step before reset in accordance with the conservation of energy argument provided in the Appendix. B.1. For $z_s = [\theta_{step},\ \omega_n]^T$ and $z_e = [-\theta_{step},\ \omega_n]^T$

$$\mathrm{e}^{\mathbf{A}t_q} z_s - z_e = 0 \tag{7.3}$$

By finding the root of the Eq. 7.3 the *time to impact* or *the time to heel strike* is obtained as follows,

$$t_q(\omega_n) = \sqrt{\frac{l}{g}} \log \left(\frac{\omega_n \sqrt{\frac{l}{g}} - \theta_{step}}{\omega_n \sqrt{\frac{l}{g}} + \theta_{step}} \right) \tag{7.4}$$

Here, t_q maps the angular velocity to corresponding *time to impact* or *time to heel strike*. The time is measured from the initial condition (which is typically the start of the toe off phase) to the heel strike. As one can observe, it is a function of the parameters of the model θ_{step}, l and g (see Table 7.1 for values). In this work the angle θ_{step} is assumed to be a constant thereby reducing the number of mechanical states to be modelled to one. Slowing down, and corresponding reduction in step length will therefore result in increased time to impact.

However, when the angular velocity is sufficiently small, the $t_q(\omega_n)$ as defined in Eq. 7.4 will not result in a positive real value. To account for this, the following definition is used,

$$T_q(\omega_n) := \begin{cases} t_q(\omega_n)\ if\ t_q(\omega_n) \in \mathbb{R}^+ \\ r_t\ if\ t_q(\omega_n) \notin \mathbb{R}^+ \end{cases} \tag{7.5}$$

where r_t is the reaction time. When there is not enough moment to push forward, this account for the minimum time for the perception and the corresponding action. As the reflexes have a less than 50 ms delay (Malcolm, 1951) one could set $r_t := 0.05\ s$. The number of times $T_q(\cdot)$ equals r_t is counted as a freezing incident. This definition

of $T_q(\cdot)$ (Eq. 7.5) is used throughout this work.

As shown in Fig. 7.1 when θ_{step} is modelled as a constant, the only mechanical state that remains to be accounted for is the change in angular velocity in each step. By symmetry, the total amount of potential energy at the start of the stance and just before the heel strike are the same (neglecting the air friction and other losses). Additionally, this energy argument assumes the ground is uniform and the step length is constant. However, after the heel strike, one must account for the losses due to impulses and other losses. This is accomplished in the model using a constant $\eta < 1$. Further, accounting for the forcing received from the CPG, the equations of motion can be prescribed as follows.

$$\omega_{n+1} := \eta\omega_n + f_t(v_{n+1},\ \tilde{v}_{n+1}); \tag{7.6}$$

The variability in forcing introduced due to postural control during walking, swaying of hands, adjustments of the centre of gravity, different levels of muscle activation are also be absorbed into the function $f(\cdot)$.

7.1.3 The General PRC Based Model for Constant Step Size

The evolution of the angular velocity and phase can be prescribed in general using the equations given below. The PRC based equations show how given an initial condition $[v_n,\ \tilde{v}_n,\ \omega_n]$, functions $f_\omega(\cdot),\ f_v(\cdot),\ f_{\tilde{v}}(\cdot)$ propagate the system to $[v_{n+1},\ \tilde{v}_{n+1},\ \omega_{n+1}]$.

$$f_t(v_n,\ \tilde{v}_n) := f_1(v_n) - f_2(\tilde{v}_n) \tag{7.7}$$

$$\begin{aligned} f_v(v_n;\ \omega_n,\ a,\ T) := v_{n+1} := (v_n + PRC(v_n,\ a) \\ + T_q(\omega_n)) \bmod T \end{aligned} \tag{7.8}$$

The function $f_t(\cdot)$ maps the *phases* of the oscillators (phenomenologically modelling the slow dynamics of a bursting oscillator) to the net force generated by the muscles. In PD the forces can act in opposite directions (Nieuwboer et al., 2004; Parakkal Unni et al., 2020b) which is modelled as $f_1(\cdot)$ and $f_2(\cdot)$. Here $f_1(\cdot)$ corresponds to the

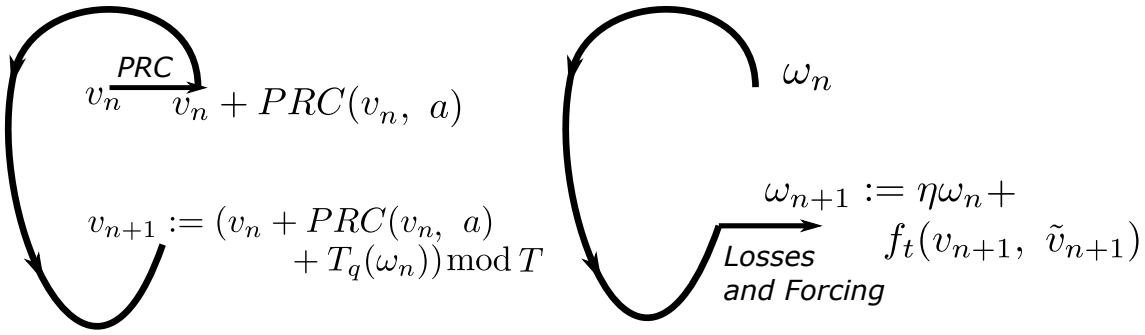

Figure 7.2: A trajectory of one of the oscillator's phase v_n and angular velocity ω_n close to a *limit cycle* is symbolized. The other oscillator's phase ($\tilde{v}_n$) also follows a similar qualitative pattern. After the heel strike, sensory input is sent to the CPGs and the phase of the oscillator jumps from v_n to $v_n + PRC(v_n,\ a)$ depending on the input received. This jump is therefore controlled by the $PRC(\cdot)$. The next heel strike happens after a time, $T_q(\omega_n)$ advancing the phase to $v_n + PRC(v_n) + T_q(\omega_n)\ mod\ T$ where T represents the oscillator's time period. The initial angular velocity ω_n after accounting for the losses $\eta\omega_n$ (due to impulse and other physiological causes) and forcing supplied by the oscillators transitions to $\omega_{n+1} := \eta\omega_n + f_t(v_{n+1},\ \tilde{v}_{n+1})$. Forcing supplied to the angular velocity at n^{th} iteration needs the phase of the oscillator at $n + 1^{th}$ step which is accounted for in Eq. 7.11.

forcing generated by the plantar flexors of the swing leg, and $f_2(\cdot)$ corresponds to that of the stance leg. The function $f_v(\cdot)$ maps the current *phase* of an oscillator to the new phase, and this phase in turn controls the amount of forcing in the next step.

$$f_\omega(\omega_n;\ v_n,\ \tilde{v}_n) := \omega_{n+1} = \eta\omega_n + f_1(v_{n+1}) - f_2(\tilde{v}_{n+1}) \tag{7.9}$$

$$= \eta\omega_n + f_t(v_{n+1},\ \tilde{v}_{n+1}) \tag{7.10}$$

$$= \eta\omega_n + f_t(f_v(v_n;\ \omega_n,\ a_1,\ T), f_v(\tilde{v}_n;\ \omega_n,\ a_2,\ T)) \tag{7.11}$$

The function $f_\omega(\cdot)$ maps angular velocity of one step to the next. As indicated in Fig. 7.2 the *phase* at the start of $n+1^{th}$ step v_{n+1} adds energy to the damped angular velocity $\eta\omega_n$. Parameters a_1 and a_2 are used to model the differences in the $PRC(\cdot)$ of the stance and swing leg respectively in each gait cycle. The value of a parametrizes the $PRC(\cdot)$. Therefore, these parameters control the change in *phase* due to the feedback (perturbations) received by these oscillators. This results in the following composition of the functions for a single gait cycle,

$$f_\omega^{p_2}(\omega_n;\ v_n,\ \tilde{v}_n,\ a_1,\ a_2,\ T) := f_\omega(f_\omega(\omega_n; v_n,\ \tilde{v}_n); f_v(\tilde{v}_n;\ \omega_n,\ a_2,\ T), f_v(v_n;\ \omega_n,\ a_1,\ T)) \tag{7.12}$$

$$f_v^{p_2}(v_n;\ \tilde{v}_n,\ \omega_n,\ a_1,\ a_2,\ T) := f_v(f_v(v_n;\ \omega_n,\ a_1,\ T); f_\omega(\omega_n;\ v_n,\ \tilde{v}_n),\ a_2,\ T) \tag{7.13}$$

$$f_{\tilde{v}}^{p_2}(v_n;\ \tilde{v}_n,\ \omega_n\ a_1,\ a_2,\ T) := f_v(f_v(\tilde{v}_n;\ \omega_n,\ a_2,\ T); f_\omega(\omega_n;\ v_n,\ \tilde{v}_n),\ a_1,\ T) \tag{7.14}$$

The functions $f_{\omega}^{p_2}$, $f_{v}^{p_2}$ and $f_{\tilde{v}}^{p_2}$ maps the states $\omega_n,\ v_n,\ \tilde{v}_n$ to $\omega_{n+2},\ v_{n+2},\ \tilde{v}_{n+2}$ respectively. All the maps required for a gait cycle as a vector valued function is given below,

$$\mathbf{f}^{p_2}(\omega_n,\ v_n,\ \tilde{v}_n;\ a_1,\ a_2,\ T) := \begin{bmatrix} f_{v}^{p_2}(v_n;\ \tilde{v}_n,\ \omega_n,\ a_1,\ a_2,\ T) \\ f_{\tilde{v}}^{p_2}(v_n;\ \tilde{v}_n,\ \omega_n,\ a_1,\ a_2,\ T) \\ f_{\omega}^{p_2}(\omega_n;\ v_n,\ \tilde{v}_n,\ a_1,\ a_2,\ T) \end{bmatrix} \tag{7.15}$$

7.2 Relevant functions

This section describes two of the functions that characterises the equations described in Eq. 7.15. Additionally, the method used for the computation of the *freezing fraction* is also provided.

7.2.1 Forcing Function

The function $f_t(v_n,\ \tilde{v}_n)$ controls the amount of 'forcing' given the phase v_n and $\tilde{v}_n$. The function $f_t(\cdot)$ combines two other functions $f_1(\cdot)$ and $f_2(\cdot)$ which phenomenologically represent the forcing supplied by the CPG on the limbs. A sinusoidal function is used for this purpose to ensure the starting of activation (of the CPG bursts) is at $v_n = 0$. The threshold operation using $\min(\cdot)$ ensures forcing is active only when the oscillator is in the active region of phase (positive region by definition),

$$f_1(v_n;\ m_{f_1}) := \min\left(m_{f_1}\sin\left(\frac{2\pi v_n}{T}\right),\ 0\right) \tag{7.16}$$

where m_{f_1} is a *muscle force constant* that controls the amplitude of the forcing generated on the limbs due to the muscles. This constant is varied to incorporate the differences in opposing ankle push-off forces (Nieuwboer et al., 2004). Similarly, the function $f_2(\cdot)$ is assumed to have m_{f_2} as the *muscle force constant*. This completes the description of the forcing functions f_1 and f_2 in Eq. 7.9. Indirectly, the *muscle force constant* also incorporates the synchronous forcing generated due to the swaying of

arms, postural adjustments, adjustments of the centre of gravity that multiplicatively amplifies the forcing. Furthermore, $|m_{f_1}| > |m_{f_2}|$ implies higher amplification of the neural forcing either due to the activation of more motor units or by the synchronous motion of the rest of the body.

7.2.2 PRC Function

PRC of the bursting neurons has been studied by several authors experimentally (Oprisan, Thirumalai and Canavier, 2003; Pinsker, 1977). The methodology described in this chapter forms a general framework for exploring these systems for understanding PD-Gait. Studying every possible form of PRC is not attempted and is very difficult. In this work, a set of general inhibitory PRC has been studied for their effect on walking. The model proposed can be modified to investigate a different PRC associated with walking by plugging in that function of the PRC rather than developing a differential-equation based neuromechanical model. Varying parameter T changes the frequency of oscillation, and varying a changes the PRC's shape. The system is simulated numerically using a family of PRC functions, and the results are plotted. The two oscillators governing the motion are assumed to have different $PRC(\cdot)$ functions. Hence, the parameter $a = a_1$ and $a = a_2$ are used to represent each of the oscillators. Neuromodulators, currents and variabilities in channel conductances affect the shape of the $PRC(\cdot)$, which can be studied by varying the parameters a and T.

Remark 6 *PRC of oscillators: Typically PRC can have regions (of phase) where an impulsive input will result in phase-advance, phase-delay or both. Typically,* integrator *types of neurons show a phase advance for excitatory impulsive input and* resonator *types of neurons can have a phase delay and phase advance against an excitatory impulsive input. The damped oscillations near a bifurcation point (e.g. subcritical Adronov-Hopf) result in the resonance behaviour (Izhikevich, 2007).*

7.2.3 Form of the PRC Functions Used in the Model

The PRC of the bursting neuron for inhibitory feedback is studied here for its influence on freezing. While this shows a plausible way of generating freezing and variability in PD patients, this is not a comprehensive list of all possible modes of inducing freezing. However, the methodology developed here generates a framework to test the multiple hypotheses as more experimental evidence emerges.

PRC relevant to the bursting CPG neurons of the form described in (Oprisan, Thirumalai and Canavier, 2003) is used in this work to represent a plausible class of bursting neurons. The convention used by mathematicians as described in Canavier, 2006 is used here. A positive value of PRC indicate an advance in phase under perturbation and vice-versa. However, biologists typically use the opposite convention (Canavier, 2006; Oprisan, Thirumalai and Canavier, 2003). As analytical expressions are not available for these PRC functions ($PRC(\cdot)$), an interpolated form of the function has been used for its study. Given a finite set of four points the interpolated $PRC(\cdot)$, between those points is defined as below.

$$PRC(v_n,\ a) := I_{fun}(I_s,\ \mathcal{O}) \tag{7.17}$$

where $I_{fun}(\cdot) \in C^0$ is an interpolation function of the order $\mathcal{O} \in \mathbb{N}$, $I_s \in \{I_m,\ I_e\}$ and $\mathcal{O} = 1$ where,

$$\begin{aligned} I_m := \{&(0,\ -0.5T),\ (0.4T,\ aT),\\ &(0.8T,\ aT),\ (T,\ 0.5T)\} \end{aligned} \tag{7.18}$$

$$\begin{aligned} I_e := \{&(0,\ -0.5T),\ (0.4T,\ 0),\\ &(0.7T + 0.25aT,\ 0),\ (T,\ 0.5T)\} \end{aligned} \tag{7.19}$$

The interpolation function is linear between the points. A general formulation of the interpolation function is used here to aid for future extensions. Hence, using the above definitions, one could generate different $PRC(\cdot)$ that correspond to different physiological scenarios by varying a. These functions map phase (v_n) to

the corresponding $PRC(\cdot)$ Substituting these $PRC(\cdot)$ in Eq. 7.9 - 7.15 generates different forcing functions and corresponding gait.

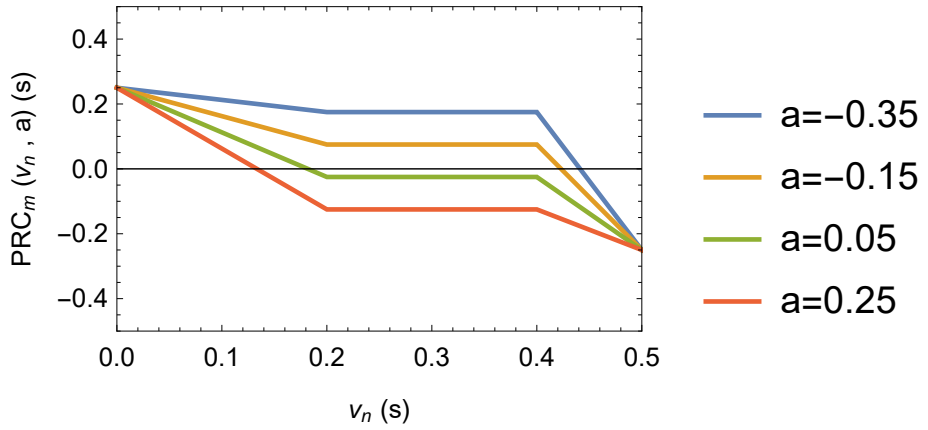

Figure 7.3: The $PRC_m(\cdot)$ parametrized by a with phase advance and delay regions having a shape similar to Oprisan, Thirumalai and Canavier, 2003 and Soofi and Prinz, 2015. Variations of a in $PRC_m(\cdot)$ further advances or delays the phase reset. If the slow variable is calcium then this shows how much change happens due to a perturbation in the accumulated calcium during a burst. Here T is chosen to be 0.5 which determines the length of the abscissa.

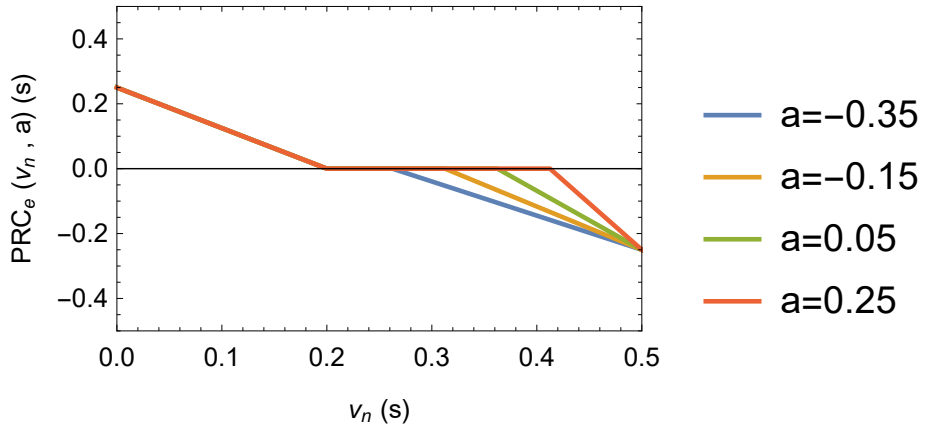

Figure 7.4: The $PRC_e(\cdot)$ parametrized by a with phase advance and delay regions having a shape similar to Oprisan, Thirumalai and Canavier, 2003 and Soofi and Prinz, 2015. Variations of a in $PRC_e(\cdot)$ changes the size of the MPR region. Here T is chosen to be 0.5 which determines the length of the abscissa.

The set of points I_m and I_e has been used to generate $PRC_m(\cdot)$ and $PRC_e(\cdot)$ respectively parametrized by a and T. This, in turn, depends on the channel which controls the slow dynamics (of the slow-fast system) and how it is modulated

(Oprisan, Thirumalai and Canavier, 2003; Ermentrout and Terman, 2010b). The effect of change in the frequency of oscillations is studied separately by varying T. As one could observe from the Fig. 7.3 the $PRC(\cdot)$ functions used in this work are piecewise-linear; parametrized by a and T. For a particular value of parameter a and T, the $PRC(\cdot)$ has three segments associated with it. For convenience, these three consecutive regions are named according to their relative locations. Region closer to the active region of the phase ($v = 0$) is defined as the beginning of phase region (BPR), a constant region in the middle is defined as the mid-phase-region (MPR), and the region closer to the next active region at the end, is defined as the end phase region (EPR). In other words, first, second and third piecewise linear segments of the $PRC(\cdot)$ defined in Eq. 7.17 correspond to BPR, MPR and EPR, respectively.

As shown in In Fig. 7.4, for $PRC_e(\cdot)$ varying a changes, the length of 'constant' phase-reset regime (MPR). A more negative a reduces the length of the MPR region. For $PRC_m(\cdot)$, as displayed in Fig. 7.3, varying a further advances or delays the phase reset. While a more negative a advances the phase reset, a positive value of a delays it. The same symbols a and T are used in both the PRC functions $PRC_m(\cdot)$ and $PRC_e(\cdot)$. Hence, one could only understand these symbols' meaning in conjunction with the PRC function it is referring to. Also, as two oscillators are there in the model, parameter a corresponding to the first and second oscillator are denoted by a_1 and a_2, respectively.

There is a multitude of plausible shapes that are observed experimentally even for inhibitory inputs as studied here (Pinsker, 1977; Soofi and Prinz, 2015) depending on the kind of physiology (e.g. conductances and perturbation levels/type) being studied. The framework developed here allows for the study of any PRC shape on FoG.

7.2.4 Freezing fraction

A set of initial phases $\{\mathbf{v}_0^i : i \in 1 \,..\, n_{init} \text{ where } \mathbf{v}_0^i \in \mathbb{R}^2\}$ is chosen from a uniform distribution defined on the grid $[-0.9T,\ 0.9T] \times [-0.9T,\ 0.9T]$. The initial angular velocity was chosen to be a constant. This was iterated for n_{iter} steps using the Eq.

No.	Parameters	Value
1	a_1	0.2
2	a_2	-0.2
3	T	0.5 s
4	r_t	0.05 s
5	m_{f_1}	-0.1
6	m_{f_2}	-0.1
7	l	0.7 m
8	η	0.98
9	g	9.8 $m\ s^{-1}$
10	$PRC(\cdot)$	$PRC_m(\cdot)$
11	ω_0	-0.7 rad. s^{-1}
12	v_0	0.05
13	$\tilde{v}_0$	0.3
14	θ_{step}	0.1 rad.

Table 7.1: Typical values of the parameters used in the simulations.

7.15 (with appropriate substitutions for the functions as described previously). The set formed by $\Omega_s := \{\omega_j^i : i \in 1\ ..\ n_{init}$ and $j \in n_{iter} - k\ ..\ n_{iter}\}$ is used for further analysis. The n_{init}, n_{iter} and k are chosen to be 10, 130 and 50 respectively. The fraction of freezing incidents in the set Ω_s is then computed by counting the number of points with $T_q(\omega_n) = r_t$ and dividing it with the cardinality of the set Ω_s.

7.3 Results

This section provides numerical simulations of the model and the analysis of its parameter variations. Unless otherwise specified, the parameters used in the model are given in Table 7.1. The simulations exhibit normal gait, FoG, variability in gait, change of gait from walking to freezing and vice versa. The model also displays orbits of different periods and chaos. Furthermore, multiple PRC shapes are studied to understand the effect of neurobiological perturbations.

7.3.1 Simulation of Normal Gait and Freezing

The Fig. 7.5 presents a numerical simulation of Eq. 7.15 using the $PRC_m(\cdot)$ and forcing function defined in Eq. 7.16. This subsection aims to demonstrate the

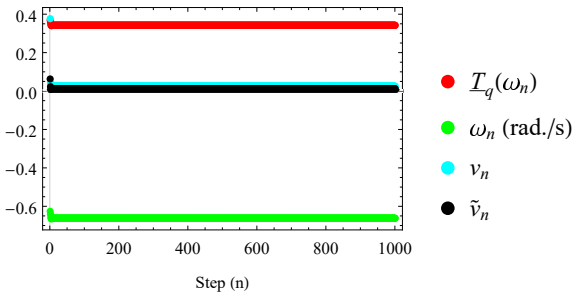

(a) *Period-1* orbit: States as a function of step number n. The parameters used in the simulations are $a_1 = 0$, $a_2 = 0.16$, $T = 0.628$, $\omega_0 = -0.626\ rad\ s^{-1}$, $v_0 = 0.1T$, $\tilde{v}_0 = 0.6T$ and $PRC_m(\cdot)$

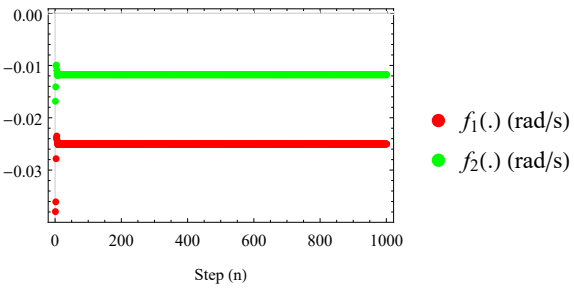

(b) *Period-1* orbit: Forcing as a function of step number n. The parameters used in the simulations are $a_1 = 0$, $a_2 = 0.1$, $T = 0.628$, $\omega_0 = -0.626\ rad\ s^{-1}$, $v_0 = 0.1T$, $\tilde{v}_0 = 0.6T$ and $PRC_m(\cdot)$

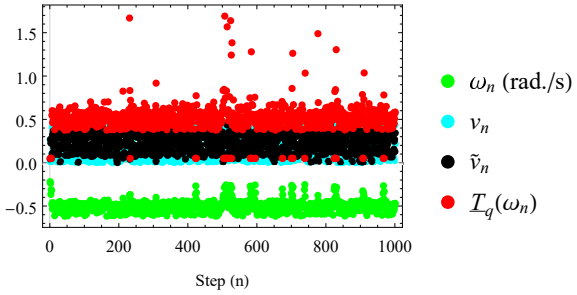

(c) *Freezing* with high variability: States as a function of step number n. The parameters used in the simulations are $a_1 = -0.416$, $a_2 = 0.198$, $T = 0.442$, $\omega_0 = -0.219\ rad\ s^{-1}$, $v_0 = 0.1T$, $\tilde{v}_0 = 0.6T$ and $PRC_m(\cdot)$

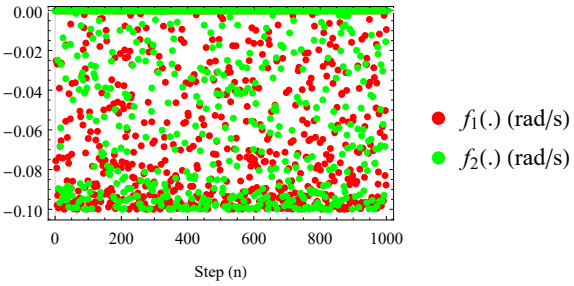

(d) *Freezing* with high variability: Forcing as a function of step number n. The parameters used in the simulations are $a_1 = -0.416$, $a_2 = 0.198$, $T = 0.442$, $\omega_0 = -0.219\ rad\ s^{-1}$, $v_0 = 0.1T$, $\tilde{v}_0 = 0.6T$ and $PRC_m(\cdot)$

Figure 7.5: Numerical simulation of Eq. 7.15 using the $PRC_m(\cdot)$ and forcing function defined in Eq. 7.16

capability of the model to exhibit freezing and normal gait. Subsequently, the role of parameters in producing freezing and normal gait are studied.

Simulation of Normal Gait: One could observe normal gait of *period-1* in Fig. 7.5a - 7.5b. In Fig. 7.5a, along with the states (ω_n, v_n, and $\tilde{v}_n$) the step time (T_q) as defined in Eq. 7.5 have also been presented. Forcing generated on both the limbs are plotted in Fig. 7.5b for the normal walking scenario. Here, the magnitude of forward forcing is larger than the opposing forcing generating a periodic orbit. One could note that the unit of forcing term expressed in rad. s^{-1} and not in Newtons.

One could interpret this forcing as increased angular velocity in a step resulting from the neural input.

Simulation of Freezing of Gait: Freezing shown in Fig. 7.5c arises from the 'untimely' generation of the forcing in the opposite direction (Fig. 7.5d) such that the forward forcing becomes incapable of pushing the centre of mass forward. At that point, $T_q(\cdot)$ gets reset to r_t as defined in Eq. 7.5. This reset results in $T_q = r_t = 0.05\ s$ in the freezing regions. One could also observe the instances of slowing down with $T_q > 1\ s$. Physiologically slowing down in the model could correspond to a reduction in step length in the real walking data. This is due to the constant step length assumption used in this model.

7.3.2 Effect of Changes in T, m_f, and η

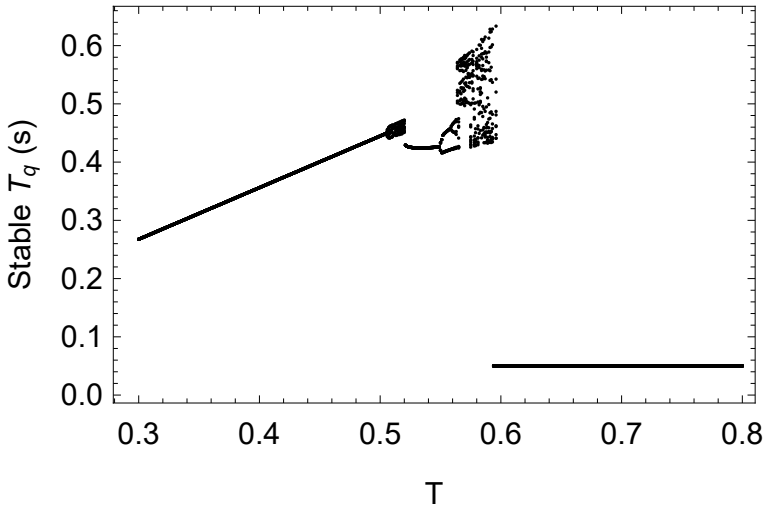

Figure 7.6: The stable T_q is shown as a function of the oscillator time period T. In the freezing region the value of Stable T_q is very low as the time to impact is defined to be $r_t = 0.05\ s$ in that case.

The oscillator's time period T and parameters m_f and η have been varied and the corresponding *time to impact* is studied in this section. The *time to impact* of the last 10 ($k = 9$) (after 1000 iterations of Eq. 7.15) iterates are plotted against the dependent variable $T,\ m_f,$ and η in Fig. 7.6, 7.7, and 7.8 respectively. $PRC_m(\cdot)$ is used in these simulations as the PRC function. Time to take a step increases (walking slows down) with an increase in oscillation time period T. After a threshold

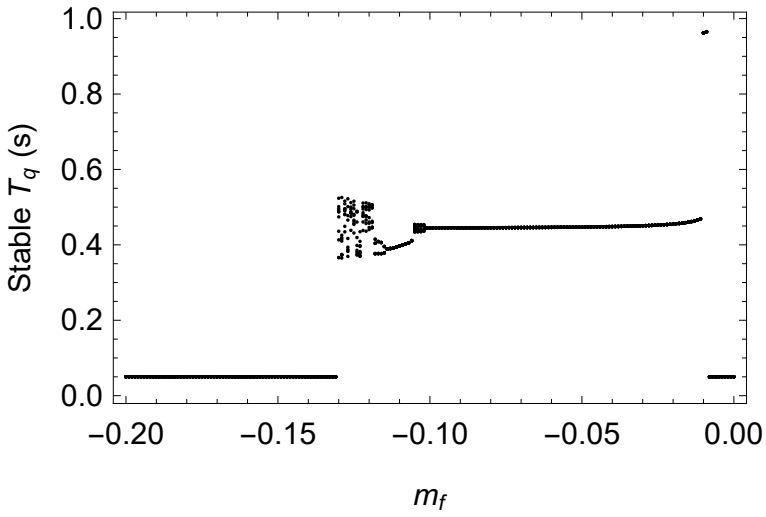

Figure 7.7: The stable T_q is shown as a function of the m_f. In the freezing region the value of Stable T_q is very low as the time to impact is defined to be $r_t = 0.05\ s$ in that case.

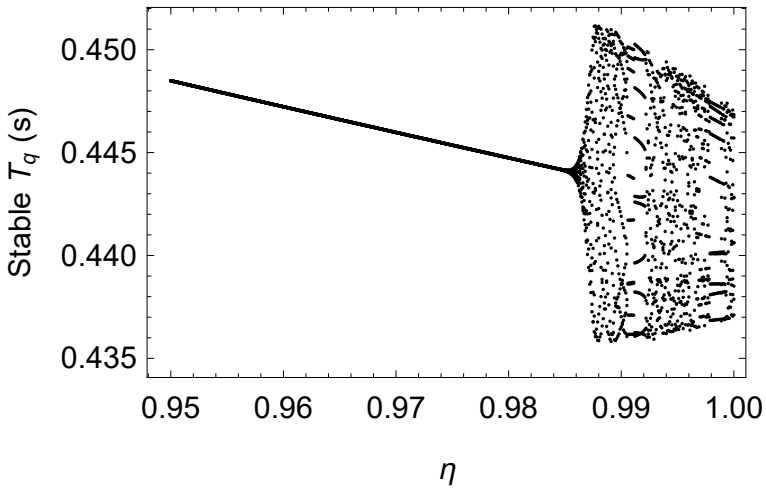

Figure 7.8: The stable T_q is shown as a function of the η. In the freezing region the value of Stable T_q is very low as the time to impact is defined to be $r_t = 0.05\ s$ in that case.

time period of oscillation, the variability in the system increases eventually leading to freezing after $T \cong 0.6\ s$ (Fig. 7.6).

As depicted in Fig. 7.7 very low $|m_f|$ results in freezing; when $|m_f|$ is increased, this results in periodic walking behaviour. However, a further increase in $|m_f|$ does not result in better walking performance but high variability, eventually leading to a freeze. Moreover, a lower absolute value of the parameter m_f could be attributed to lower muscle-tone. One could hypothesise PPN stimulation (known to result in lowering the muscle tone (Snijders et al., 2016)) plausibly moves the system to the region of the optimal muscle-tone, helping to avoid a freeze.

As shown in Fig. 7.8, an increase in η results in an increase in the walking speeds (decrease in time to impact). However, a further increase close to $\eta \cong 1$ results in high variability. The parameter η phenomenologically controls the losses which are proportional to the angular velocity such as impulse losses.

7.3.3 Varying the shape of the PRC

Two qualitative variations of the PRC, namely $PRC_m(\cdot)$ and $PRC_e(\cdot)$, are studied in this work. Variation of the PRC using $PRC_m(\cdot)$ is studied in Figs. 7.9a and 7.9b showing freezing fraction and coefficient of dispersion (CD) respectively. Freezing fraction and CD are computed by varying the parameter a of oscillators, that corresponds to the forward forcing (a_1), and backward forcing (a_2) in the model, individually. The freezing region and the normal gait region have low CD, while those regions' transition has a higher variability (higher CD). Varying a_1 and a_2 in $PRC_m(\cdot)$ does not show a clear demarcation for walking and freezing regions. However, one could note that when $a_1 \cong a_2$ the freezing fraction (Fig. 7.9a) and variability (Fig. 7.9b) is high. Variation of the EPR using $PRC_e(\cdot)$ is studied in Figs. 7.9c and 7.9d; showing freezing fraction and CD respectively. As described previously, the freezing fraction and CD are computed by individually varying the parameter corresponding to the forward forcing (a_1) and the backward forcing (a_2). The Fig. 7.9c indicates that $a_1 > 0$ and $a_2 < 0$ is better for walking. The region between walking and freezing exhibit high variability, as shown in Fig. 7.9d.

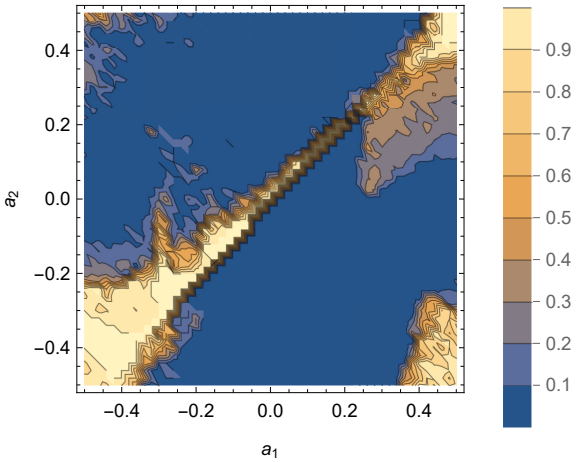

(a) Freezing fraction as function of $(a_1,\ a_2)$ at high initial angular velocity conditions. Constant Parameters $T = 0.5\ s,\ \omega_0 = -0.7\ rad.\ s^{-1}$. PRC function used is $PRC_m(\cdot)$

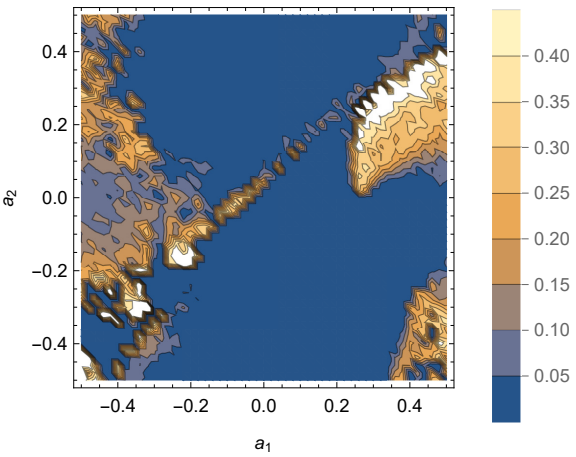

(b) coefficient of dispersion (CD) as function of $(a_1,\ a_2)$ at high initial angular velocity conditions. Constant Parameters $T = 0.5\ s,\ \omega_0 = -0.7\ rad.\ s^{-1}$. PRC function used is $PRC_m(\cdot)$

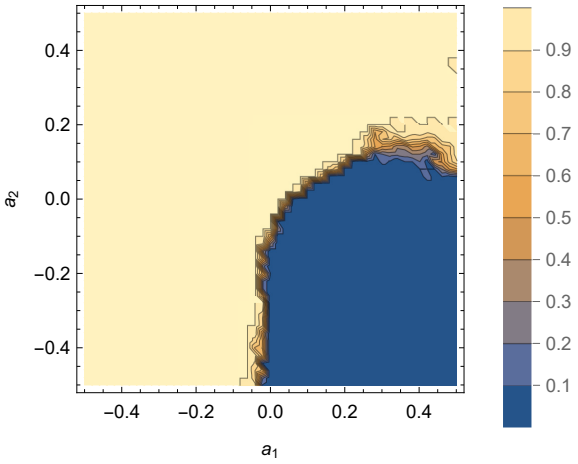

(c) Freezing fraction as function of $(a_1,\ a_2)$ at high initial angular velocity conditions. Constant Parameters $T = 0.5\ s,\ \omega_0 = -0.7\ rad.\ s^{-1}$. PRC function used is $PRC_e(\cdot)$

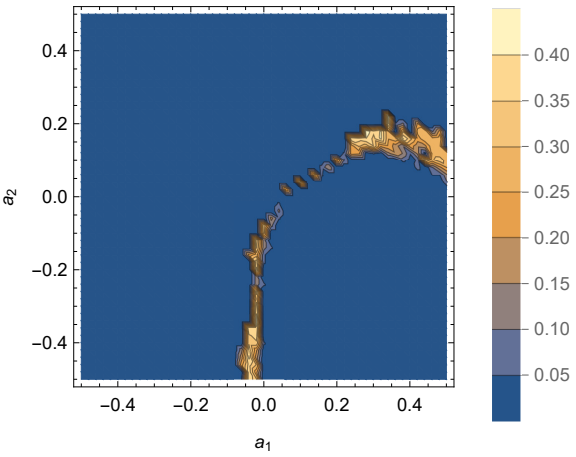

(d) Coefficient of dispersion (CD) as function of $(a_1,\ a_2)$ at high initial angular velocity conditions. Constant Parameters $T = 0.5\ s,\ \omega_0 = -0.7\ rad.\ s^{-1}$. PRC function used is $PRC_e(\cdot)$

Figure 7.9: Result for the PRCs of the type shown in Fig. 7.4. One must note that parameters a_1 and a_2 has different meanings in different $PRC(\cdot)$s and hence in different figures.

7.4 Discussion

Freezing of gait is a debilitating phenomenon, the mechanism of which is still unclear. In this work, PRC of CPG oscillators and walking mechanics have been used to generate a map to understand how feedback and related perturbations to the CPG systems affect PD locomotion. The plantar flexors of stance and swing legs are modelled following the observations given in (Nieuwboer et al., 2004). Hence, this model is specific to PD. The model shows the effect of PPN stimulation phenomenologically, and the modular structure of the model makes it compatible for testing out different PRC functions. Moreover, the modular structure aids in understanding the plausible neural correlates of PD variability and freezing of gait. Furthermore, as different models converge to similar PRC shapes, the results obtained using PRC based methodologies generalises to a larger class of models. The model has been studied to understand different perturbations on the PRC function and change in different parameters that potentially correspond to the PPN stimulation and oscillator time periods. Parameters of the CPG such as $T,\ m_f,\ \eta$ have been investigated in this chapter. The parameter m_f controls the total energy supplied from the muscles, and a higher absolute value of m_f could be attributed to higher muscle tone. Therefore, this parameter is a phenomenological representation of the PPN, which, when stimulated, decreases the muscle tone (Snijders et al., 2016). Plausibly, PPN stimulations that reduce muscle tone can be attributed to reducing the parameter $|m_f|$ in the model such that one achieves periodic walking. A related parameter is η, a lower value of which results in higher energy loss in each step. Therefore, this parameter is affected by impulsive dynamics and energy loss due to antagonistic muscles' activation. The time period (T) of oscillations is prone to be altered by different kinds of cellular perturbations, (e.g. neuro-modulators, temperature). Increasing the time period of oscillations beyond a threshold results in high variability and freezing. Further, this dependence on time period could be proposed as a plausible mechanism of freezing, necessitating further experimentation. The effect of change in time-period is studied independently, even though this change can affect $PRC(\cdot)$ shape. However, it could be argued that homeostatic mechanisms

such as intracellular calcium dependent readjustment of conductance make PRC and time-period independent. One of the novel aspects of this work lies in generating a PD-Gait model which is modular enough to accommodate different PRC shapes. These PRC functions abstractly represent the oscillator dynamics and control the forcing generated at each step, determining the system's future evolution to FoG and normal gait. There are disparate parameter sets such as conductances and currents, which could elicit similar circuit activity (Prinz, Bucher and Marder, 2004). Also, there are multiple underlying redundancies in the currents, which help bring in resilience to the neuronal activity against perturbations (e. g. temperature (Alonso and Marder, 2020)). In other words, in a set of cases, variations in individual conductances get balanced out by homeostatic mechanisms such that stable network activity is maintained (Liu et al., 1998). Hence, talking about the effect of individual conductances without correctly modelling the intracellular feedback mechanisms of homeostasis (e.g. calcium-sensing) can be meaningless. Hence, a framework is developed such that the FoG could be studied without focusing on individual conductances and other cellular dynamics.

The framework developed could be used to analyse several plausible PRCs and their variations. This is demonstrated using two 'variations' in PRC functions adapted from the works of Oprisan, Thirumalai and Canavier, 2003 and Soofi and Prinz, 2015. In Fig. 7.3 decreasing the parameter a could be interpreted as an increased H current (Soofi and Prinz, 2015). One could see from Fig. 7.9a that a similar (high or low) H current on both the oscillators can result in freezing of gait. Moreover, shrinking of the constant (MPR) region is studied using the PRC functions given in Fig. 7.4. This type of change in PRC function can be seen in the experimental study by Oprisan, Thirumalai and Canavier, 2003, depending on the perturbation duration. A further study is required on the effects of the relevant PD-Pathologies on PRC. From the simulations, it is clear that different neuropathologies may lead to PRC changes, leading to the freezing phenomenon. These simulations also explain the discrepancy in the different neurophysiological characteristics leading to a freeze (Pozzi et al., 2019). The high variability regions are closer to the freezing

regions, which align with the experimental evidence. Also, experimentally, one can only look at different subregions of the overall parameter space. Hence, this generates discrepancies in the effectiveness of the treatment methodologies. Model-driven experimentation would help more personalised treatment methodologies. Moreover, in future work, one could design experiments to estimate the PRC of the CPG in PD patients. These estimated PRC functions could then be plugged into the model and tested if the walking data observed experimentally and generated by the model match. Additionally, one could stimulate the anatomical structure PPN with different current intensities, thereby controlling the overall muscle tones. The result should then match with the variations in gait (step times) introduced by the variations of the parameter m_f.

The $PRC(\cdot)$ developed in this work describes only the *slow* dynamics of the *slow fast* bursting system. The modulation of bursting *fast* dynamics can be explained by *slow* outward (inactivation of inward) voltage-dependent or Ca^{2+} - dependent current (Izhikevich, 2003). The $PRC(\cdot)$ can be controlled by controlling these slow currents' dynamics either through input from the brain-stem locomotor areas or motor cortex (Grillner, 1985; Ermentrout and Terman, 2010a). Neurotransmitters or neuromodulators could mediate these inputs (Golowasch, 2019). One could observe from the study of parameters a_1 and a_2 that normal walking can exhibit in large parameter space. Neuromodulation controls the 'normal' operating parameter range of the neurons (Golowasch, 2019); hence, treatments targeting them could be beneficial in PD. Therefore, a computational and experimental study of neuromodulatory effects on the PRC of the CPG in PD subjects is highly warranted. Moreover, rehabilitative training in PD could be studied as minimising CD by varying parameters a_1 and a_2. Training essentially results in the convergence of the parameters to the 'walking regimes' explaining the recovery processes.

8. Summary and Conclusion

The thesis presented an analysis of stepping data for FoG prediction and mathematical modelling methodologies for understanding PD-Gait, specifically FoG.

Data Analysis: On the data analysis front, a prediction algorithm was developed to forecast FoG in PD. The prediction algorithm was implemented using a rolling window-based approach, rather than the FoG/Pre-FoG classification based approach typically seen in literature (Pardoel et al., 2019). Moreover, the algorithm was tested with a different offset length than it was trained for, demonstrating a valuable real-time prediction system. Typically, in pre-FoG/FoG classification literature, varied lengths of pre-FoG data are used for analysis ranging from 1 s-11 s (Mazilu et al., 2013; Pardoel et al., 2019). Though not directly comparable to the Pre-FoG time period chosen, our analysis demonstrated an optimum input length (1.13s) of data to be used for prediction FoG. Individual variations are very high in the FoG prediction literature (Pardoel et al., 2019). A personalization methodology is proposed in this thesis to give control of the trade-off between the sensitivity and specificity to the user. The methodology developed forms a potential tool to be used in conjunction with the augmented feedback given to the people affected with PD. Moreover, the cross-validation technique used in the thesis aims to avoid the reuse of the data in training and testing. A key limitation of the data analysis work, is the low number of patients, which needs to be addressed in future extensions.

Modelling: Mathematical modelling of PD-Gait and FoG is accomplished in three stages using a bottom-up approach. In this thesis, modelling is done from the leg upwards and is referred to as the bottom-up approach. There are other meanings for the word bottom-up such as starting from the smallest details of the system (e.g. cellular level), which are not applicable in this work. This is done first by

modelling the essential aspects of kinetics of the lower limbs under a physiologically meaningful forcing. Successively, going upward, modelling the influence of the CPG and then generalizing the model using a phase reset curve based approach. This methodology helped constrain the number of variables in the model to a lower value while explaining a set of possible mechanisms of freezing.

In Chapter 5, the ankle-push-off based model addressed the defective limb kinetics, taking into account the abnormal EMG patterns shown in Nieuwboer et al., 2004. In the proposed model, an inverted pendulum abstracts the dynamics of the stance leg. The novelty in the model comes from the physiologically meaningful forcing proposed and the model's ability in exhibiting PD-Gait abnormalities and normal gait. A salient parameter of the model is the phase; this quantifies the premature activations of the plantar flexors. Variations of the phase parameter showed period-doubling, chaos and freezing in the model, delineating the role of coordination in the model. This finding, the role of phase in freezing and variability, is central to the future developments of the model. Apart from explaining the effects of lack of coordination, the ankle-push-off model also studies the effect of forcing and the step sizes. In this model, even though inputs from the brain is not modelled explicitly, one could speculate that the parameter τ_l could be influenced non-motor aspects such as anxiety. This result in higher premature activation of the plantar flexors and can lead to a freeze. The focus on mechanics, ability to exhibit FoG and variability distinguishes the proposed model from the previously proposed models of PD in the literature (Muralidharan et al., 2018; Sarbaz et al., 2012; Montazeri Moghadam et al., 2018). Key aspects missing from the ankle push-off model are the following (1) It does not show how gait transitions from a freeze to walking (2) How the lack of synchrony in the phase is generated and (3) What is the effect of feedback in PD-Gait. The subsequent models aim to address these questions.

The inverted pendulum model derived in Chapter 5 is extended with the CPG oscillator proposed by Ijspeert, Crespi and Cabelguen, 2005 in Chapter 6. Apart from the FoG and variability, numerical simulations of this model showed gait transitions from freezing to walking and the effect of feedback. The lack of synchrony arises in

this model as an emergent characteristic of interactions between the hybrid-walking mechanics and the non-linear *limit-cycle* oscillator. The oscillator based model has implications to both in understanding PD walking and has the potential to be used to understand augmented feedback (Hwang et al., 2012). Continuing the trend from Chapter 5 the parameters which govern the phase, such as the time constant and feedback, play an important role in the extended model as well. Moreover, the freezing region and the region with high variability are close by. To address stability, the method used in the model is inspired by the Poincare based methodology proposed in Goswami, Thuilot and Espiau, 1996b. This is done by constructing a map numerically for every gait cycle involving two steps and computing its stability, considering it as a map. While this model solves the limitations of the ankle-push-off based simple model, there is further scope for generalization. The aim of the further generalization is the following (1) ability of the model to generalize to several oscillator types (2) simplify the model to include only the most salient aspects.

The PRC based model is built as a generalization of the models described in Chapters 5 and 6. The vital aspect of the oscillator described in Chapter 6 relevant to FoG is, synchronization and desynchronization of phase, which in turn is governed by the PRC of the oscillator. The discrete model in Chapter 7 makes use of the relevant experimental studies on phase resets in Oprisan, Thirumalai and Canavier, 2003. The proposed method explored different variations of the PRC according to the relevant experimental and simulation studies by Soofi and Prinz, 2015 and Oprisan, Thirumalai and Canavier, 2003. The modularization of the system allows for its further exploration with minor modifications. The generalized model exhibited PD-Gait characteristics previously shown by other models, such as freezing and variability. The role of the oscillator's time period parameter (T) in Eq. 7.16 controlling the freezing and variability follows the trend shown in other models in Chapters 5 and 6, where phase and coordination affect the FoG and variability. Moreover, the parameter exploration in PRC based model also shows the freezing and variability regions to be closer to each other. The discrete based model reduced the computational complexity of the system, helping to explore a

set of initial conditions for 1000 iterations corresponding to 500 gait cycles. The generalization aspect of the PRC model is that the PRC is modelling not one particular differential equation set but rather the family of differential equations with the same PRC. Moreover, brain activity of several regions are correlated with seemingly different symptoms related to freezing of gait (Pozzi et al., 2019; Heremans, Nieuwboer and Vercruysse, 2013b). From the understanding gained from the PRC based model, one could speculate why gait abnormalities (freezing, highly variable stepping) in PD could be the manifestations of the same underlying cause as there are several parameter regimes at which one observes normal walking, variable walking and FoG. For example, one could move from walking to freezing and then to the walking regime by continuously increasing the same parameter of the model. These parameters phenomenologically represent the neuromodulators or other neuronal inputs controlling the CPG. In an experimental setting, different governing parameters need to be measured simultaneously to generate conclusive results. The modelling studies need further experimental validation to make it useful for clinical applications. Further experimental studies on the CPG and spinal-chord is needed to generate the right PRC function governing gait in a patient affected with PD.

8.1 Future Work

There are several ways by which one could extend the PRC based work proposed in this thesis. The neuromodulators and internal cellular feedback control the PRC of the system. There is a need for exploring the correlations between neuromodulation, cellular dynamics and PRC, which could be a future work. One could achieve this either by experimentation as the one by Oprisan, Thirumalai and Canavier, 2003 or by numerical simulations of the biophysical models, such as one by Soofi and Prinz, 2015. Successively, one could test the effects of these PRCs on gait. Furthermore, one could immediately explore the effect of positively perturbed (depolarization) CPG by looking at its PRC and its effect on the gait model. However, the physical plausibility of a positively perturbed CPG system should be considered simultaneously. Moreover, the ankle push-off based model developed in chapter 5 extended in chapter

6 has further scope for extension using detailed biomechanical models of the ankle (Chatzistefani et al., 2017; Wynarsky and Greenwald, 1983). These extended models could be used for developing wearable solutions for FoG (Yetisen et al., 2018).

The proposed PRC based model can be further used with the stepping time data extracted from accelerometer data or step sensor data (e.g. one available in mobile phones) for model parameter estimation. One could do this with a right distance measure between the experimental data, and the model generated data and an optimization methodology. The parameter estimation would generate personalized models for the patient, which could then be used for (1) prediction, and (2) understanding their disease progression. Further validation of these parameters with patients of different UPDRS scores or with patients at different stages of disease progression would essentially help develop a clinical tool for evaluating the response of the patient to treatment methodologies.

The postural control during gait and gait initiation need further study. A clear understanding of this has not yet been established in the experimental literature (Snijders et al., 2016). Work in this direction would involve phenomenological modelling of the muscles involved in postural adjustments, helping to readjust the centre of gravity before the initiation of walking. Successively the effect from the higher centres also needs to be established, especially CPG, PPN, MLR and MC. EMG measurements of the gait initiation also would be very beneficial in validating the model. One could also make a robotics driven approach to understand gait initiation. In this case, a bipedal robot could be programmed with a neural controller for walking from a set of initial conditions. A reinforcement-based learning approach may be used to learn several strategies to bring the bipedal system from various initial conditions to the stable walking limit cycle. The learned strategies can then be compared with the biological neuromechanical system to understand pathophysiology.

There are several other possible ways one could extend the Oscillator and PRC based models. The effect of noise and external environments are not fully explored in the thesis, which could be future work. One could also use inverse-optimal control to learn cost functions, which could then be assumed to control the model.

This would require additional data collection of the normal and PD subjects. The learned cost function could then be used as a clinical tool.

A. Appendix: Background Physiology

A.1 Motor Control Physiology - General structure and function

At the lowest level, the neural reflexes carry out locomotion in the spinal cord (Kandel et al., 2000). These are a set of self inhibiting neurons (Kandel et al., 2000) with interneurons hardwired (Kandel et al., 2000) to generate oscillations. The next level of organisation and control happens at the brain (Kandel et al., 2000), with several regions interacting in learning, integrating feedback and other finer controls. Even though the neural pathways of motor control are deciphered to some extent, the exact mechanism of motor control of limbs is an active area of research. Excitation of motor cortex activate muscles in different parts of our body, eliciting a direct or indirect projection of the motor cortex to the spinal cord and motor neurons(Lemon, 2008). The primary motor cortex and supplementary motor areas control the planning and execution of movements. Motor actions are believed to be controlled via two different routes: the pyramidal tract and the extrapyramidal tract. The pyramidal tract consists of the cortico-spinal tract and corticobulbar tract. The corticospinal tract originates from the pyramidal cells of the cerebral cortex, the majority of which, projecting from the supplementary motor area and primary motor cortex traversing through the posterior limb of the internal capsule, cerebral peduncle, to brain stem and medulla oblongata. Part of these neurons travels down the tract and synapse with the lower motor neurons in the spinal cord majorly via interneurons (Hall, 2015)

therefore the name 'corticospinal'. The corticobulbar tracts also originate from the cerebral cortex traversing through the brain stem to synapse on the lower motor neurons of the cranial nerves. The corticobulbar tract, being composed of the cranial nerves' upper motor neurons, controls the facial and head muscles in contrast with the corticospinal tracts controlling the upper and lower limbs through lower motor neurons.

The extrapyramidal system controls movement through a non-pyramidal route composing of the nigrostriatal pathway modulated by the basal ganglia, the cerebellum, the vestibular nuclei, and different sensory areas of the cerebral cortex (Hall and John, 2005). Parkinson's disease(PD) is a disorder associated with the extrapyramidal system, mainly the BG, the physiology of which will be described in detail in the section below.

A.2 Pathophysiology of Parkinson's Disease

Basal ganglia situated at the base of the forebrain consists of a set of substructures - striatum (dorsal (caudate nucleus, putamen) and ventral (nucleus accumbens, olfactory tubercle)), globus pallidus externus (GPe), global pallidus internus (GPi), ventral pallidum, substantia nigra and subthalamic nuclei (STN) (Kandel et al., 2000) (Graybiel, 2000). Models of BG conceptualises its function using direct and indirect pathways as depicted in Fig. A.1. According to this model, the thalamus with excitatory effects on the cortex is inhibited by globus pallidus internus. The direct pathway is known to inhibit globus pallidus internus, thereby helping initiate movement, while the indirect pathway that involves the subthalamic nucleus suppresses the thalamic excitation. Moreover, BG has connections towards the PPN (Pedunculopontine nucleus) (Weinberger et al., 2008) which influences the postural control and limb movements.

The direct and indirect pathways and the SNc modulation of these pathways are given below in brief.

Direct Pathway: The striatum, a structure consisting predominantly of inhibitory medium spiny neurons, receives inputs from the cerebral cortex, thalamus,

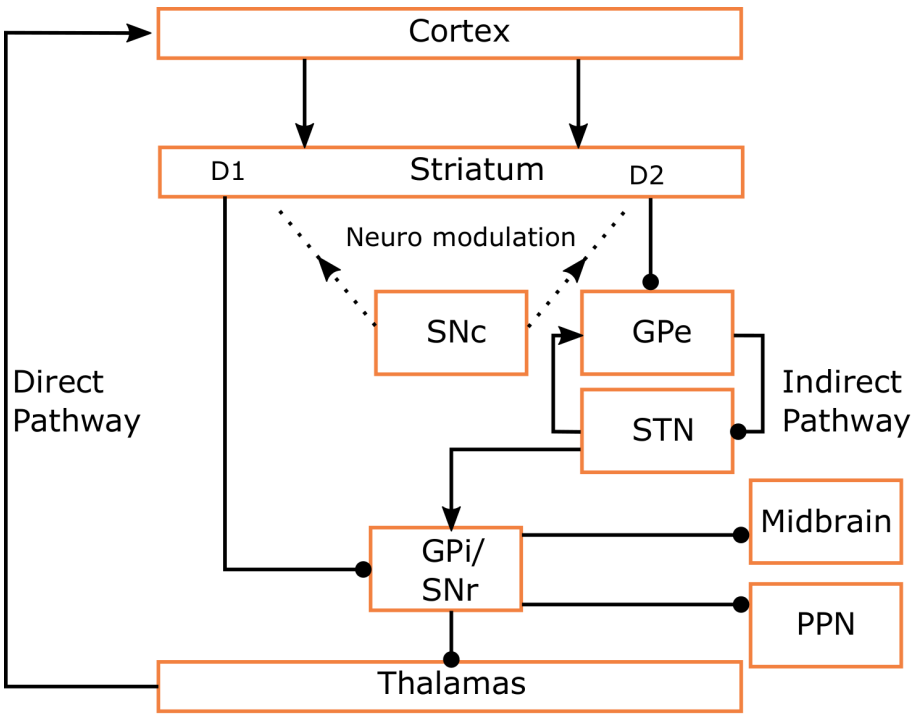

Figure A.1: A detailed description of the basal ganglia functional dynamics is provided. The direct and indirect pathways and the connections to the PPN (Pedunculopontine nucleus) and midbrain are also indicated. The arrows in the diagram indicate excitatory input and the disk end points show inhibitory input. The dashed lines from SNc are used to indicate neuromodulation of the D1 and D2 receptors of striatum.

and limbic system. Substantia nigra pars reticularis(SNr) and globus pallidus acts as the output units which projects to the thalamus and the cortex Fig.A.1. The cortex provides excitatory inputs to the striatum, providing inhibitory output to the GPi and SNr. These structures then inhibit the thalamus, which then excites the cortex. The overall effect of the direct pathway is to increase the activity of the motor cortex.

Indirect Pathway: In the indirect pathway, the striatum receives excitatory inputs from the cortex and sends inhibitory projections to the GPe. The GPe then sends inhibitory connections to the STN while STN sends excitatory projections to the SNr and GPi. These structures then send inhibitory signals to the thalamus, which in turn sends excitatory signals to the cortex Fig. A.1. The overall effect of the indirect pathway is to reduce the activity of the motor cortex.

SNc - Modulation of Direct and indirect pathways: Dopaminergic projections from the SNc modulate the effect of direct and indirect pathways in the BG and control the cortex's activity. This modulation happens in the following way. When SNc projects onto the striatum, the cells of the direct pathway which has D1 dopamine receptors gets excited (increases the chances of firing) by binding to the dopamine; in contrast, the D2 dopamine receptors of the indirect pathway reduces its chance of firing by binding with the dopamine Fig.A.1. A higher amount of dopamine generates an increased direct pathway activity and a decreased indirect pathway activity. In PD the neurons associated with SNc dies, affecting the dopaminergic neuromodulation of striatum.

A.3 PD interventions

Pharmacological interventions of PD typically target the metabolic pathway of dopamine synthesis and clearance. However, there are other pharmacological approaches as well to treating PD, such as the use of anticholinergics and amantadine (Connolly and Lang, 2014). Treatment methodologies aim to increase the concentration of dopamine in the brain in one of the following ways 1) being a dopamine substitute by acting on the receptors (e.g. Rotigotine, pramipexole) 2) turning into dopamine (e.g.

Levodopa) 3) inhibiting the breakdown of dopamine (e.g. Monoamine Oxidase B (MAO-B) inhibitors) (Kopin, 1993; Goetz et al., 2005; Zahoor, Shafi and Haq, 2018). These treatment methodologies are relatively more efficient against bradykinesia, rigidity and tremor than gait and posture-related abnormalities.

DBS is a surgical treatment methodology where high-frequency electrical pulses are delivered to regions of the brain using an implanted device. DBS has an effect similar to lesioning the brain region and, therefore, reduces that region's pathophysiological effect. VIM (ventral intermediate nucleus of the thalamus), STN, and GPi are the common areas where the stimulation is targeted and can be beneficial against tremor, bradykinesia, rigidity and gait impairment. DBS can also help reduce the time a patient spends in the 'off' state of the medication and reducing the untoward effects of the dopa-induced medications such as dyskinesias and involuntary movements (Perlmutter and Mink, 2006). DBS on STN has been shown to have a frequency-dependent effect on FoG (Moreau et al., 2008) helping to maintain stepping (Yokochi, 2006; Fischer et al., 2020), pointing to synchronisation. The effect of STN-DBS is not shown to change with dorsal or ventral STN stimulation, pointing to a diffused effect (McNeely et al., 2011). However, GPi stimulation can trigger hypokinetic gait disorder with FoG (Schrader et al., 2011). PPN - stimulation has been identified for stimulation and has shown promise in FoG recently (Molina et al., 2020; Snijders et al., 2016). While there are empirical observation of improvements in PD-Gait upon the stimulation of PPN, the exact mechanism of action is still unclear.

B. Appendix: PRC Model

B.1 Another way to arrive at the equation of motion

As the total energy is conserved, one could equate the total energy at the beginning of a step with the end of the step before impulsive loss as follows,

$$\frac{1}{2}I(\omega_n)^2 + PE_1 = \frac{1}{2}I(\omega_{n+1})^2 + PE_2 \tag{B.1}$$

Here, I is the moment of inertia of the inverted pendulum, PE_1 and PE_2 are the potential energies, and ω_n and ω_{n+1} are the angular velocities. However, as one assumes constant step size ($\theta_n = \theta_{n+1}$),

$$PE_1 = PE_2 \tag{B.2}$$

Therefore, before the impulse loss,

$$\omega_{n+1} = \omega_n \tag{B.3}$$

Considering the energy loss after an impulse, and the forcing added from the neural system the EoM takes the following form.

$$\omega_{n+1} := \eta\omega_n + f_t(v_{n+1},\ \tilde{v}_{n+1}); \tag{B.4}$$

Here the function $f_t(.)$ depends on the *phase* v_{n+1} and $\tilde{v}_{n+1}$ of the neural oscillators at the time of stepping.

Bibliography

S. Aich, P. M. Pradhan, J. Park, N. Sethi, V. S. S. Vathsa and H.-C. Kim (2018). 'A validation study of freezing of gait (FoG) detection and machine-learning-based FoG prediction using estimated gait characteristics with a wearable accelerometer'. In: *Sensors* 18.10, p. 3287 (Cited on page 53).

M. Alam, K. Schwabe and J. K. Krauss (2011). 'The pedunculopontine nucleus area: critical evaluation of interspecies differences relevant for its use as a target for deep brain stimulation'. In: *Brain* 134.1, pp. 11–23 (Cited on page 13).

L. M. Alonso and E. Marder (2019). 'Visualization of currents in neural models with similar behavior and different conductance densities'. In: *Elife* 8, e42722 (Cited on page 30).

L. M. Alonso and E. Marder (2020). 'Temperature compensation in a small rhythmic circuit'. In: *Elife* 9, e55470 (Cited on page 142).

A. D. Ames (2014). 'Human-inspired control of bipedal walking robots'. In: *IEEE Transactions on Automatic Control* 59.5, pp. 1115–1130 (Cited on page 29).

A. Amini, K. Banitsas and W. R. Young (2019). 'Kinect4FOG: monitoring and improving mobility in people with Parkinson's using a novel system incorporating the Microsoft Kinect v2'. In: *Disability and Rehabilitation: Assistive Technology* 14.6, pp. 566–573 (Cited on pages 21, 57 and 93).

C. Anidi, J. J. O'Day, R. W. Anderson, M. F. Afzal, J. Syrkin-Nikolau, A. Velisar and H. M. Bronte-Stewart (2018). 'Neuromodulation targets pathological not physiological beta bursts during gait in Parkinson's disease'. In: *Neurobiology of disease* 120, pp. 107–117 (Cited on page 1).

S. Aoi, N. Ogihara, T. Funato, Y. Sugimoto and K. Tsuchiya (2010). 'Evaluating functional roles of phase resetting in generation of adaptive human bipedal

walking with a physiologically based model of the spinal pattern generator'. In: *Biological cybernetics* 102.5, pp. 373–387 (Cited on pages 3, 4, 22, 23 and 31).

S. Aoi, T. Ohashi, R. Bamba, S. Fujiki, D. Tamura, T. Funato, K. Senda, Y. Ivanenko and K. Tsuchiya (2019). 'Neuromusculoskeletal model that walks and runs across a speed range with a few motor control parameter changes based on the muscle synergy hypothesis'. In: *Scientific reports* 9.1, pp. 1–13 (Cited on pages 11, 22, 26 and 120).

S. Aoi and K. Tsuchiya (2006). 'Stability analysis of a simple walking model driven by an oscillator with a phase reset using sensory feedback'. In: *IEEE Transactions on robotics* 22.2, pp. 391–397 (Cited on pages 4, 22, 23 and 120).

A. Arami, A. Poulakakis-Daktylidis, Y. F. Tai and E. Burdet (2019). 'Prediction of gait freezing in Parkinsonian patients: a binary classification augmented with time series prediction'. In: *IEEE Transactions on Neural Systems and Rehabilitation Engineering* 27.9, pp. 1909–1919 (Cited on page 18).

M. Bachlin, M. Plotnik, D. Roggen, I. Maidan, J. M. Hausdorff, N. Giladi and G. Troster (2009). 'Wearable assistant for Parkinson's disease patients with the freezing of gait symptom'. In: *IEEE Transactions on Information Technology in Biomedicine* 14.2, pp. 436–446 (Cited on pages 99 and 109).

M. T. Barbe, M. Amarell, A. H. Snijders, E. Florin, E.-L. Quatuor, E. Schönau, G. R. Fink, B. R. Bloem and L. Timmermann (2014). 'Gait and upper limb variability in Parkinson's disease patients with and without freezing of gait'. In: *Journal of neurology* 261.2, pp. 330–342 (Cited on page 123).

C. Barthel, E. Mallia, B. Debû, B. R. Bloem and M. U. Ferraye (2016). 'The practicalities of assessing freezing of gait'. In: *Journal of Parkinson's disease* 6.4, pp. 667–674 (Cited on page 46).

C. Barthel, J. Nonnekes, M. Van Helvert, R. Haan, A. Janssen, A. Delval, V. Weerdesteyn, B. Debû, R. Van Wezel, B. R. Bloem et al. (2018). 'The laser shoes: a new ambulatory device to alleviate freezing of gait in Parkinson disease'. In: *Neurology* 90.2, e164–e171 (Cited on page 55).

W Berger, V Dietz and J Quintern (1984). 'Corrective reactions to stumbling in man: neuronal co-ordination of bilateral leg muscle activity during gait.' In: *The Journal of physiology* 357.1, pp. 109–125 (Cited on page 98).

B. R. Bloem, J. M. Hausdorff, J. E. Visser and N. Giladi (2004). 'Falls and freezing of gait in Parkinson's disease: a review of two interconnected, episodic phenomena'. In: *Movement Disorders* 19.8, pp. 871–884 (Cited on pages 1 and 54).

B. Bloem, N. Voermans, M. Aerts, K. Bhatia, B. van Engelen and B. Van de Warrenburg (2016). 'The wrong end of the telescope: neuromuscular mimics of movement disorders (and vice versa)'. In: *Practical neurology*, practneurol–2015 (Cited on page 1).

L. Borzì, I. Mazzetta, A. Zampogna, A. Suppa, G. Olmo and F. Irrera (2021). 'Prediction of freezing of gait in Parkinson's disease using wearables and machine learning'. In: *Sensors* 21.2, p. 614 (Cited on pages 18 and 19).

S. Breit, J. B. Schulz and A.-L. Benabid (2004). 'Deep brain stimulation'. In: *Cell and tissue research* 318.1, pp. 275–288 (Cited on page 1).

A. Büschges (2005). 'Sensory control and organization of neural networks mediating coordination of multisegmental organs for locomotion'. In: *Journal of neurophysiology* 93.3, pp. 1127–1135 (Cited on page 10).

C. C. Canavier (2006). 'Phase response curve'. In: *Scholarpedia* 1.12. revision #91651, p. 1332. DOI: 10.4249/scholarpedia.1332 (Cited on page 132).

N Chatzistefani, M. Chappell, C Hutchinson, S Kletzenbauer and N. Evans (2017). 'A mathematical model characterising Achilles tendon dynamics in flexion'. In: *Mathematical biosciences* 284, pp. 92–102 (Cited on page 148).

R. Chee, A. Murphy, M. Danoudis, N. Georgiou-Karistianis and R. Iansek (2009). 'Gait freezing in Parkinson's disease and the stride length sequence effect interaction'. In: *Brain* 132.8, pp. 2151–2160 (Cited on pages 54 and 55).

Z. Chen, G. Li, C. Gao, Y. Tan, J. Liu, J. Zhao, Y. Ling, X. Yu, K. Ren and S. Chen (2021). 'Prediction of Freezing of Gait in Parkinson's Disease Using a Random Forest Model Based on an Orthogonal Experimental Design: A Pilot Study'. In: *Frontiers in human neuroscience* 15, p. 79 (Cited on page 19).

V. C. Cheung, A. d'Avella, M. C. Tresch and E. Bizzi (2005). 'Central and sensory contributions to the activation and organization of muscle synergies during natural motor behaviors'. In: *Journal of Neuroscience* 25.27, pp. 6419–6434 (Cited on pages 99, 101 and 114).

E. A. Clancy, O. Bida and D. Rancourt (2006). 'Influence of advanced electromyogram (EMG) amplitude processors on EMG-to-torque estimation during constant-posture, force-varying contractions'. In: *Journal of biomechanics* 39.14, pp. 2690–2698 (Cited on page 99).

B. T. Cole, S. H. Roy and S. H. Nawab (2011). 'Detecting freezing-of-gait during unscripted and unconstrained activity'. In: *2011 Annual International Conference of the IEEE Engineering in Medicine and Biology Society*. IEEE, pp. 5649–5652 (Cited on page 16).

B. S. Connolly and A. E. Lang (2014). 'Pharmacological treatment of Parkinson disease: a review'. In: *Jama* 311.16, pp. 1670–1683 (Cited on page 153).

A. G. Cresswell, W. Löscher and A. Thorstensson (1995). 'Influence of gastrocnemius muscle length on triceps surae torque development and electromyographic activity in man'. In: *Experimental Brain Research* 105.2, pp. 283–290 (Cited on page 99).

H. Dai and R. Tedrake (2013). 'L 2-gain optimization for robust bipedal walking on unknown terrain'. In: *2013 IEEE International Conference on Robotics and Automation*. IEEE, pp. 3116–3123 (Cited on pages 3, 22 and 24).

S. Dean, Ó. Gearóid, R. Margaret, M. Pauline, R. Lois, M. Aimi, C. Anne-Louise and R. Q. Leo (2020). 'Effect of auditory, visual and somatosensory cueing strategies on On-State Freezing of Gait in Parkinson's disease'. In: *Parkinsonism & related disorders* 77, pp. 1–4 (Cited on pages 2 and 20).

S. L. Delp, F. C. Anderson, A. S. Arnold, P. Loan, A. Habib, C. T. John, E. Guendelman and D. G. Thelen (2007). 'OpenSim: open-source software to create and analyze dynamic simulations of movement'. In: *IEEE transactions on biomedical engineering* 54.11, pp. 1940–1950 (Cited on page 3).

R. Devaney (2018). *An introduction to chaotic dynamical systems*. CRC Press (Cited on page 111).

V. Dietz (2003). 'Spinal cord pattern generators for locomotion'. In: *Clinical Neurophysiology* 114.8, pp. 1379–1389 (Cited on pages 98, 99, 101 and 114).

V. Dietz and G. Colombo (1998). 'Influence of body load on the gait pattern in Parkinson's disease'. In: *Movement disorders: official journal of the Movement Disorder Society* 13.2, pp. 255–261 (Cited on pages 1 and 99).

M. R. Dimitrijevic, Y. Gerasimenko and M. M. Pinter (1998). 'Evidence for a spinal central pattern generator in humans a'. In: *Annals of the New York Academy of Sciences* 860.1, pp. 360–376 (Cited on page 103).

E. Dorschky, M. Nitschke, A.-K. Seifer, A. J. van den Bogert and B. M. Eskofier (2019). 'Estimation of gait kinematics and kinetics from inertial sensor data using optimal control of musculoskeletal models'. In: *Journal of biomechanics* 95, p. 109278 (Cited on page 3).

X. Duan, R. Allen and J. Sun (1997). 'A stiffness-varying model of human gait'. In: *Medical engineering & physics* 19.6, pp. 518–524 (Cited on page 25).

J Duysens, M Trippel, G. Horstmann and V Dietz (1990). 'Gating and reversal of reflexes in ankle muscles during human walking'. In: *Experimental brain research* 82.2, pp. 351–358 (Cited on page 14).

K. A. Ehgoetz Martens, C. G. Ellard and Q. J. Almeida (Sept. 2014). 'Does Anxiety Cause Freezing of Gait in Parkinson's Disease?' In: *PLOS ONE* 9.9, pp. 1–10. DOI: 10.1371/journal.pone.0106561. URL: https://doi.org/10.1371/journal.pone.0106561 (Cited on page 93).

K. A. Ehgoetz Martens, J. M. Shine, C. C. Walton, M. J. Georgiades, M. Gilat, J. M. Hall, A. J. Muller, J. Y. Szeto and S. J. Lewis (2018). 'Evidence for subtypes of freezing of gait in Parkinson's disease'. In: *Movement Disorders* 33.7, pp. 1174–1178 (Cited on page 50).

M. S. El-Tamawy, M. H. Darwish and M. E. Khallaf (2012). 'Effects of augmented proprioceptive cues on the parameters of gait of individuals with Parkinson's disease'. In: *Annals of Indian Academy of Neurology* 15.4, p. 267 (Cited on page 20).

B. Ermentrout and D. H. Terman (2010a). *Foundations of mathematical neuroscience*. Citeseer (Cited on pages 30, 33 and 143).

G. B. Ermentrout and D. H. Terman (2010b). *Mathematical foundations of neuroscience*. Vol. 35. Springer Science & Business Media (Cited on pages 33 and 134).

S. A. Factor (2008). 'The clinical spectrum of freezing of gait in atypical parkinsonism'. In: *Movement disorders: official journal of the Movement Disorder Society* 23.S2, S431–S438 (Cited on page 11).

M. Fathizadeh, H. Mohammadi and S. Taghvaei (2019). 'A modified passive walking biped model with two feasible switching patterns of motion to resemble multi-pattern human walking'. In: *Chaos, Solitons & Fractals* 127, pp. 83–95 (Cited on pages 3, 22 and 24).

M. Fathizadeh, S. Taghvaei and H. Mohammadi (2018). 'Analyzing bifurcation, stability and chaos for a passive walking biped model with a sole foot'. In: *International Journal of Bifurcation and Chaos* 28.09, p. 1850113 (Cited on pages 3, 22 and 24).

A. G. Feldman (1986). 'Once more on the equilibrium-point hypothesis (λ model) for motor control'. In: *Journal of motor behavior* 18.1, pp. 17–54 (Cited on pages 25, 26, 92 and 93).

P. Fischer, S. He, A. de Roquemaurel, H. Akram, T. Foltynie, P. Limousin, L. Zrinzo, J. Hyam, H. Cagnan, P. Brown et al. (2020). 'Entraining stepping movements of Parkinson's patients to alternating subthalamic nucleus deep brain stimulation'. In: *Journal of Neuroscience* 40.46, pp. 8964–8972 (Cited on pages 120 and 154).

T. Flash and N. Hogan (1985). 'The coordination of arm movements: an experimentally confirmed mathematical model'. In: *Journal of neuroscience* 5.7, pp. 1688–1703 (Cited on page 3).

H Frohlich, K Claes, C. W. De, X. D. Van and A Michel (2017). 'A Machine Learning Approach to Automated Gait Analysis for the Noldus Catwalk (TM) System.' In: *IEEE transactions on bio-medical engineering* (Cited on page 21).

R. Frost, J. Skidmore, M. Santello and P. Artemiadis (2015). 'Sensorimotor control of gait: a novel approach for the study of the interplay of visual and proprioceptive feedback'. In: *Frontiers in human neuroscience* 9, p. 14 (Cited on page 14).

T. Funato, Y. Yamamoto, S. Aoi, T. Imai, T. Aoyagi, N. Tomita and K. Tsuchiya (2016). 'Evaluation of the phase-dependent rhythm control of human walking using phase response curves'. In: *PLoS computational biology* 12.5 (Cited on page 31).

G. Gede, D. L. Peterson, A. S. Nanjangud, J. K. Moore and M. Hubbard (2013). 'Constrained multibody dynamics with Python: From symbolic equation generation to publication'. In: *International Design Engineering Technical Conferences and Computers and Information in Engineering Conference*. Vol. 55973. American Society of Mechanical Engineers, V07BT10A051 (Cited on page 61).

W. Genadry, R. Kearney and I. Hunter (1988). 'Dynamic relationship between EMG and torque at the human ankle: variation with contraction level and modulation'. In: *Medical and Biological Engineering and Computing* 26.5, pp. 489–496 (Cited on pages 58 and 99).

S. Ghai, I. Ghai, G. Schmitz and A. O. Effenberg (2018). 'Effect of rhythmic auditory cueing on parkinsonian gait: a systematic review and meta-analysis'. In: *Scientific reports* 8.1, pp. 1–19 (Cited on pages 116 and 120).

N Giladi, M. McDermott, S Fahn, S Przedborski, J Jankovic, M Stern, C Tanner, P. S. Group et al. (2001). 'Freezing of gait in PD Prospective assessment in the DATATOP cohort'. In: *Neurology* 56.12, pp. 1712–1721 (Cited on page 1).

M. Gilat (2019). 'How to annotate freezing of gait from video: a standardized method using open-source software'. In: *Journal of Parkinson's disease* 9.4, pp. 821–824 (Cited on page 42).

M. Gilat, S. Lewis, J. Shine, A. M. Handojoseno, Q. T. Ly, G. R. Naik, H. T. Nguyen and T. Nguyen (2018a). 'Prediction of Freezing of Gait in Patients with Parkinson's Disease Using EEG Signals'. In: (Cited on page 18).

M. Gilat, A. L. S. de Lima, B. R. Bloem, J. M. Shine, J. Nonnekes and S. J. Lewis (2018b). 'Freezing of gait: promising avenues for future treatment'. In: *Parkinsonism & related disorders* 52, pp. 7–16 (Cited on pages 1, 2 and 20).

P. Ginis, E. Nackaerts, A. Nieuwboer and E. Heremans (2018). 'Cueing for people with Parkinson's disease with freezing of gait: a narrative review of the state-of-the-art and novel perspectives'. In: *Annals of physical and rehabilitation medicine* 61.6, pp. 407–413 (Cited on page 20).

P. Glendinning (1994). *Stability, instability and chaos: an introduction to the theory of nonlinear differential equations*. Vol. 11. Cambridge university press (Cited on pages 26, 76 and 89).

J.-M. Goaillard and E. Marder (2021). 'Ion channel degeneracy, variability, and covariation in neuron and circuit resilience'. In: *Annual review of neuroscience* 44 (Cited on page 30).

C. G. Goetz, W. Poewe, O. Rascol and C. Sampaio (2005). 'Evidence-based medical review update: pharmacological and surgical treatments of Parkinson's disease: 2001 to 2004'. In: *Movement disorders: official journal of the Movement Disorder Society* 20.5, pp. 523–539 (Cited on page 154).

J. Golowasch (2019). 'Neuromodulation of central pattern generators and its role in the functional recovery of central pattern generator activity'. In: *Journal of neurophysiology* 122.1, pp. 300–315 (Cited on page 143).

A. Goswami, B. Thuilot and B. Espiau (1996a). *Compass-Like Biped Robot Part I : Stability and Bifurcation of Passive Gaits*. Research Report RR-2996. INRIA. URL: `https://hal.inria.fr/inria-00073701` (Cited on pages 3, 22, 24, 27 and 111).

A. Goswami, B. Thuilot and B. Espiau (1996b). 'Compass-like biped robot part I: Stability and bifurcation of passive gaits'. In: (Cited on page 146).

A. M. Graybiel (2000). 'The basal ganglia'. In: *Current biology* 10.14, R509–R511 (Cited on page 151).

S. Grillner (1985). 'Neurobiological bases of rhythmic motor acts in vertebrates'. In: *Science* 228.4696, pp. 143–149 (Cited on page 143).

S. Grillner (2003). 'The motor infrastructure: from ion channels to neuronal networks'. In: *Nature Reviews Neuroscience* 4.7, pp. 573–586 (Cited on page 10).

S. Grillner (2021). 'The execution of movement: A spinal affair'. In: *Journal of Neurophysiology* 125.2, pp. 693–698 (Cited on page 10).

S. Grillner, T. Deliagina, A El Manira, R. Hill, G. Orlovsky, P Wallén, Ö Ekeberg and A Lansner (1995). 'Neural networks that co-ordinate locomotion and body orientation in lamprey'. In: *Trends in neurosciences* 18.6, pp. 270–279 (Cited on pages 98 and 99).

S. Grillner, P. Wallén, R. Hill, L. Cangiano and A. E. Manira (2001). 'Ion channels of importance for the locomotor pattern generation in the lamprey brainstem-spinal cord'. In: *The Journal of physiology* 533.1, pp. 23–30 (Cited on page 98).

J. W. Grizzle, G. Abba and F. Plestan (2001). 'Asymptotically stable walking for biped robots: Analysis via systems with impulse effects'. In: *IEEE Transactions on automatic control* 46.1, pp. 51–64 (Cited on page 59).

S. Gupta and A. Kumar (2017). 'A brief review of dynamics and control of underactuated biped robots'. In: *Advanced Robotics* 31.12, pp. 607–623 (Cited on page 24).

T. Gurevich and N. Giladi (2003). 'Freezing of gait in multiple system atrophy (MSA)'. In: *Parkinsonism & related disorders* 9.3, pp. 169–174 (Cited on page 11).

S. Haghighi, M. Jasemi, S. Hessabi and A. Zolanvari (2018). 'PyCM: Multiclass confusion matrix library in Python'. In: *Journal of Open Source Software* 3.25, p. 729. DOI: 10.21105/joss.00729. URL: https://doi.org/10.21105/joss.00729 (Cited on page 43).

A. C. G. Hall and E John (2005). *Textbook of medical physiology . Philadelphia: WB Saunders*. Tech. rep. ISBN 978-0-7216-0240-0 (Cited on page 151).

J. E. Hall (2015). *Guyton and Hall Textbook of Medical Physiology E-Book*. Elsevier Health Sciences (Cited on page 150).

A. A. Handojoseno, J. M. Shine, T. N. Nguyen, Y. Tran, S. J. Lewis and H. T. Nguyen (2012). 'The detection of Freezing of Gait in Parkinson's disease patients using EEG signals based on Wavelet decomposition'. In: *2012 Annual International*

Conference of the IEEE Engineering in Medicine and Biology Society. IEEE, pp. 69–72 (Cited on page 16).

A. A. Handojoseno, J. M. Shine, T. N. Nguyen, Y. Tran, S. J. Lewis and H. T. Nguyen (2014). 'Analysis and prediction of the freezing of gait using EEG brain dynamics'. In: *IEEE transactions on neural systems and rehabilitation engineering* 23.5, pp. 887–896 (Cited on pages 18 and 19).

J. Hausdorff, J. Schaafsma, Y Balash, A. Bartels, T Gurevich and N Giladi (2003). 'Impaired regulation of stride variability in Parkinson's disease subjects with freezing of gait'. In: *Experimental brain research* 149.2, pp. 187–194 (Cited on page 114).

E. Heremans, A. Nieuwboer and S. Vercruysse (2013a). 'Freezing of Gait in Parkinson's Disease: Where Are We Now?' In: *Current Neurology and Neuroscience Reports* 13.6, p. 350. ISSN: 1534-6293. DOI: 10.1007/s11910-013-0350-7. URL: https://doi.org/10.1007/s11910-013-0350-7 (Cited on pages 2, 3, 57, 59 and 119).

E. Heremans, A. Nieuwboer and S. Vercruysse (2013b). 'Freezing of gait in Parkinson's disease: where are we now?' In: *Current neurology and neuroscience reports* 13.6, p. 350 (Cited on pages 123 and 147).

A. Hof and J. Van Den Berg (1977). 'Linearity between the weighted sum of the EMGs of the human triceps surae and the total torque'. In: *Journal of biomechanics* 10.9, pp. 529–539 (Cited on pages 58 and 99).

S. Hwang, Y. Woo, S.-Y. Lee, S.-S. Shin and S. Jung (2012). 'Augmented feedback using visual cues for movement smoothness during gait performance of individuals with Parkinson's disease'. In: *Journal of Physical Therapy Science* 24.6, pp. 553–556 (Cited on pages 1, 2, 20 and 146).

A. J. Ijspeert (2008). 'Central pattern generators for locomotion control in animals and robots: a review'. In: *Neural networks* 21.4, pp. 642–653 (Cited on pages 23 and 98).

A. J. Ijspeert, A. Crespi and J.-M. Cabelguen (2005). 'Simulation and robotics studies of salamander locomotion'. In: *Neuroinformatics* 3.3, pp. 171–195 (Cited on pages 101, 103, 109 and 145).

W. R. Inc. *Mathematica, Version 12.0*. URL: `https://www.wolfram.com/mathematica` (Cited on pages 75 and 109).

M. Iosa, A. Fusco, G. Morone and S. Paolucci (2014). 'Development and decline of upright gait stability'. In: *Frontiers in aging neuroscience* 6, p. 14 (Cited on page 109).

S. Iqbal, X. Zang, Y. Zhu and J. Zhao (2014). 'Bifurcations and chaos in passive dynamic walking: A review'. In: *Robotics and Autonomous Systems* 62.6, pp. 889–909 (Cited on pages 3, 22 and 24).

K. Ishihara, T. D. Itoh and J. Morimoto (2019). 'Full-body optimal control toward versatile and agile behaviors in a humanoid robot'. In: *IEEE Robotics and Automation Letters* 5.1, pp. 119–126 (Cited on page 25).

Y. P. Ivanenko, R. E. Poppele and F. Lacquaniti (2004). 'Five basic muscle activation patterns account for muscle activity during human locomotion'. In: *The Journal of physiology* 556.1, pp. 267–282 (Cited on page 23).

E. M. Izhikevich (2003). 'Simple model of spiking neurons'. In: *IEEE Transactions on neural networks* 14.6, pp. 1569–1572 (Cited on pages 24, 99, 103, 104 and 143).

E. M. Izhikevich (2007). *Dynamical systems in neuroscience*. MIT press (Cited on pages 30, 32, 33, 34, 98, 99, 120, 125 and 131).

K. Josic, E. T. Shea-Brown and J. Moehlis (2006). 'Isochron'. In: *Scholarpedia* 1.8. revision #182469, p. 1361. DOI: `10.4249/scholarpedia.1361` (Cited on pages 32 and 124).

E. R. Kandel, J. H. Schwartz, T. M. Jessell, S. A. Siegelbaum and A. J. Hudspeth (2000). *Principles of neural science*. Vol. 4. McGraw-hill New York (Cited on pages 1, 150 and 151).

T. R. Kane and D. A. Levinson (1985). *Dynamics, theory and applications*. McGraw Hill (Cited on page 61).

A. Kharb, V. Saini, Y. Jain and S. Dhiman (2011). 'A review of gait cycle and its parameters'. In: *IJCEM International Journal of Computational Engineering & Management* 13, pp. 78–83 (Cited on page 59).

E. Khudados, F. W. Cody and D. J. O'Boyle (1999). 'Proprioceptive regulation of voluntary ankle movements, demonstrated using muscle vibration, is impaired by Parkinson's disease'. In: *Journal of Neurology, Neurosurgery & Psychiatry* 67.4, pp. 504–510 (Cited on page 14).

T. Klockgether, M. Borutta, H. Rapp, S. Spieker and J. Dichgans (1995). 'A defect of kinesthesia in Parkinson's disease'. In: *Movement disorders: official journal of the Movement Disorder Society* 10.4, pp. 460–465 (Cited on page 14).

P. Knobl, L. Kielstra and Q. Almeida (2012). 'The relationship between motor planning and freezing of gait in Parkinson's disease'. In: *Journal of Neurology, Neurosurgery & Psychiatry* 83.1, pp. 98–101 (Cited on page 18).

J. Konczak, D. M. Corcos, F. Horak, H. Poizner, M. Shapiro, P. Tuite, J. Volkmann and M. Maschke (2009). 'Proprioception and motor control in Parkinson's disease'. In: *Journal of motor behavior* 41.6, pp. 543–552 (Cited on pages 14 and 20).

I. J. Kopin (1993). 'The pharmacology of Parkinson's disease therapy: an update'. In: *Annual review of pharmacology and toxicology* 33.1, pp. 467–495 (Cited on page 154).

Y. Kuramoto (1984). 'Cooperative dynamics of oscillator communitya study based on lattice of rings'. In: *Progress of Theoretical Physics Supplement* 79, pp. 223–240 (Cited on page 34).

M. L. Latash (2010). 'Motor synergies and the equilibrium-point hypothesis'. In: *Motor control* 14.3, pp. 294–322 (Cited on page 26).

M. L. Latash, J. P. Scholz and G. Schöner (2002). 'Motor control strategies revealed in the structure of motor variability'. In: *Exercise and sport sciences reviews* 30.1, pp. 26–31 (Cited on pages 25 and 122).

M. Lemieux and F. Bretzner (2019). 'Glutamatergic neurons of the gigantocellular reticular nucleus shape locomotor pattern and rhythm in the freely behaving mouse'. In: *PLoS biology* 17.4, e2003880 (Cited on page 13).

R. N. Lemon (2008). 'Descending pathways in motor control'. In: *Annu. Rev. Neurosci.* 31, pp. 195–218 (Cited on page 150).

S. J. Lewis and R. A. Barker (2009). 'A pathophysiological model of freezing of gait in Parkinson's disease'. In: *Parkinsonism & related disorders* 15.5, pp. 333–338 (Cited on page 1).

S. J. Lewis and J. M. Shine (2016). 'The next step: a common neural mechanism for freezing of gait'. In: *The Neuroscientist* 22.1, pp. 72–82 (Cited on page 24).

D. C. Liu and J. Nocedal (1989). 'On the limited memory BFGS method for large scale optimization'. In: *Mathematical programming* 45.1-3, pp. 503–528 (Cited on page 46).

Z. Liu, J. Golowasch, E. Marder and L. Abbott (1998). 'A model neuron with activity-dependent conductances regulated by multiple calcium sensors'. In: *Journal of Neuroscience* 18.7, pp. 2309–2320 (Cited on page 142).

L. Livi, A. Sadeghian and H. Sadeghian (2016). 'Discrimination and Characterization of Parkinsonian Rest Tremors by Analyzing Long-Term Correlations and Multifractal Signatures'. In: *IEEE Transactions on Biomedical Engineering* 63.11, pp. 2243–2249. DOI: 10.1109/TBME.2016.2515760 (Cited on page 21).

W. Lohmiller and J.-J. E. Slotine (1998). 'On contraction analysis for non-linear systems'. In: *Automatica* 34.6, pp. 683–696 (Cited on pages 27 and 97).

R. Lozi (2013). 'Can we trust in numerical computations of chaotic solutions of dynamical systems?' In: *Topology and dynamics of Chaos: In celebration of Robert Gilmore's 70th birthday*. World Scientific, pp. 63–98 (Cited on page 73).

J. Lunze and F. Lamnabhi-Lagarrigue (2009). *Handbook of hybrid systems control: theory, tools, applications*. Cambridge University Press (Cited on page 61).

F. Magrinelli, A. Picelli, P. Tocco, A. Federico, L. Roncari, N. Smania, G. Zanette and S. Tamburin (2016). 'Pathophysiology of motor dysfunction in Parkinson's disease as the rationale for drug treatment and rehabilitation'. In: *Parkinson's disease* 2016 (Cited on page 121).

P Mahmoodi, R. Ransing and M. Friswell (2013). 'Modelling the effect of 'heel to toe'roll-over contact on the walking dynamics of passive biped robots'. In: *Applied Mathematical Modelling* 37.12-13, pp. 7352–7373 (Cited on pages 3, 22 and 24).

D. S. Malcolm (1951). 'A method of measuring reflex times applied in sciatica and other conditions due to nerve-root compression'. In: *Journal of neurology, neurosurgery, and psychiatry* 14.1, p. 15 (Cited on pages 99, 103 and 126).

I. R. Manchester, M. M. Tobenkin, M. Levashov and R. Tedrake (2011). 'Regions of attraction for hybrid limit cycles of walking robots'. In: *IFAC Proceedings Volumes* 44.1, pp. 5801–5806 (Cited on pages 3, 22 and 24).

A. Mandali, M. Rengaswamy, V. S. Chakravarthy and A. A. Moustafa (2015). 'A spiking Basal Ganglia model of synchrony, exploration and decision making'. In: *Frontiers in neuroscience* 9, p. 191 (Cited on page 21).

C. Marsden and J. Parkes (1977). 'Success and problems of long-term levodopa therapy in Parkinson's disease'. In: *The Lancet* 309.8007, pp. 345–349 (Cited on page 1).

K. E. Martens, J. M. Hall, M. Gilat, M. J. Georgiades, C. C. Walton and S. Lewis (2016). 'Anxiety is associated with freezing of gait and attentional set-shifting in Parkinson's disease: a new perspective for early intervention'. In: *Gait & posture* 49, pp. 431–436 (Cited on page 93).

S. Mazilu, A. Calatroni, E. Gazit, A. Mirelman, J. M. Hausdorff and G. Tröster (2015). 'Prediction of freezing of gait in Parkinson's from physiological wearables: an exploratory study'. In: *IEEE journal of biomedical and health informatics* 19.6, pp. 1843–1854 (Cited on pages 1, 2, 16, 18, 19, 50 and 54).

S. Mazilu, A. Calatroni, E. Gazit, D. Roggen, J. M. Hausdorff and G. Tröster (2013). 'Feature learning for detection and prediction of freezing of gait in Parkinson's disease'. In: *International workshop on machine learning and data mining in pattern Recognition*. Springer, pp. 144–158 (Cited on pages 2, 18, 19, 53, 54 and 144).

T. McGeer et al. (1990). 'Passive dynamic walking'. In: *I. J. Robotic Res.* 9.2, pp. 62–82 (Cited on pages 3, 24 and 59).

M. McNeely, T Hershey, M. Campbell, S. Tabbal, M Karimi, J. Hartlein, H. Lugar, F. Revilla, J. Perlmutter and G. Earhart (2011). 'Effects of deep brain stimulation of dorsal versus ventral subthalamic nucleus regions on gait and balance in Parkinson's disease'. In: *Journal of Neurology, Neurosurgery & Psychiatry* 82.11, pp. 1250–1255 (Cited on page 154).

K. Minassian, U. S. Hofstoetter, F. Dzeladini, P. A. Guertin and A. Ijspeert (2017). 'The human central pattern generator for locomotion: Does it exist and contribute to walking?' In: *The Neuroscientist* 23.6, pp. 649–663 (Cited on pages 11 and 98).

K. Minassian, I. Persy, F. Rattay, M. M. Pinter, H. Kern and M. R. Dimitrijevic (2007). 'Human lumbar cord circuitries can be activated by extrinsic tonic input to generate locomotor-like activity'. In: *Human movement science* 26.2, pp. 275–295 (Cited on page 124).

R. Molina, C. J. Hass, K. Sowalsky, A. C. Schmitt, E. Opri, J. A. Roper, D. Martinez-Ramirez, C. W. Hess, K. D. Foote, M. S. Okun et al. (2020). 'Neurophysiological correlates of gait in the human basal ganglia and the PPN region in Parkinson's disease'. In: *Frontiers in Human Neuroscience* 14 (Cited on page 154).

K. Mombaur, A. Truong and J.-P. Laumond (2010). 'From human to humanoid locomotion—an inverse optimal control approach'. In: *Autonomous robots* 28.3, pp. 369–383 (Cited on page 25).

S. Montazeri Moghadam, M. Sadeghi Talarposhti, A. Niaty, F. Towhidkhah and S. Jafari (2018). 'The simple chaotic model of passive dynamic walking'. In: *Nonlinear Dynamics* 93.3, pp. 1183–1199. ISSN: 1573-269X. DOI: 10.1007/s11071-018-4252-8. URL: https://doi.org/10.1007/s11071-018-4252-8 (Cited on pages 4, 21, 22 and 145).

C Moreau, L Defebvre, A Destee, S Bleuse, F Clement, J. Blatt, P Krystkowiak and D Devos (2008). 'STN-DBS frequency effects on freezing of gait in advanced Parkinson disease'. In: *Neurology* 71.2, pp. 80–84 (Cited on page 154).

V. Muralidharan, P. Balasubramani, S. Chakravarthy, S. J. G. Lewis and A. Moustafa (2014). 'A COMPUTATIONAL MODEL OF ALTERED GAIT PATTERNS IN PARKINSON'S DISEASE PATIENTS NEGOTIATING NARROW DOOR-

WAYS'. In: *Frontiers in Computational Neuroscience* 7, p. 190. ISSN: 1662-5188. DOI: 10.3389/fncom.2013.00190. URL: https://www.frontiersin.org/article/10.3389/fncom.2013.00190 (Cited on page 21).

V. Muralidharan, P. P. Balasubramani, V. S. Chakravarthy and A. A. Moustafa (2018). 'A Basal Ganglia Model of Freezing of Gait in Parkinson's Disease'. In: *Computational Neuroscience Models of the Basal Ganglia*. Springer, pp. 113–129 (Cited on pages 3, 4, 22 and 145).

N. Muthukrishnan, J. J. Abbas, H. A. Shill and N. Krishnamurthi (2019). 'Cueing paradigms to improve gait and posture in Parkinson's disease: A narrative review'. In: *Sensors* 19.24, p. 5468 (Cited on page 20).

I. J. Myung (2003). 'Tutorial on maximum likelihood estimation'. In: *Journal of mathematical Psychology* 47.1, pp. 90–100 (Cited on page 45).

J. Nantel, C. de Solages and H. Bronte-Stewart (2011). 'Repetitive stepping in place identifies and measures freezing episodes in subjects with Parkinson's disease'. In: *Gait & posture* 34.3, pp. 329–333 (Cited on pages 41 and 42).

A. Nieuwboer (2008). 'Cueing for freezing of gait in patients with Parkinson's disease: a rehabilitation perspective'. In: *Movement disorders: official journal of the Movement Disorder Society* 23.S2, S475–S481 (Cited on pages 116 and 120).

A. Nieuwboer (2015). 'Cueing effects in Parkinson's disease: Benefits and drawbacks'. In: *Annals of Physical and Rehabilitation Medicine* 58, e70–e71 (Cited on page 20).

A. Nieuwboer, R. Dom, W. De Weerdt, K. Desloovere, L. Janssens and V. Stijn (2004). 'Electromyographic profiles of gait prior to onset of freezing episodes in patients with Parkinson's disease'. In: *Brain* 127.7, pp. 1650–1660 (Cited on pages 14, 56, 57, 58, 63, 92, 99, 105, 127, 130, 141 and 145).

J. Nonnekes, A. H. Snijders, J. G. Nutt, G. Deuschl, N. Giladi and B. R. Bloem (2015). 'Freezing of gait: a practical approach to management'. In: *The Lancet Neurology* 14.7, pp. 768–778 (Cited on pages 2 and 20).

A. J. Northcutt and D. J. Schulz (2020). 'Molecular mechanisms of homeostatic plasticity in central pattern generator networks'. In: *Developmental neurobiology* 80.1-2, pp. 58–69 (Cited on page 121).

J. G. Nutt, B. R. Bloem, N. Giladi, M. Hallett, F. B. Horak and A. Nieuwboer (2011). 'Freezing of gait: moving forward on a mysterious clinical phenomenon'. In: *The Lancet Neurology* 10.8, pp. 734–744 (Cited on pages 1, 57, 58, 59, 78 and 92).

W. Olszewski and A. Sandroni (2011). 'Falsifiability'. In: *American Economic Review* 101.2, pp. 788–818 (Cited on page 26).

J. Opitz and S. Burst (2019). 'Macro F1 and Macro F1'. In: *arXiv preprint arXiv:1911.03347* (Cited on pages 43, 46 and 47).

S. Oprisan, V Thirumalai and C. Canavier (2003). 'Dynamics from a time series: can we extract the phase resetting curve from a time series?' In: *Biophysical journal* 84.5, pp. 2919–2928 (Cited on pages 31, 131, 132, 133, 134, 142, 146 and 147).

N. K. Orphanidou, A. Hussain, R. Keight, P. Lishoa, J. Hind and H. Al-Askar (2018). 'Predicting freezing of gait in Parkinsons disease patients using machine learning'. In: *2018 IEEE Congress on Evolutionary Computation (CEC)*. IEEE, pp. 1–8 (Cited on page 19).

R. Ospina and F. Marmolejo-Ramos (2019). 'Performance of Some Estimators of Relative Variability'. In: *Frontiers in Applied Mathematics and Statistics* 5, p. 43. ISSN: 2297-4687. DOI: 10.3389/fams.2019.00043. URL: https://www.frontiersin.org/article/10.3389/fams.2019.00043 (Cited on page 117).

L. Palmerini, L. Rocchi, S. Mazilu, E. Gazit, J. M. Hausdorff and L. Chiari (2017). 'Identification of characteristic motor patterns preceding freezing of gait in Parkinson's disease using wearable sensors'. In: *Frontiers in neurology* 8, p. 394 (Cited on pages 17, 18 and 19).

M. Parakkal Unni, P. P. Menon, M. R. Wilson and K. Tsaneva-Atanasova (2020a). 'Ankle Push-Off Based Mathematical Model for Freezing of Gait in Parkinson's Disease'. In: *Frontiers in Bioengineering and Biotechnology* 8, p. 1197. DOI: 10.3389/fbioe.2020.552635. URL: https://www.frontiersin.org/article/10.3389/fbioe.2020.552635 (Cited on page 104).

M. Parakkal Unni, P. P. Menon, M. R. Wilson and K. Tsaneva-Atanasova (2020b). 'Ankle Push-Off Based Mathematical Model for Freezing of Gait in Parkinson's Disease'. In: *Frontiers in Bioengineering and Biotechnology* 8, p. 1197. ISSN: 2296-

4185. DOI: 10.3389/fbioe.2020.552635. URL: https://www.frontiersin.org/article/10.3389/fbioe.2020.552635 (Cited on page 127).

M. Parakkal Unni, A. Sinha, K. Chakravarty, D. Chatterjee and A. Das (2017). 'Neuro-mechanical cost functionals governing motor control for early screening of motor disorders'. In: *Frontiers in Bioengineering and Biotechnology* 5, p. 78 (Cited on pages 3, 25 and 55).

S. Pardoel, J. Kofman, J. Nantel and E. D. Lemaire (2019). 'Wearable-sensor-based detection and prediction of freezing of gait in Parkinson's disease: A review'. In: *Sensors* 19.23, p. 5141 (Cited on pages 2, 16 and 144).

F. Pedregosa, G. Varoquaux, A. Gramfort, V. Michel, B. Thirion, O. Grisel, M. Blondel, P. Prettenhofer, R. Weiss, V. Dubourg et al. (2011). 'Scikit-learn: Machine Learning in Python'. In: *Journal of Machine Learning Research* 12, pp. 2825–2830 (Cited on page 46).

D. Pekarek, A. D. Ames and J. E. Marsden (2007). 'Discrete mechanics and optimal control applied to the compass gait biped'. In: *2007 46th IEEE Conference on Decision and Control*. IEEE, pp. 5376–5382 (Cited on pages 3 and 25).

J. S. Perlmutter and J. W. Mink (2006). 'Deep brain stimulation'. In: *Annu. Rev. Neurosci.* 29, pp. 229–257 (Cited on page 154).

T. T. Pham, S. T. Moore, S. J. G. Lewis, D. N. Nguyen, E. Dutkiewicz, A. J. Fuglevand, A. L. McEwan and P. H. Leong (2017). 'Freezing of gait detection in Parkinson's disease: a subject-independent detector using anomaly scores'. In: *IEEE Transactions on Biomedical Engineering* 64.11, pp. 2719–2728 (Cited on pages 2, 16 and 21).

H. M. Pinsker (1977). 'Aplysia bursting neurons as endogenous oscillators. I. Phase-response curves for pulsed inhibitory synaptic input'. In: *Journal of Neurophysiology* 40.3, pp. 527–543 (Cited on pages 131 and 134).

J. C. Polese, L. F. Teixeira-Salmela, L. R. Nascimento, C. D. M. Faria, R. N. Kirkwood, G. C. Laurentino and L. Ada (2012). 'The effects of walking sticks on gait kinematics and kinetics with chronic stroke survivors'. In: *Clinical Biomechanics* 27.2, pp. 131–137 (Cited on page 61).

K. Popper (2002). *Popper: The logic of scientific discovery*. Routledge Classics New York, NY, pp. 17–21 (Cited on page 26).

N. G. Pozzi, A. Canessa, C. Palmisano, J. Brumberg, F. Steigerwald, M. M. Reich, B. Minafra, C. Pacchetti, G. Pezzoli, J. Volkmann et al. (2019). 'Freezing of gait in Parkinson's disease reflects a sudden derangement of locomotor network dynamics'. In: *Brain* 142.7, pp. 2037–2050 (Cited on pages 123, 142 and 147).

A. A. Prinz, D. Bucher and E. Marder (2004). 'Similar network activity from disparate circuit parameters'. In: *Nature neuroscience* 7.12, pp. 1345–1352 (Cited on page 142).

A Ranavolo, C Conte, S Iavicoli, M Serrao, A Silvetti, G Sandrini, F Pierelli and F Draicchio (2011). 'Walking strategies of visually impaired people on trapezoidal- and sinusoidal-section tactile groundsurface indicators'. In: *Ergonomics* 54.3, pp. 246–256 (Cited on page 61).

J. R. Rebula, S. Schaal, J. Finley and L. Righetti (2019). 'A Robustness Analysis of Inverse Optimal Control of Bipedal Walking'. In: *IEEE Robotics and Automation Letters* 4.4, pp. 4531–4538 (Cited on page 25).

C. Rickards and F. Cody (1997). 'Proprioceptive control of wrist movements in Parkinson's disease. Reduced muscle vibration-induced errors.' In: *Brain: a journal of neurology* 120.6, pp. 977–990 (Cited on page 14).

L. Rochester, V. Hetherington, D. Jones, A. Nieuwboer, A.-M. Willems, G. Kwakkel and E. Van Wegen (2005). 'The effect of external rhythmic cues (auditory and visual) on walking during a functional task in homes of people with Parkinson's disease'. In: *Archives of physical medicine and rehabilitation* 86.5, pp. 999–1006 (Cited on pages 57 and 93).

J. Ros, J. M. Font-Llagunes, A. Plaza and J. Kövecses (2015). 'Dynamic considerations of heel-strike impact in human gait'. In: *Multibody system dynamics* 35.3, pp. 215–232 (Cited on page 3).

T. C. Rubinstein, N. Giladi and J. M. Hausdorff (2002). 'The power of cueing to circumvent dopamine deficits: a review of physical therapy treatment of gait

disturbances in Parkinson's disease'. In: *Movement disorders: official journal of the Movement Disorder Society* 17.6, pp. 1148–1160 (Cited on pages 2 and 20).

H. Sadeghian and M. Barkhordari (2020). 'Orbital Analysis of Passive Dynamic Bipeds; the Effect of Model Parameters and Stabilizing Arm'. In: *International Journal of Mechanical Sciences*, p. 105616. ISSN: 0020-7403. DOI: https://doi.org/10.1016/j.ijmecsci.2020.105616. URL: http://www.sciencedirect.com/science/article/pii/S0020740319336641 (Cited on pages 3, 22 and 24).

R. L. Sainburg (2015). 'Should the Equilibrium Point Hypothesis (EPH) be considered a scientific theory?' In: *Motor control* 19.2, pp. 142–148 (Cited on pages 26 and 92).

G. J. Sammarco (1995). 'Peroneus longus tendon tears: acute and chronic'. In: *Foot & ankle international* 16.5, pp. 245–253 (Cited on page 14).

R. San-Segundo, R. Torres-Sánchez, J. Hodgins and F. De la Torre (2019). 'Increasing Robustness in the Detection of Freezing of Gait in Parkinson's Disease'. In: *Electronics* 8.2, p. 119 (Cited on page 109).

Y. Sarbaz, M. Banaie, M. Pooyan, S. Gharibzadeh, F. Towhidkhah and A. Jafari (2012). 'Modeling the gait of normal and Parkinsonian persons for improving the diagnosis'. In: *Neuroscience letters* 509.2, pp. 72–75 (Cited on pages 4, 22 and 145).

A. H. Schapira, K. R. Chaudhuri and P. Jenner (2017). 'Non-motor features of Parkinson disease'. In: *Nature Reviews Neuroscience* 18.7, p. 435 (Cited on page 1).

C Schrader, H.-H. Capelle, T. Kinfe, C Blahak, H Bäzner, G Lütjens, D Dressler and J. Krauss (2011). 'GPi-DBS may induce a hypokinetic gait disorder with freezing of gait in patients with dystonia'. In: *Neurology* 77.5, pp. 483–488 (Cited on page 154).

J. Shine, A. Handojoseno, T. Nguyen, Y Tran, S. Naismith, H Nguyen and S. Lewis (2014). 'Abnormal patterns of theta frequency oscillations during the temporal evolution of freezing of gait in Parkinson's disease'. In: *Clinical Neurophysiology* 125.3, pp. 569–576 (Cited on page 24).

F. H. Sieling, C. C. Canavier and A. A. Prinz (2009). 'Predictions of phase-locking in excitatory hybrid networks: excitation does not promote phase-locking in pattern-generating networks as reliably as inhibition'. In: *Journal of neurophysiology* 102.1, pp. 69–84 (Cited on page 31).

R. W. Sinnet, M. J. Powell, R. P. Shah and A. D. Ames (2011). 'A human-inspired hybrid control approach to bipedal robotic walking'. In: *IFAC Proceedings Volumes* 44.1, pp. 6904–6911 (Cited on page 59).

A. H. Snijders, M. J. Nijkrake, M. Bakker, M. Munneke, C. Wind and B. R. Bloem (2008). 'Clinimetrics of freezing of gait'. In: *Movement disorders: official journal of the Movement Disorder Society* 23.S2, S468–S474 (Cited on pages 56 and 57).

A. H. Snijders, K. Takakusaki, B. Debu, A. M. Lozano, V. Krishna, A. Fasano, T. Z. Aziz, S. M. Papa, S. A. Factor and M. Hallett (2016). 'Physiology of freezing of gait'. In: *Annals of neurology* 80.5, pp. 644–659 (Cited on pages 13, 14, 98, 121, 139, 141, 148 and 154).

W. Soofi and A. A. Prinz (2015). 'Differential effects of conductances on the phase resetting curve of a bursting neuronal oscillator'. In: *Journal of computational neuroscience* 38.3, pp. 539–558 (Cited on pages 31, 133, 134, 142, 146 and 147).

S. J. Spaulding, B. Barber, M. Colby, B. Cormack, T. Mick and M. E. Jenkins (2013). 'Cueing and gait improvement among people with Parkinson's disease: a meta-analysis'. In: *Archives of physical medicine and rehabilitation* 94.3, pp. 562–570 (Cited on pages 116 and 120).

J. Su and H. Zhang (2006). 'A fast decision tree learning algorithm'. In: *Aaai*. Vol. 6, pp. 500–505 (Cited on page 46).

X. Sun and J. Lei (2013). 'Limit Cycle'. In: *Encyclopedia of Systems Biology*. Ed. by W. Dubitzky, O. Wolkenhauer, K.-H. Cho and H. Yokota. New York, NY: Springer New York, pp. 1126–1127. ISBN: 978-1-4419-9863-7. DOI: 10.1007/978-1-4419-9863-7_533. URL: https://doi.org/10.1007/978-1-4419-9863-7_533 (Cited on page 29).

J. Syrkin-Nikolau, M. M. Koop, T. Prieto, C. Anidi, M. F. Afzal, A. Velisar, Z. Blumenfeld, T. Martin, M. Trager and H. Bronte-Stewart (2017). 'Subthalamic

neural entropy is a feature of freezing of gait in freely moving people with Parkinson's disease'. In: *Neurobiology of disease* 108, pp. 288–297 (Cited on page 1).

G. Taga (1994). 'Emergence of bipedal locomotion through entrainment among the neuro-musculo-skeletal system and the environment'. In: *Physica D: Nonlinear Phenomena* 75.1-3, pp. 190–208 (Cited on page 24).

G. Taga (1995). 'A model of the neuro-musculo-skeletal system for human locomotion'. In: *Biological cybernetics* 73.2, pp. 97–111 (Cited on pages 3, 4, 11, 23, 59 and 120).

K. Takakusaki (2013). 'Neurophysiology of gait: from the spinal cord to the frontal lobe'. In: *Movement Disorders* 28.11, pp. 1483–1491 (Cited on page 13).

D. Tamura, S. Aoi, T. Funato, S. Fujiki, K. Senda and K. Tsuchiya (2020). 'Contribution of Phase Resetting to Adaptive Rhythm Control in Human Walking Based on the Phase Response Curves of a Neuromusculoskeletal Model'. In: *Frontiers in Neuroscience* 14 (Cited on pages 4, 23, 26, 31 and 120).

J. Z. Tang and I. R. Manchester (2014). 'Transverse contraction criteria for stability of nonlinear hybrid limit cycles'. In: *53rd IEEE Conference on decision and control*. IEEE, pp. 31–36 (Cited on pages 27 and 97).

E. Taub, G. Uswatte and T. Elbert (2002). 'New treatments in neurorehabiliation founded on basic research'. In: *Nature Reviews Neuroscience* 3.3, pp. 228–236 (Cited on page 98).

H. Teasdale, E. Preston and G. Waddington (2017). 'Proprioception of the Ankle is Impaired in People with Parkinson's Disease'. In: *Movement disorders clinical practice* 4.4, pp. 524–528 (Cited on page 14).

V. G. Torvi, A. Bhattacharya and S. Chakraborty (2018). 'Deep Domain Adaptation to Predict Freezing of Gait in Patients with Parkinson's Disease'. In: *2018 17th IEEE International Conference on Machine Learning and Applications (ICMLA)*. IEEE, pp. 1001–1006 (Cited on page 19).

M. C. Tresch and A. Jarc (2009). 'The case for and against muscle synergies'. In: *Current opinion in neurobiology* 19.6, pp. 601–607 (Cited on page 26).

J. C. Tuthill and E. Azim (2018). 'Proprioception'. In: *Current Biology* 28.5, R194–R203 (Cited on pages 14, 99, 101 and 114).

J. R. Usherwood (2005). 'Why not walk faster?' In: *Biology letters* 1.3, pp. 338–341 (Cited on page 61).

M. Wahde and J. Pettersson (2002). 'A brief review of bipedal robotics research'. In: *Proceedings of the 8th UK Mechatronics Forum International Conference (Mechatronics 2002)*, pp. 480–488 (Cited on page 59).

M. Weinberger, C. Hamani, W. D. Hutchison, E. Moro, A. M. Lozano and J. O. Dostrovsky (2008). 'Pedunculopontine nucleus microelectrode recordings in movement disorder patients'. In: *Experimental brain research* 188.2, pp. 165–174 (Cited on page 151).

E. D. Wendel and A. D. Ames (2010). 'Rank properties of Poincaré maps for hybrid systems with applications to bipedal walking'. In: *Proceedings of the 13th ACM international conference on Hybrid systems: computation and control*, pp. 151–160 (Cited on page 29).

A. M. Willems, A. Nieuwboer, F Chavret, K. Desloovere, R. Dom, L. Rochester, D. Jones, G. Kwakkel and E. Van Wegen (2006). 'The use of rhythmic auditory cues to influence gait in patients with Parkinson's disease, the differential effect for freezers and non-freezers, an explorative study'. In: *Disability and rehabilitation* 28.11, pp. 721–728 (Cited on pages 116 and 120).

A. T. Winfree (1967). 'Biological rhythms and the behavior of populations of coupled oscillators'. In: *Journal of theoretical biology* 16.1, pp. 15–42 (Cited on page 34).

G. T. Wynarsky and A. S. Greenwald (1983). 'Mathematical model of the human ankle joint'. In: *Journal of biomechanics* 16.4, pp. 241–251 (Cited on page 148).

S. Yakovenko and T. Drew (2009). 'A motor cortical contribution to the anticipatory postural adjustments that precede reaching in the cat'. In: *Journal of neurophysiology* 102.2, pp. 853–874 (Cited on page 14).

T. Yamasaki, T. Nomura and S. Sato (2003). 'Possible functional roles of phase resetting during walking'. In: *Biological cybernetics* 88.6, pp. 468–496 (Cited on pages 23 and 31).

A. K. Yetisen, J. L. Martinez-Hurtado, B. Ünal, A. Khademhosseini and H. Butt (2018). 'Wearables in medicine'. In: *Advanced Materials* 30.33, p. 1706910 (Cited on page 148).

F. Yokochi (2006). 'Effect of deep brain stimulation on FOG'. In: *Parkinsonism & Related Disorders* 12, S67–S69 (Cited on page 154).

W. R. Young, M. W. Rodger and C. M. Craig (2014). 'Auditory observation of stepping actions can cue both spatial and temporal components of gait in Parkinson's disease patients'. In: *Neuropsychologia* 57, pp. 140–153 (Cited on pages 57 and 93).

W. R. Young, L. Shreve, E. J. Quinn, C. Craig and H. Bronte-Stewart (2016). 'Auditory cueing in Parkinson's patients with freezing of gait. What matters most: action-relevance or cue-continuity?' In: *Neuropsychologia* 87, pp. 54–62 (Cited on pages 39, 40 and 42).

I. Zahoor, A. Shafi and E. Haq (2018). 'Pharmacological treatment of Parkinson's disease'. In: *Exon Publications*, pp. 129–144 (Cited on page 154).

K. E. Zelik and P. G. Adamczyk (2016). 'A unified perspective on ankle push-off in human walking'. In: *Journal of Experimental Biology* 219.23, pp. 3676–3683 (Cited on pages 58 and 67).

H. Zhang (2004). 'The optimality of naive Bayes'. In: *AA* 1.2, p. 3 (Cited on page 45).

C. Zhu, R. H. Byrd, P. Lu and J. Nocedal (1997). 'Algorithm 778: L-BFGS-B: Fortran subroutines for large-scale bound-constrained optimization'. In: *ACM Transactions on Mathematical Software (TOMS)* 23.4, pp. 550–560 (Cited on page 46).

J. Zia, A. Tadayon, T. McDaniel and S. Panchanathan (2016). 'Utilizing neural networks to predict freezing of gait in parkinson's patients'. In: *Proceedings of the 18th International ACM SIGACCESS Conference on Computers and Accessibility*, pp. 333–334 (Cited on page 19).

W. Znegui, H. Gritli and S. Belghith (2020). 'Design of an explicit expression of the Poincaré map for the passive dynamic walking of the compass-gait biped model'. In: *Chaos, Solitons & Fractals* 130, p. 109436 (Cited on pages 3, 22 and 24).